OUT-OF-STEP RELAYING PRINCIPLES AND ADVANCES

Antans Sauļus Sauhats
Andrejs Utāns

Rīgas Tehniskā universitāte
1862 2022

OUT-OF-STEP RELAYING PRINCIPLES AND ADVANCES

Antans Sauļus Sauhats
Andrejs Utāns

Scientific monograph

RTU Press
2022

Sauhats, A. S., Utāns, A. **Out-of-Step Relaying Principles and Advances.** Scientific monograph. Riga, RTU Press, 2022. 168 pp.

The book is devoted to out-of-step (OOS) protection systems. It consists of two parts. Chapters 1–6 are dedicated to the problem of angular stability and OOS relaying principles. Traditional protection systems as well as potential prospective implementations are considered in these chapters. An outline of the most recent achievements in OOS relaying philosophy is provided. A new algorithm for generator grouping and OOS protection is presented. Chapters 7 and 8 review the existing and emerging communication technologies and communication standards that are already in use in power systems and can be used in the future to improve the performance of OOS protection systems.

Reviewers
Vladimirs Čuvičins
Arturas Klementavičius

Scientific editor
Andrejs Utāns

The monograph is published in accordance with the resolution of RTU Scientific Council of 24.10.2022, Minutes No. 04000-3/09.

Layout design Baiba Puriņa
Cover design Paula Lore

https://doi.org/10.7250/9789934227929
ISBN 978-9934-22-791-2 (print)
ISBN 978-9934-22-792-9 (pdf)

ABOUT THE AUTHORS

Antans Saulus Sauhats

Antans Sauhats is a professor and Director at the Power Engineering Institute of Riga Technical University, Latvia. He holds Dr. Sc. ing and Dr. habil. Sc.ing degrees in power system control and network operation optimisation. He is a corresponding member of the Latvian Academy of Sciences, a longtime member of the Latvian Electrical Engineering Society and a member of International Scientific Committees of Latvian, Lithuanian, Polish and Slovak Scientific Simposiums and conferences. Having more than 45 years of experience, Professor Sauhats is a well-known authority in the field of power system control and optimisation. He is the author of over 350 scientific publications and leads many Latvian and international research projects. His research specialty and interests include power system stability, power plant control and operation optimisation, high voltage transmission line fault location, protection relays and power system automation-related issues. He is the author of the idea and the scientific director of the out-of-step protection system, which is widely used nowadays in the power system of the Baltic States.

Andrejs Utans

Andrejs Utans received a Dr. Sc. ing degree from Riga Technical University in 1997. He is currently a professor at the Faculty of Electrical and Environmental Engineering of Riga Technical University. He is a leading researcher in several international and Latvian scientific projects and has more than 25 years of experience in the field of protection relays and automation systems. He is an author of more than 25 scientific publications. His current research is focused on power system stability and system resiliency-related problems. In addition to purely theorethical aspects of the problem, his area of interest is also a possible practical implementation of the problem being solved. He is also a developer and the technical director of out-of-step protection terminals, which are used in power system presently.

CONTENTS

INTRODUCTION

Power systems rank among the most complex technical objects created by mankind, ensuring a progressive civilisation development process and a relatively high standard of living so that people should be content and could perform their usual daily activities. Over the last ten years, the dependence on electricity has increased several times, since electricity has found wide use in various electrical devices (electrification of means of transport and of district heating, mobile phones, laptop computers, etc.). At present, mankind's dependence on electricity has become almost unquestionable; by analysing the development tendencies, it can be concluded that this dependence will only increase. Cases of power system blackouts, which last for several hours or even several days, have a considerable impact on everyday life and the economy. The functioning of the key systems, for example, communications or transport, will be hindered; water supply and district heating will be interrupted; manufacturing processes and trading at exchanges will be stopped. Emergency services (firefighting service, police or emergency medical services) will be unable to communicate due to the collapse of the telecommunication systems. Hospitals will remain in operation only as long as fuel is provided for the emergency generators. Financial exchanges, ATMs and shops will be closed, which will lead to a catastrophic scenario.

Striving to increase the economic efficiency of power supply, many countries have started using a joint electricity market. Trends in electricity market liberalisation affect considerably the operation of interconnected power systems. Power system operational mode changes due to various economic and environmental constraints. This may often lead to a contradiction between an attempt to achieve maximum economic efficiency and, at the same time, maintain power system stability and security at the highest possible level. Great efforts are being made to resolve this contradiction; still, in the realm of electricity market liberalisation, modern interconnected power systems are being operated much closer to their limits. For example, in striving to increase the economic efficiency, the typical power transfer profiles may be changed or even the transfer capabilities might be temporarily violated, which unavoidably diminishes the power system's stability reserve. These new tendencies leave the system planners and engineers faced with rather different and much more complex modes of power system operation.

While considerable efforts are being made in achieving stable and secure operation of the system for nearly any possible mode of operation, there always exists a probability that a sequence of unexpected and overlapping events may eventually push the power system into instability. The problem of the stability of large interconnected systems is becoming increasingly

topical due to the extensive development of electric power systems and their increasing complexity. The likelihood of a power system losing stability was confirmed by several blackouts and large-scale power outages that were found in many power systems during the past decades [1]–[5]. Analysing the reasons of recent blackouts, it can be concluded that there are always multiple causes for system collapse. The most typical reasons are: human-related factors; unavailability or misinterpretation of online information; underestimation of the extremity of the weather conditions; unpredictability of some power system events; inappropriate or incorrect response of various protection systems; unsatisfactory coordination between system operators or between control and automation systems. All of these factors may appear in different combinations; therefore, a power system that is able to withstand all the possible emergencies could hardly be implemented.

Recognising the fact that severe contingencies are unavoidable and the stability of the power system could be eventually lost, the main goal lies in avoiding a complete collapse of the system, that is, specific actions should be taken to mitigate the disastrous consequences of system instability. It is often the case that the process of loss of stability evolves much faster than the power system operator is able to respond to it. Therefore, special protection systems should respond to the system-wide emergency to preserve the network integrity as far as possible. One of such protection systems is the out-of-step (OOS) protection system, which is intended to minimise the harmful effect of angular instability. It is recognised that among several types of instability that may occur in a power system, the angular instability of the generator rotor is the one that should be addressed most urgently; therefore, the significance of the OOS protection system should not be underestimated.

It has to be noted that the problem of generator angle stability is as old as power system networks themselves. An enormous amount of studies and publications have been devoted exactly to this problem and research is still continuing. The reason for this is the extreme complexity of the problem, especially when large interconnected power systems are concerned. The complexity of the problem calls for a reasonable solution, which should be achieved by making allowance for already existing technologies as well as emerging ones. In the creation of reliable, cost-efficient and technically accomplished emergency control systems, it has been generally accepted in the recent twenty years to use microprocessor element basis, high-speed optical communication channels and the Global Positioning System (GPS). Using the above systems and elements offers new opportunities in creating complex, technically accomplished protection relaying and emergency control devices that operate within a unified system.

A significant contribution to the evaluation of the OOS protection relaying and automation systems, simulation of processes and synthesis of appropriate automatic equipment has also been made by Latvian researchers

Jānis Bubenko, Veniamin Fabrikant, Jēkabs Kuzmins, Zigurds Krišāns, Vilnis Krēsliņš, Kārlis Brinķis, Jēkabs Barkāns, Vladimirs Čuvičins, Aleksandrs Dolgicers, Galina Bočkarjova. Thanks to them, the power systems of the Baltic region use many effective technologies and control systems. Significant efforts were taken in OOS relaying. Latvia-manufactured OOS relays have already been in use in all the Baltic countries for more than twenty-five years. The authors of this book have participated in the development of the above automation equipment. The experience gained during the development and the results of the research have greatly contributed to the structure and contents of this book.

The scope of this book is devoted to OOS protection systems. The book consists of two parts. The first part (Chapters 1–6) is dedicated to the problem of angular stability and OOS relaying principles. Traditional protection systems as well as potential prospective implementations are considered in the first part of the book. An outline of the most recent achievements in OOS relaying philosophy is provided. The second part of the book (Chapters 7 and 8) reviews the existing and emerging communication technologies and communication standards that are already in use in power systems and can be used in the future to improve the performance of OOS protection systems.

1. POWER SYSTEM STABILITY

Power system stability is a fundamental concept, which has to do with the ability of a power system to maintain its operational parameters at a satisfactory level in the presence of various types of disturbances. Since the stability problem has been recognised to be paramount for any power system, many definitions of the power system stability term have been given. One of the most recent definitions of stability was formulated in [6] and is as follows:

> "Power system stability is the ability of an electric power system, for a given initial operating condition, to regain a state of operating equilibrium after being subjected to a physical disturbance, with most system variables bounded so that practically the entire system remains intact."

Conversely, in the case when the power system (or some part of the power system) is unable to attain a new state of equilibrium, the system is recognised to be unstable. This formulation treats the stability problem as a whole, without specifying the causes of power system instability. The reason for such a formulation is that power system instability is a complex phenomenon. All the major parameters of the power system are closely interrelated, and therefore a critical change in one parameter inevitably affects other parameters of the system. On the other hand, it is due to the exceptional complexity of the problem that it becomes necessary to divide the entire problem into separate problems that could be classified and addressed separately. An overall picture of the power system stability problem with a stability classification is presented in Fig. 1.1.

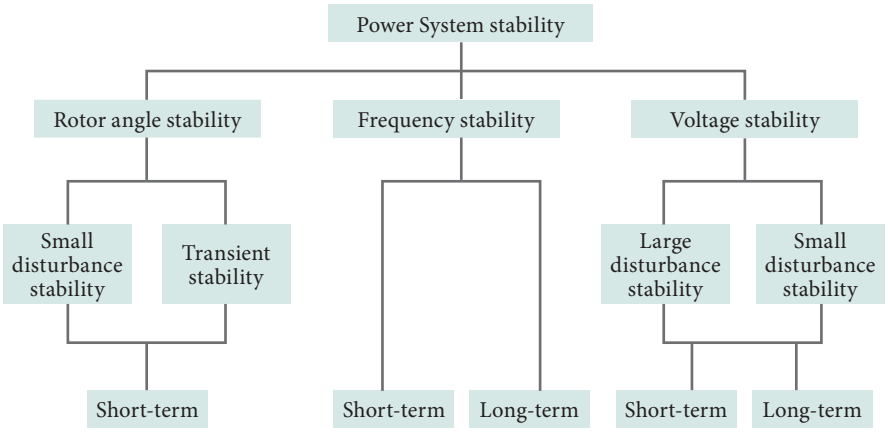

Fig. 1.1. Classification of power system stability (adopted from [6])

Depending on the essential factors that contribute to power system instability, three main types of stability can be distinguished:

1. Generator rotor angle stability.
2. Frequency stability.
3. Voltage stability.

Each type of system instability can be further classified depending on the severity of the disturbance (large/small) and depending on the time interval during which the specific phenomenon is developing and can be observed (short-term/long-term). Although there is no exact definition for short-term and long-term time frames, the approximate time scales to be considered could be defined as follows:

- short-term or transient – from 0 to 10 seconds;
- long-term – from 10 seconds to several minutes.

Because of the limited scope of this book, only the rotor angle stability problem will be considered further.

1.1. Rotor angle stability

> "Rotor angle stability is the ability of the synchronous machines of an interconnected power system to remain in synchronism after being subjected to a disturbance" [6].

A power system under steady-state conditions operates at a near-constant frequency with a maximum permissible frequency deviation of ±0.1…0.3 % from the rated value. The rotors of all the generators are rotating with the same speed, and the difference between the rotor angles of any two generators is near-constant. The rotation speed of all the machines is maintained within strict limits by the generators' governors. Under steady-state operation there should always be a balance between generated and consumed power. The mechanical input power of each generator should be balanced by the generator's electrical power output, thus providing a state of equilibrium for the entire system. This state of equilibrium is also known as the steady state; however, in real power systems, the steady-state condition never exists. Random changes in load and generation are taking place all the time; the network topology may be changed occasionally in response to a command from the system operator or due to some unexpected events like equipment faults and short circuits. From the power system point of view, any such change can be classified as a disturbance because it upsets the state of equilibrium to a greater or lesser degree. As soon as the equilibrium is lost, the generators' rotors start to accelerate or decelerate depending on the unbalance that exists between the input mechanical torque and the output electromagnetic torque. An adjustment of generation follows any

such change to restore the balance and attain a new state of equilibrium. Therefore, the operation of the power system can be described as a sequence of incessant adjustments aimed at attaining a new equilibrium point. The dynamical behaviour of the generator's rotor in response to various disturbances will be different and is highly dependent on the initial operating condition of the machines and the severity of the disturbance.

The motion of the rotor of a synchronous machine is described by the mechanical laws for rotating bodies (1.1).

$$J\frac{\mathrm{d}^2\theta_\mathrm{m}}{\mathrm{d}t^2} = T_\mathrm{m} - T_\mathrm{e} = T_\mathrm{a}, \tag{1.1}$$

where:

J – the total moment of inertia of the rotor masses, kg · m^2;
θ_m – the angular displacement of the rotor with respect to the stationary axis, rad. mechanical;
t – time, s;
T_a – net accelerating torque, N · m;
T_m – mechanical torque from the prime mover corrected for rotational losses, N · m;
T_e – electromagnetic torque corrected for electrical losses, N · m.

The angular displacement of rotor δ_m with respect to the reference axis, which rotates at a constant synchronous speed, $\omega_{0\mathrm{m}}$, is:

$$\delta_\mathrm{m} = \theta_\mathrm{m} - \omega_{0\mathrm{m}}t. \tag{1.2}$$

Then

$$\frac{\mathrm{d}\delta_\mathrm{m}}{\mathrm{d}t} = \frac{\mathrm{d}\theta_\mathrm{m}}{\mathrm{d}t} - \omega_{0\mathrm{m}}; \tag{1.3}$$

$$\frac{\mathrm{d}^2\delta_\mathrm{m}}{\mathrm{d}t^2} = \frac{\mathrm{d}^2\theta_\mathrm{m}}{\mathrm{d}t^2}, \tag{1.4}$$

where $\mathrm{d}\delta_\mathrm{m}/\mathrm{d}t$ is the deviation of the rotor speed from the synchronous speed, rad. mechanical / s.

Then, by substituting (1.4) in (1.1):

$$J\frac{\mathrm{d}^2\delta_\mathrm{m}}{\mathrm{d}t^2} = T_\mathrm{m} - T_\mathrm{e} = T_\mathrm{a}. \tag{1.5}$$

Let us define the angular velocity of the rotor, ω_m, in mechanical radians per second:

$$\omega_\mathrm{m} = \frac{\mathrm{d}\theta_\mathrm{m}}{\mathrm{d}t}. \tag{1.6}$$

By multiplying (1.5) by (1.6) we get

$$J\omega_\mathrm{m}\frac{\mathrm{d}^2\delta_\mathrm{m}}{\mathrm{d}t^2} = T_\mathrm{m}\omega_\mathrm{m} - T_\mathrm{e}\omega_\mathrm{m} = T_\mathrm{a}\omega_\mathrm{m}. \tag{1.7}$$

In a rotational system, power is a product of torque and angular velocity. Then

$$J\omega_m \frac{d^2 \delta_m}{dt^2} = P_m - P_e = P_a. \tag{1.8}$$

The quantity $J\omega_m$ is the angular momentum of the rotor. For the steady-state condition $\omega_m \approx \omega_{0m}$ and angular momentum at synchronous speed, $J\omega_{0m}$, is known as the generator's inertia constant M. Mechanical radians are related with electrical radians through the number of poles of the machine, p:

$$\omega_0 = \omega_{0m} \frac{p}{2};\ \delta = \delta_m \frac{p}{2}. \tag{1.9}$$

Then (1.8) can be rewritten as follows:

$$M \frac{d^2 \delta}{dt^2} = P_m - P_e = P_a, \tag{1.10}$$

where:

M – angular momentum (inertia constant);
δ – rotor angle deviation with respect to a synchronously rotating axis;
P_m – mechanical power input corrected for mechanical losses;
P_e – electrical power output corrected for electrical losses;
P_a – accelerating power.

Equation (1.10) is known as the "swing equation" of the synchronous generator. The angular momentum of a machine is often represented in the form of the value of its stored kinetic energy at rated speed. This constant is known as the H-constant and is typically given in the machine data:

$$H = \frac{stored\,energy, \text{MJ}}{machine\,rating, \text{MVA}};$$

$$H = \frac{1}{2} \frac{M\omega_0}{S_R}, \tag{1.11}$$

where H is expressed in MJ/MVA and S_R is the genrator's rated power in MVA.

The inertia constant H states how much time it would take to bring the machine from synchronous speed to a standstill if the machine is loaded at rated power but no mechanical power is fed into it. When dividing both sides of (1.10) by machine rated power S_R, the swing equation can be rewritten in per-unit notation:

$$\frac{2H}{\omega_0} \frac{d^2 \delta}{dt^2} = P_m - P_e = P_a. \tag{1.12}$$

Equations (1.10) and (1.12) describe the motion of the generator's rotor in the presence of accelerating power, which can be positive (in this case, the rotor accelerates with respect to a synchronous reference) or negative (in this case, the rotor decelerates).

1.2. Small-disturbance stability

Rotor angle stability is roughly divided into small-disturbance stability and transient stability.

> Small-disturbance stability is the ability of generators to remain in synchronism after a small disturbance.

The disturbance is considered small if linearisation of system equations is permissible for the purposes of analysis [6]. Typically, after a small disturbance the system reaches the new equilibrium point within a short period of time and the new steady-state condition coincides with (or is close to) the pre-disturbed one. Examples of small disturbances are the minor fluctuation of load or generation, transformer tap changing, switching of VAR compensators, etc.

Equation (1.12) does not take into account the damping effect. Without positive damping, even a small disturbance results in undamped oscillations of the rotor. The damping effect is negligible in the steady-state condition but manifests itself when the rotor starts to oscillate. During an oscillation, the flux linkage of a machine is not invariant and the rate of change of the flux linkage produces an electrical damping force. Due to the rate of change of the rotor angle with respect to the armature flux, there will be an induced current in the rotor, which also produces a damping effect. The degree of damping is affected by the action of the automatic voltage regulator and the governor and also depends on the presence of damper windings. To account for the damping, the swing equation can be rewritten as follows:

$$\frac{2H}{\omega_0}\frac{\mathrm{d}^2\delta}{\mathrm{d}t^2} = P_\mathrm{m} - P_\mathrm{e} - D\frac{\mathrm{d}\delta}{\mathrm{d}t} = P_\mathrm{a}. \tag{1.13}$$

Consider the generator/infinite-bus system presented in Fig. 1.2. By neglecting the resistance and using the classical model of a synchronous generator, the electrical power output is as follows:

$$P_\mathrm{e} = \frac{E_1 E_2}{X'_\mathrm{d} + X_\mathrm{e}}\sin\delta = P_\mathrm{max}\sin\delta. \tag{1.14}$$

For a small disturbance, Equation (1.13) can be linearised near initial operating point a (Fig. 1.2) and, assuming that the mechanical power is constant ($\mathrm{d}P_\mathrm{m}/\mathrm{d}t = 0$), the swing equation will be as follows:

$$\frac{2H}{\omega_0}\frac{\mathrm{d}^2\Delta\delta}{\mathrm{d}t^2} = -K_\mathrm{s}\Delta\delta - \frac{K_\mathrm{d}}{\omega_0}\frac{\mathrm{d}\Delta\delta}{\mathrm{d}t}, \tag{1.15}$$

where:

$K_\mathrm{s} = \dfrac{\mathrm{d}P_\mathrm{e}}{\mathrm{d}\delta} = \dfrac{E_1 E_2}{X'_\mathrm{d} + X_\mathrm{e}}\cos\delta_0$ is the synchronising power coefficient;

K_d is the damping coefficient.

According to (1.15), the small-disturbance stability of the synchronous generator is dependent on both the synchronising power coefficient and the damping coefficient. Looking at Fig. 1.2, it can be seen that synchronising power is positive at the rising slope of the power-angle curve ($-\pi/2 \le \delta \le \pi/2$) and becomes negative as soon as point b is crossed. In order not to lose stability after a small transient, the generator's operating point should reside on the left part of the power-angle curve, that is, where $K_s > 0$.

The effect of positive and negative damping coefficients is shown in Fig. 1.3.

For a system to remain stable, both the synchronising power and the damping coefficients should be positive. Insufficient synchronising torque may lead to the angular difference between machines increasing aperiodically. Further, a deficient damping torque may lead to rotor angle oscillations with an increasing amplitude.

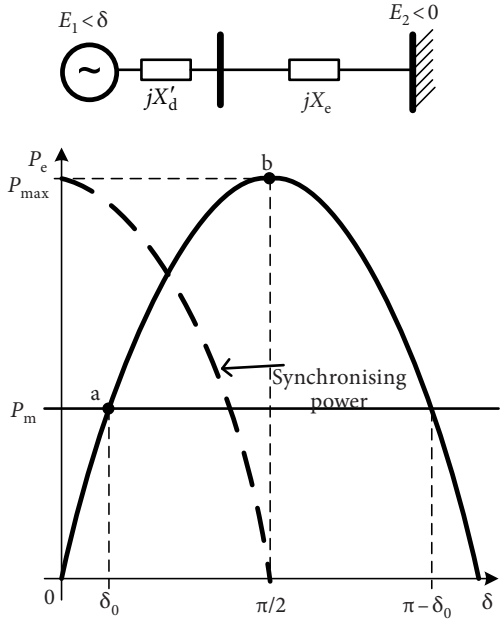

Fig. 1.2. The power transfer curve of the generator/infinite-bus system

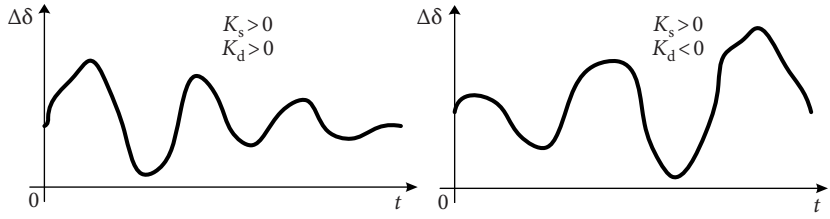

Fig. 1.3. Angle responses for positive and negative damping

1.3. Transient stability

Large-disturbance rotor angle stability or transient stability has to do with the ability of the power system to maintain synchronism when subjected to a severe disturbance, such as a short circuit on a transmission line [6]. The system's response to a large disturbance is characterised by large excursions of the generator rotor angle, which exhibit a nonlinear power-angle relationship. Severe disturbances often result in aperiodic angular separation without the rotors of the machines swinging back after the initial disturbance. This type of instability is known as first-swing instability. Because of the highly nonlinear behaviour, it is difficult to obtain pure analytical solutions to the system equations, and the graphical method, also known as the equal area criterion (EAC), is often used to determine whether the system will lose stability after a disturbance or not. The mathematical justification of the EAC as it has been derived in [7] is presented below. Equation (1.13) can be rewritten as follows:

$$M\frac{\mathrm{d}\delta^2}{\mathrm{d}t^2} = P_\mathrm{a} = P_\mathrm{m} - P_\mathrm{e} - D\frac{\mathrm{d}\delta}{\mathrm{d}t}. \tag{1.16}$$

The effect of damping has a little impact during the first swing of the generator rotor and can thus be neglected. Due to the relatively slow response of the generator's governor, the mechanical input power P_m is assumed to be constant during a short period of time (1 to 3 s). Multiplication of (1.16) by $2\mathrm{d}\delta / M\mathrm{d}t$ and rearrangement provide the following:

$$2\frac{\mathrm{d}\delta^2}{\mathrm{d}t^2}\frac{\mathrm{d}\delta}{\mathrm{d}t} = 2\frac{P_a}{M}\frac{\mathrm{d}\delta}{\mathrm{d}t}; \tag{1.17}$$

$$\frac{\mathrm{d}}{\mathrm{d}t}\left[\left(\frac{\mathrm{d}\delta}{\mathrm{d}t}\right)^2\right] = 2\frac{P_\mathrm{a}}{M}\frac{\mathrm{d}\delta}{\mathrm{d}t}. \tag{1.18}$$

After multiplying (1.18) by $\mathrm{d}t$ and integrating, we obtain the following:

$$\left(\frac{\mathrm{d}\delta}{\mathrm{d}t}\right)^2 = \frac{2}{M}\int_{\delta_0}^{\delta} P_\mathrm{a}\,\mathrm{d}\delta. \tag{1.19}$$

If the generator does not lose stability after a disturbance, then a new equilibrium point will be achieved, for which the generator's speed with respect to the infinite bus is zero:

$$\frac{\mathrm{d}\delta}{\mathrm{d}t} = \sqrt{\frac{2}{M}\int_{\delta_0}^{\delta} P_\mathrm{a}\,\mathrm{d}\delta} = 0; \tag{1.20}$$

$$\int_{\delta_0}^{\delta_m} P_\mathrm{a}\,\mathrm{d}\delta = 0. \tag{1.21}$$

Equation (1.21) is a criterion of generator stability, which can be represented graphically as shown in Fig. 1.4. Consider generator G supplying

power to the infinite bus through the two transmission lines. Assuming that the network consists only of reactances, the power-angle curves take the form of an undisplaced sinusoid. Different states of the network will be described with three different power-angle curves: curve 1 corresponds to the initial state at which both transmission lines are in operation; curve 2 corresponds to the state of fault (short circuit, SC) of one of the transmission lines; curve 3 corresponds to the post-fault state when the faulted line has been removed from operation and the power is supplied over the remaining healthy line.

At a steady state, the generator's operating point a is determined by the equilibrium between the input mechanical power fed to the generator and the output electrical power. At the moment when a short circuit occurs, the electrical power output decreases abruptly to point b. At point b, the input power exceeds the output power, and therefore, the input/output torque equilibrium is lost. An excess of input torque accelerates the rotor and the generator's operating point is moving along the power-angle "Fault" curve with the rotor angle increasing. At point c, the faulted line is removed from operation and the generator's output power jumps from point c to point d.

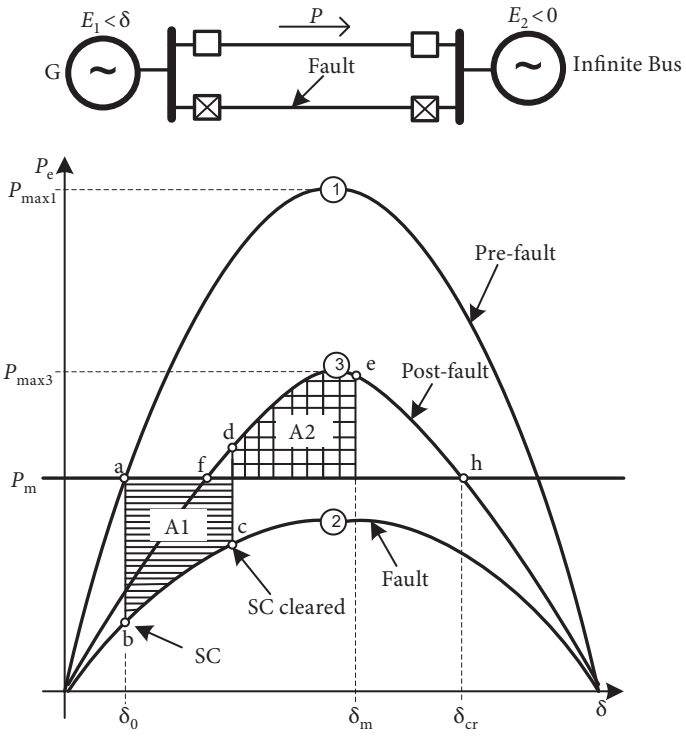

Fig. 1.4. The equal area criterion for stability

At point d, the generator's electrical torque exceeds the input torque, but the generator's speed is higher than the synchronous speed, and the generator's operating point is moving along the "Post-fault" curve with the rotor angle still increasing. While moving along the "Post-fault" curve, the excess of output power decelerates the generator's rotor and the relative speed of the rotor vanishes to zero at point e. At point e, the maximum angular excursion is reached and then the rotor angle starts to decrease due to an excess in decelerating torque. In the presence of positive damping, the rotor will reach a new point of equilibrium, f, after several oscillations.

The existence of point e on the power-angle curve is determined by the equality of two areas (Fig. 1.4): A1 = A2, where area A1 represents the energy that accelerates the rotor; and area A2 represents the energy that decelerates the rotor. In other words, the generator does not lose stability after a disturbance if the acceleration energy is counterbalanced by the deceleration energy. The last point on the power-angle curve for which this condition can be fulfilled, is the critical point h with the corresponding angle δ_{cr}. In case point h has been reached with the rotor speed above synchronous speed, the angle difference between the generator and the infinite bus will increase infinitely and the synchronism will be lost. The condition for which the angle difference exceeds 180 degrees is often referred to as the generator pole slip. Typically, after exhibiting pole slipping, the generator loses stability and goes out of step (OOS) with respect to the rest of the system.

The EAC principle can be used to assess the stability of the one-machine infinite-bus (OMIB) system and can also be applied to those configurations that could be adequately transformed into an OMIB system.

Transient stability depends on both the initial operating point of the machines and the severity and location of the fault [6]. The time frame of interest in the first-swing stability study typically lies within 0.5 s to 2 s, but this time may be prolonged significantly when large interconnected systems are concerned. The reason for this lies in the very complex nature of interactions produced by different parts of the system in response to the local disturbance. In some remote parts of the system, the effect of the disturbance may be felt with some lag, thus complicating the overall analysis. In some cases, part of the system generators remain stable immediately after the disturbance but may lose stability as a result of a power mismatch in other parts of the system. It is often the case when the initial disturbance, which causes the power swings in one part of the system, causes other disturbances in neighbouring areas. Therefore, the angular stability problem should be considered in all its diversity, accounting for the unpredictability of contingency scenarios.

1.4. Out-of-step condition characteristics

Large power system disturbances can eventually lead to loss of synchronism between the generator and the system or between groups of machines operating in different parts of the large interconnected system. Angular instability is manifested as aperiodic angular separation among different generation sources. A typical example of generators' angle variation after loss of synchronism is presented in Fig. 1.5.

The angular difference between generator G1 and the remaining machines increases infinitely, thus evidencing that the synchronism has been lost. Generator G4 slips the pole but eventually settles down and remains in synchronism. Massive power swings along the lines interconnecting asynchronously rotating generation sources can be observed during the OOS condition. Power swings are three-phase symmetrical phenomena, which result from generators' internal voltage vectors rotating at different speeds. The currents along the lines and the voltages at the system buses oscillate with a frequency equal to the generators' speed difference (Fig. 1.6). When the difference of the generators' phase angles passes through the value of 180 degrees, the values of the currents reach their maximum and at the same time the voltage drops to its minimum. At its maximum, the current may exceed the rated value several times and the voltage at some system buses may drop to zero.

There is a whole list of various problems related with the OOS condition. During unstable power swings, the power fluctuations follow the current and voltage waveforms and thus power supply to the load will be interrupted. Unexpected rejection of load may occur for several network buses

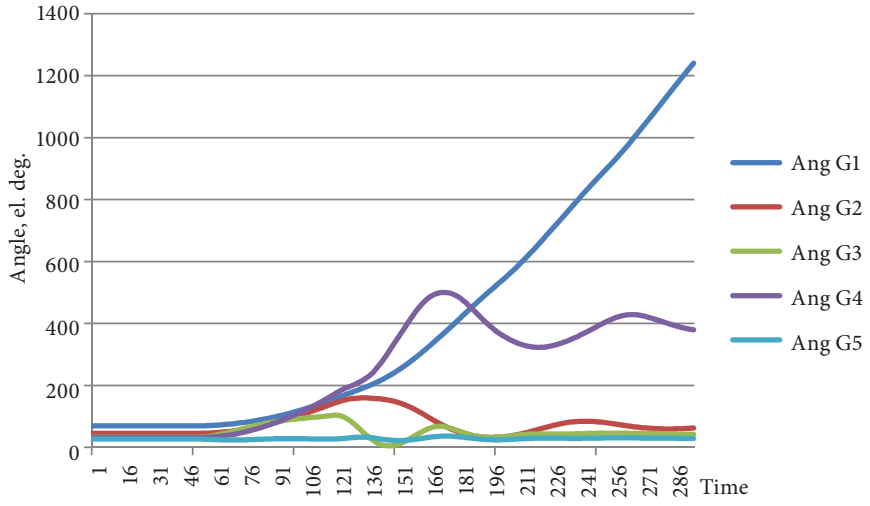

Fig. 1.5. Generators' rotor angle deviation after disturbance

in response to a voltage drop. Pole slipping is an unacceptable condition for generators because of the serious mechanical stress produced on the generator shaft, which may lead to physical damage to the turbine-generator set. Line tripping during power swings may become problematic due to the presence of a large transient recovery voltage across the circuit breaker contacts when the voltage sources are out of phase. Some types of relays may incorrectly respond to current and voltage swings and may superfluously trip the respective lines. As a result of such misinterpretation, the power balance, which is already troubled, will worsen further. Cascaded tripping of lines may lead to uncontrolled splitting of the network into highly unbalanced islands with unpredictable consequences. Thereby, the OOS condition, if not addressed adequately, may represent a significant risk to system integrity and, in the worst-case scenario, may lead to widespread outages and blackouts.

To avoid the above problems, it is imperative that the network areas operating asynchronously be separated as soon as the OOS condition has been detected. The power network should be separated in such locations as to maintain the best possible load-generation balance in each of the separated areas. The main goal of such controlled splitting is an attempt to preserve independent operation of the islands, thus providing the power supply to the customers while the quality and quantity of service may be reduced.

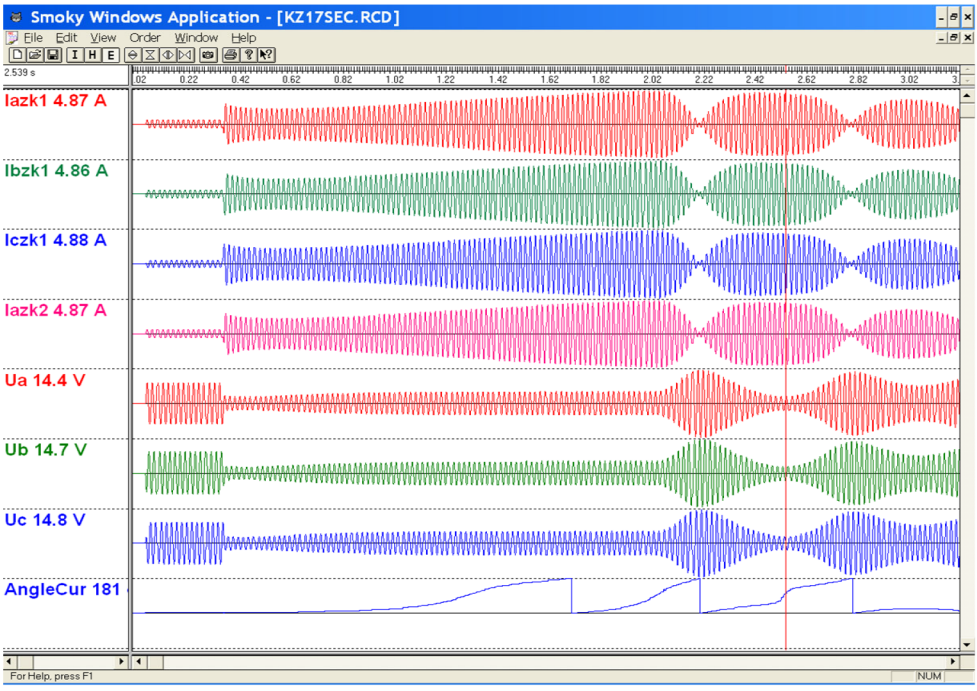

Fig. 1.6. Voltage and current waveforms during OOS condition (secondary values)

1.5. OOS protection tasks

The response of the power network operator may be too slow and even inconsistent in the case of a fast-evolving emergency, and therefore automated action should be taken to reach the goal. These automated actions are assigned to a protection system of a special type – the OOS protection system. Thereby, OOS protection should be capable of accomplishing the following tasks:

1. Reliable detection of the OOS condition, preferably at the very onset of the OOS condition.
2. Detection of the generator or group of generators which operates asynchronously with respect to the remaining system or with respect to one another.
3. Determination of the locations in the network which allow separating asynchronously rotating parts of the system.
4. Among all possible splitting decisions, selection of the one which provides the best-balanced islands after network-splitting.
5. Sending control signals to the appropriate circuit breakers to accomplish network separation.
6. The highest possible degree of security and dependability should be provided in the presence of various abnormal conditions in the power system.

2. OOS PROTECTION. LOCAL-MEASUREMENT-BASED APPROACH

2.1. Impedance-measurement-based OOS protection

The power swings observed in the network during generator rotor pole slip result in voltage and current amplitude and phase oscillations. These oscillations will lead to corresponding oscillations of the measured impedance. An impedance-calculation-based distance relay will see the impedance locus changes on the complex impedance plane, and this indication can be used for power swing detection. The distance relay measures voltage on bus V_s and current through the line of interest, I (Fig. 2.1), calculates the impedance and checks if the calculated impedance falls within protection *zone1…zone3*. For any time moment, the complex impedance Z_d seen by the relay is expressed by (2.1).

$$Z_d = \frac{\dot{V}_s}{\dot{I}} = \frac{\dot{E}_s - \dot{I}Z_s}{\dot{I}} = \frac{\dot{E}_s}{\dot{I}} - Z_s; \dot{I} = \frac{\dot{E}_s - \dot{E}_r}{Z_\Sigma}; Z_d = Z_\Sigma \frac{\dot{E}_s}{\dot{E}_s - \dot{E}_r} - Z_s, \quad (2.1)$$

where $Z_\Sigma = Z_s + Z_{line} + Z_r$ is the total complex impedance of the system.

Let $K = \left|\frac{E_s}{E_r}\right|$ and δ be the angle between the sending-side (E_s) and receiving-side (E_r) emf vectors, then:

$$Z_d = Z_\Sigma \frac{KE_r e^{j\delta}}{KE_r e^{j\delta} - E_r} - Z_s = Z_\Sigma \frac{Ke^{j\delta}}{Ke^{j\delta} - 1} - Z_s. \quad (2.2)$$

According to (2.2), the impedance seen by the relay is a function of the angle between the generation sources (assuming K is near-constant), and when angle δ changes, the impedance locus will travel from the right to the left (if the sending-side machine accelerates with respect to the receiving-side machine) or from the left to the right (if the sending-side machine decelerates with respect to the receiving-side machine).

When the amplitudes of the emfs of both machines are equal ($K = 1$), the impedance locus crosses the straight line of Z_Σ at the point of the electrical swing centre (SC). For $K > 1$ or $K < 1$, the impedance locus travels along the circular arcs and crosses the line when the angle reaches 180°.

If impedance falls within the distance protection operating characteristics during the power swing, then tripping of the transmission line is possible and special care should be taken to avoid such undesired operation. The distance relay should be able to distinguish a stable power-swing condition from an unstable one and should not trip the line when a stable power swing occurs. Inability to discriminate between the two may lead to uncontrolled tripping of several lines at random places of the network, which may lead to system disruption. On the other hand, in case of severe swings, and

especially OOS, operation of protection can be desirable if the transmission line corresponds to the network-splitting scenario.

To achieve both goals simultaneously, two functions are implemented within distance relays:

- The power-swing blocking (PSB, ANSI No. 68) function is intended to block tripping of the distance relay at a stable power-swing condition.
- The OOS tripping (OST, ANSI No. 78) function is intended to trip the controlled line if an OOS condition has been detected.

Both functions are based on impedance measurements and both use similar approaches in power swing detection logic. The main criterion that allows discriminating power swings from all the other conditions (short circuits, bulk power transfer) is the way impedance changes during power swings. Power swings are electromechanical phenomena and the rate of impedance change is relatively slow due to the large inertia of generators. Generators' rotor angles cannot change abruptly, and this translates into smooth variations in the impedance measured by the protection. This is in contrast with the short-circuit condition when the impedance "jumps" instantly from the pre-fault point (*load*) to the new, fault-specific point (*fault*) in the complex plane (Fig. 2.2).

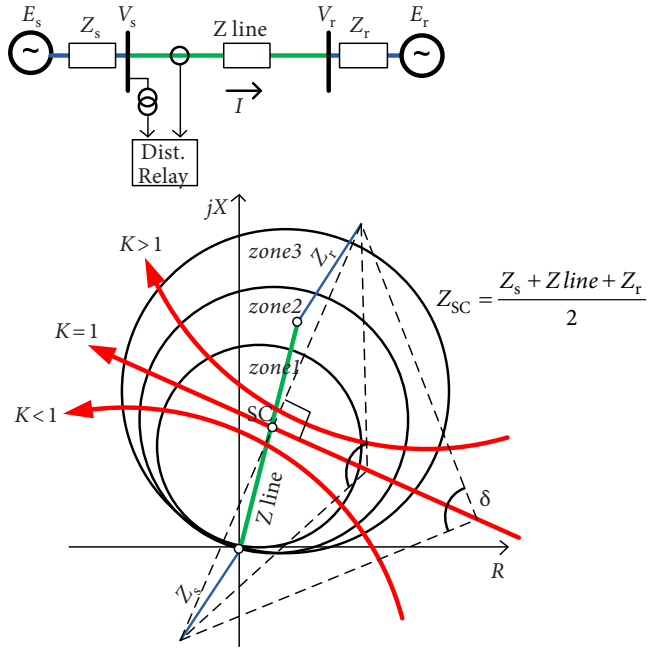

Fig. 2.1. Power swing impedance locus as seen by relay

Two methods are typically implemented to control the rate of change of impedance: the concentric characteristic and the blinder-based characteristic (Fig. 2.2 a), b)). The concentric characteristic outlines the last active zone of protection at a distance of ΔZ. As soon as the impedance locus crosses the outer characteristic, the internal countdown timer is started and if the timer expires upon entering the active protection zone, a power swing condition is declared. In a blinder-based scheme the same principle is implemented except that two blinders (the inner one and the outer one) are used at both sides of the active zone instead of the concentric characteristic. Some manufacturers allow additional shaping of the concentric characteristics using blinders.

OOS is a symmetrical condition and thus, independent positive-sequence impedance calculation for each phase allows additional logic to be implemented for power swing detection and PSB. Considerable efforts are being taken by relay designers to ensure disconnection of the faulty element even if the fault is superimposed on power swings. Because of the possible differences in the particular implementation of PSB and OST functions, the following discussion will concern solely the OST functionality. A brief overview of the OST function as implemented by different manufacturers is presented below.

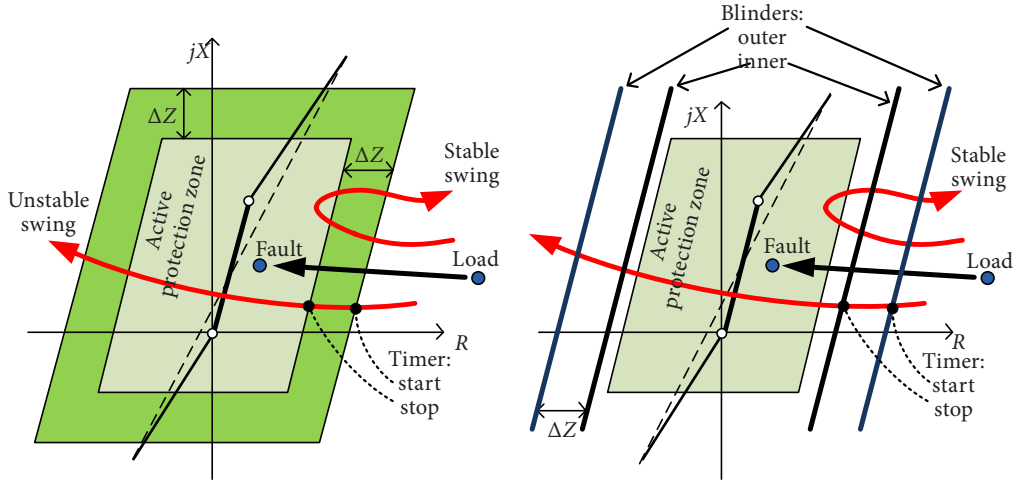

a) concentric characteristic **b)** blinder-based characteristic

Fig. 2.2. Power swing detection

The **SIEMENS 7SA522xx** distance protection terminal implements the concentric characteristic principle but without dedicated timer settings. Instead, continuous impedance calculation is used and then a special algorithm is implemented to ensure smooth transition of the swing impedance in the complex plane (Fig. 2.3) [8]. The impedance trajectory is continuously monitored, and the power swings are detected only if three conditions are fulfilled:

- Monotony of impedance trajectory: between two subsequent impedance calculations, only one parameter (ΔX or ΔR) may change sign.
- Continuity of impedance trajectory: the impedance variation between two subsequent samples (ΔX and ΔR) should exceed a minimum threshold to ensure that the impedance is not stationary.
- Smoothness of impedance trajectory: the ratio of impedance variation between two subsequent samples

$$\left|\frac{\Delta X_n}{\Delta X_{n+1}}\right| < thr; \left|\frac{\Delta R_n}{\Delta R_{n+1}}\right| < thr$$

should be less than a maximum threshold to ensure that the impedance does not change abruptly.

If all the three conditions are met and the impedance enters the swing detection polygon, then a power swing is declared. To differentiate between stable and unstable swing, the protection checks the sign of R upon the entrance and exit of the swing pickup polygon. If the sign of R remains the same, then a stable swing is declared [8]. When the impedance locus crosses the polygon at point 1 (crossing the transmission line impedance characteristic), an alarm signal is generated, announcing that the swing is unstable. A line tripping command is issued as soon as point 2 is crossed.

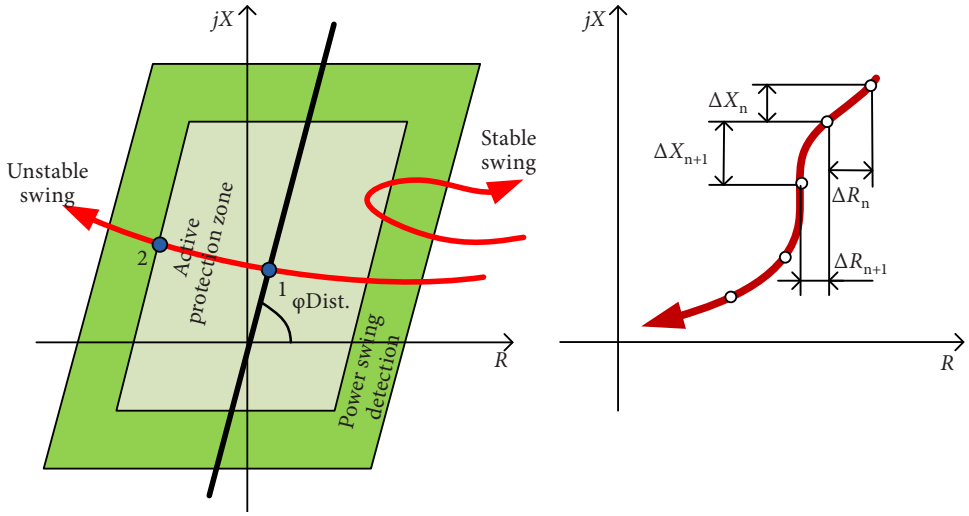

Fig. 2.3. Detection of stable and unstable power swing by SIEMENS 7SA522

The **ABB REL 670** distance protection terminal implements two independent concentric characteristics (inner and outer) for power swing detection. If the impedance transit timing between the inner and the outer polygon exceeds the maximum time setting, then a power swing is declared. Depending on the place of terminal installation, two applications are considered: generator pole slip protection (Fig. 2.4) and transmission line application. The difference lies only in the impedance values in the forward (ZA) and reverse (ZB) directions as viewed from the protection installation place. Impedance *ZA* is the sum of transformer impedance X_t and the system's equivalent impedance Z_s. Impedance ZB is equal to transient reactance X'_d of the generator (Fig. 2.4) [9]. Impedance *ZC* in this case should be equal to X_t and is the borderline between protection *zone1* and *zone2*. Power swing detection uses a concentric-characteristic and timer-based approach, whereas the OST function uses an angle-based approach. An alarm signal is generated as soon as the power swings have been detected and the *StartAngle* has been exceeded (Fig. 2.4). When the apparent impedance crosses the ZA–ZB line, the direction of impedance locus movement is checked and, if it remains the same as at the beginning, then a trip command will be issued as soon as the *TripAngle* threshold is reached. The number of pole slips before a trip command is generated is a variable and can be set independently for *zone1* and *zone2*. This feature is intended to provide some degree of OST selectivity if several OST protection terminals are installed on neighbouring lines.

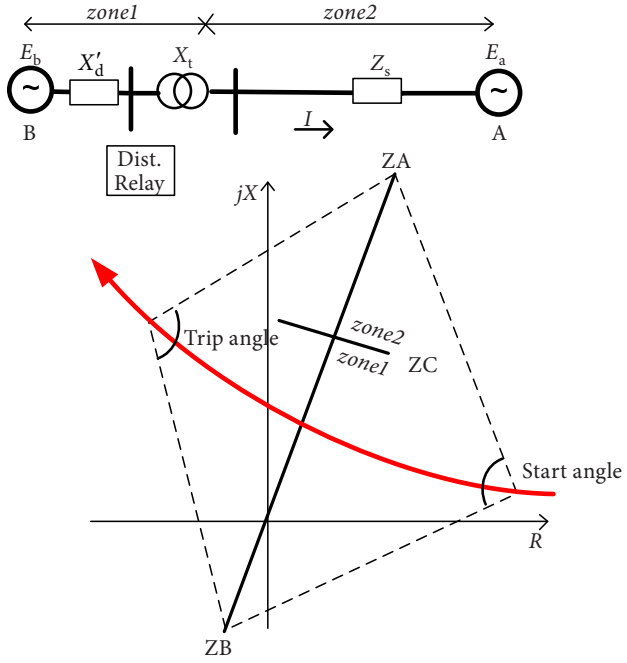

Fig. 2.4. Generator pole slip protection as implemented in REL 670 series relays

The **General Electric D60** line distance protection measures the positive-sequence apparent impedance and traces its locus with respect to either two or three user-selectable operating characteristic boundaries: the inner, middle and outer one (Fig. 2.5 a)).

The presence of impedance within each particular polygon is time-graded and the appropriate latch is triggered if the impedance stays within the zone longer than the timer pre-set. Depending on the number of characteristics chosen, the OST function operates as follows for three-step and two-step power swing detection modes [10]:

- Three-step operation. The trip sequence identifies unstable power swings by determining if the impedance locus spends a finite time between the outer and middle zones and then a finite time between the middle and inner zones. After the outer zone timer has timed out, latch 1 is set. If afterwards, at any time, the locus enters the middle zone but stays outside the inner zone for a period of time defined by the middle zone timer, latch 2 is set. If afterwards the locus enters the inner zone and stays there for a period of time defined by the inner zone timer, the OOS element is ready to trip.
  If the "Early" trip mode is selected, the power swing trip operand is set immediately. If the "Delayed" trip mode is selected, the element waits until the impedance locus leaves the inner characteristic, then times out for the middle zone timer and sets latch 4 – the element is now ready to trip. The trip operand is set later, when the impedance locus leaves the outer characteristic [10].

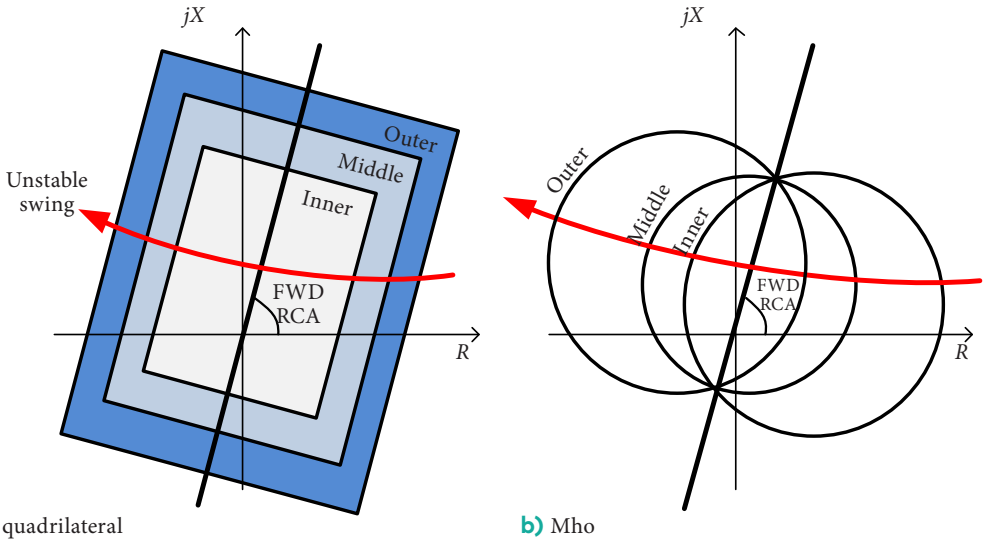

a) quadrilateral **b)** Mho

Fig. 2.5. Power swing detection characteristic

- The two-step operation principle is similar to the three-step mode except that the middle-zone logic is skipped.
  The power swing detection element can be set to use either lens (Mho) or rectangular (quadrilateral) characteristics (Fig. 2.5). A set of left and right blinders can be additionally applied to the "Mho" type of characteristic.

Similar approaches in OOS detection (with some minor variations) are used by MiCOM P44 series distance relays and the Toshiba GRZ 100 distance relay [11], [12].

2.2. Difficulties with impedance-based OST function

Two main requirements should be fulfilled when classical concentric characteristic and blinder schemes are used:

- The impedance setting of the inner power swing detection element should be placed outside the active protection zone. This ensures reliable PSB before the impedance enters the active zone.
- The outer element should be placed away from the load region to ensure absence of PSB under a heavy-load condition.

These requirements unavoidably lead to the shrinking of the power swing detection area with the appropriate timer settings becoming too small. The situation even worsens in cases when load encroachment needs to be used to guarantee correct functioning of the protection at heavy power transfer conditions. Thus, the choice of optimal settings for the power swing detection function becomes a non-trivial task and extensive stabilities studies are needed to identify the fastest possible rate of change of impedance. The continuous impedance calculation method (Fig. 2.3) seems to be free from these deficiencies because the impedance trajectory is continuously monitored and the impedance trace is time-graded by the impedance sampling rate of the device.

Some other important impedance-related considerations should be taken into account when choosing OST settings. While the line impedance is known, the system's equivalent impedances in forward and backward directions from the place of relay installation are not well defined. System impedance may vary significantly depending on the network configuration, the generation capacities currently in use and the network operating regime. When referring to Fig. 2.4 and if OST is used to split the network, uncertainty may appear in the *StartAngle* and the *TripAngle* because of the variation of the system impedances over time.

Another system-impedance-related issue that may affect the performances of OOS protection is the ratio between the line impedance and the

system's source impedance. If the line impedance is large compared with the system impedance, then the power swing centre is likely to be located within the limits of the line. If the system impedances are much larger than the line impedance, the swing centre will be located somewhere outside the protected line zones. If the system sources are interconnected by means of several lines in series, the problem of OST function coordination (selectivity) between the line protection terminals becomes very significant. Overlapping of different relay zones may lead to uncontrolled and random tripping if the OST functions are not properly coordinated. Here, the flexibility of OST settings for *zone1* and *zone2* implemented in REL 670 may provide the solution (Fig. 2.4). Still, the problem of an optimal

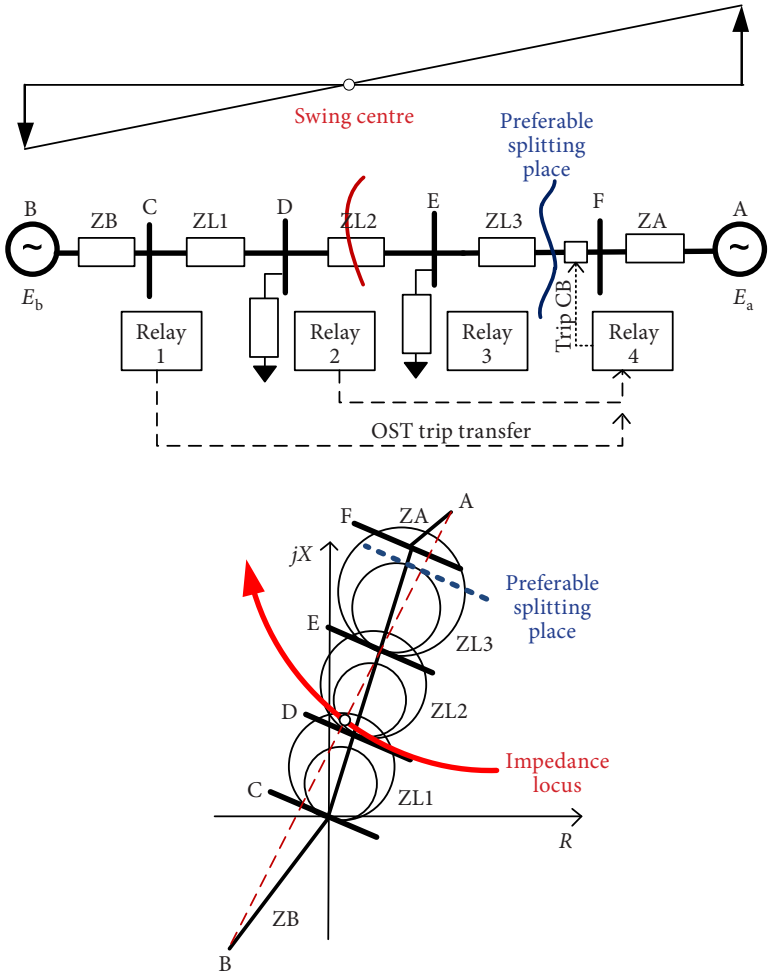

Fig. 2.6. Relay coordination using OST command transfer

network-splitting solution remains unanswered. The optimal relay location for OOS detection will be the one that is close to the system's electrical centre. However, because of the voltage drop at the swing centre point, the performance of the impedance calculation may be violated. Additionally, splitting the network near the swing centre does not always provide the best solution in terms of generation/load balance. The preferred splitting place depends on the actual dynamic behaviour of the system, which can hardly be assessed online by a distance relay. The simplest and most straightforward approach is to split the network in a pre-defined place, taking into account the acceptable generation/load balance after splitting. This can be accomplished by using OST signal transfer from the relays that sense the power swings (*Relay1* and *Relay2*) to the splitting point located at *Relay4* (Fig. 2.6). This approach prevents unwanted tripping of lines in a random order. Also, the post-fault network configuration will be known in this case while it may not be optimal.

If more than one power transfer path exists between sources within the network (which usually is the case), then a set of lines should be tripped to split asynchronously rotating parts. The choice of the network cutset points becomes a complex task, which, once again, assumes that extensive stability studies should be carried out for the network. Concluding about distance-relay-based OOS protection, the best outcome that could be achieved is avoiding the random tripping of lines and splitting the network at pre-defined cutset points. The main advantage of distance-relay-based OOS protection is that the OST function is an integral part of the line distance relay and is thus readily available on every transmission line. This ensures that power swings will always be detected wherever they appear in the complex network (supposing that the generator-transformer zone can also be covered by a dedicated distance relay).

2.3. Line differential protection with OST function

Toshiba line differential protection terminal GRL 100B has an integrated OST function, which is based on positive-sequence voltage phase comparison between local and remote terminals. The OST function operates only if the OOS loci cross the protected line (Fig. 2.7) [13]. The voltage phase of remote terminal B is compared with the voltage phase of terminal A, and a trip signal is generated as soon as angle θ exceeds 180°. The main deficiency of such a principle is that OOS can be detected only if the power swing centre is located within the protected zone.

2.4. Swing centre voltage control method

One of the major disadvantages of distance relay-based OOS protection is the difficulty in estimating the proper value of settings. Extensive stability studies need to be made to determine the optimal settings and even then there is no absolute guarantee that the real-life contingency exactly matches one of the simulated scenarios. The swing centre voltage (SCV) control method is attractive because the quantities used by the method do not depend on the system impedances, power transfer, generation/load capacities or any other system parameters. The SCV method has been described in several publications, and a detailed description of the OST function based on the SCV method has been provided in [14]. The essence of the method is explained by using a two-source network, which is presented in Fig. 2.8. When the emf vectors at the sending end, E_s, and at the receiving end, E_r, are completely out of phase (180°), then the voltage at the electrical swing centre, SCV, decreases to zero. For any angle between two voltage vectors, the instant value of SCV can be represented as a sine wave of the average frequency $(\omega + 1/2\,\mathrm{d}\delta/\mathrm{d}t)$, which is amplitude-modulated by the cosine wave of the two machines' slip frequency (2.3), [14].

$$SCV(t) = \sqrt{2}E \cdot \sin\left(\omega t + \frac{\delta(t)}{2}\right) \cdot \cos\left(\frac{\delta(t)}{2}\right). \tag{2.3}$$

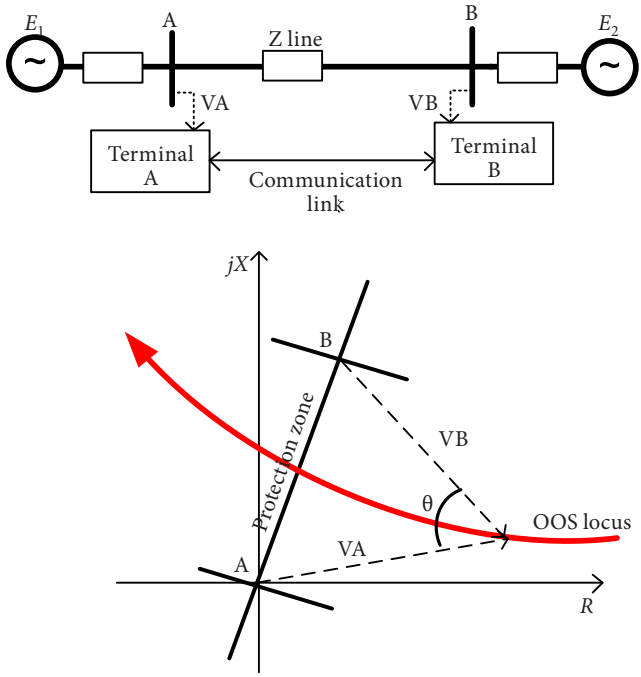

Fig. 2.7. OST function implemented within line differential protection terminals

Therefore, the SCV amplitude changes over time from its nominal value (at 0°) to zero value when the angle between the two machines reaches 180°. If we assume that the impedance angle θ is close to 90° for the entire system, then SCV can be approximated by using locally measured voltage *Vs* as follows:

$$SCV \approx |Vs| \cdot \cos\varphi. \tag{2.4}$$

This approximation may lead to significant errors in the SCV amplitude, considering a real network with lines and systems that have different impedance angles. However, for the purpose of power swing detection, the SCV amplitude is not so important. What is of importance is the rate of change of the SCV amplitude $\left(\mathrm{d}(SCV)/\mathrm{d}t\right)$ because voltage and current swings are exactly the result of two generators' slip frequency $\left(\mathrm{d}\delta/\mathrm{d}t\right)$. Assuming that $E_s = E_r = E$, the SCV amplitude can be calculated as follows [14]:

$$SCV = E \cdot \cos\left(\frac{\delta}{2}\right), \tag{2.5}$$

and then the SCV rate of change is as follows:

$$\frac{\mathrm{d}(SCV)}{\mathrm{d}t} = -\frac{E}{2} \cdot \sin\left(\frac{\delta}{2}\right)\frac{\mathrm{d}\delta}{\mathrm{d}t}. \tag{2.6}$$

The SCV rate of change is zero when two machines' voltage vectors are in phase and attains its maximum value when the angle between the machines reaches 180°. This method can be successfully implemented for

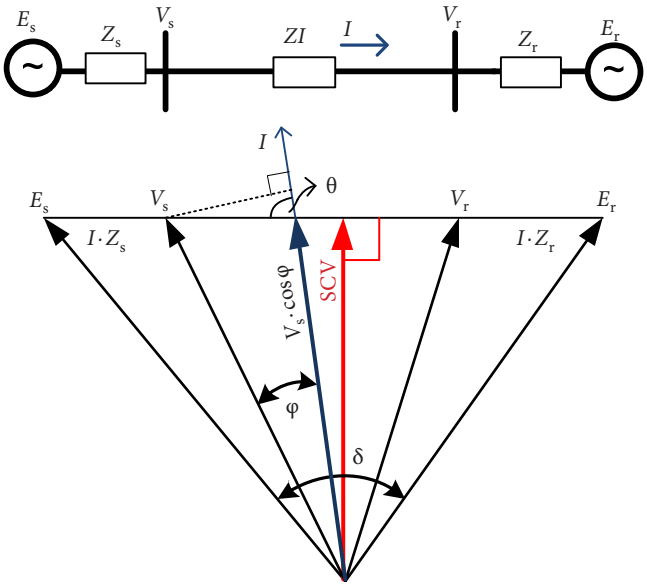

Fig. 2.8. SCV approximation: $V \cdot \cos\varphi$ is a projection of local voltage V_s onto local current I

PSB as well as the OST function with additional care to be taken to avoid possible discontinuities in $\mathrm{d}(SCV)/\mathrm{d}t$. OST function implementation algorithms as well as the method validation results are provided in [14].

2.5. Control of the angle between two modelled voltage vectors

This method is based on the estimation of the angle between two modelled voltage vectors. The method is implemented by a dedicated OOS protection terminal, AGNA, and is widely used within the interconnected networks of the Baltic States. As a general rule, AGNA should be located in such way as to allow control of the most critical transmission lines with bulk power transfer. Historically, the place of splitting the Baltic States network was chosen along the boundaries of the networks of the Latvian, Estonian and Lithuanian transmission system operators (TSO). The reason for this is the relatively small number of transmission lines interconnecting different TSOs.

The entire power system should be represented by its two-machine equivalent network (Fig. 2.9), where $E_{1\Sigma}$, $E_{2\Sigma}$ are equivalent generator voltages and $Z_{1\Sigma}$, $Z_{2\Sigma}$ – equivalent impedances of the network. The AGNA

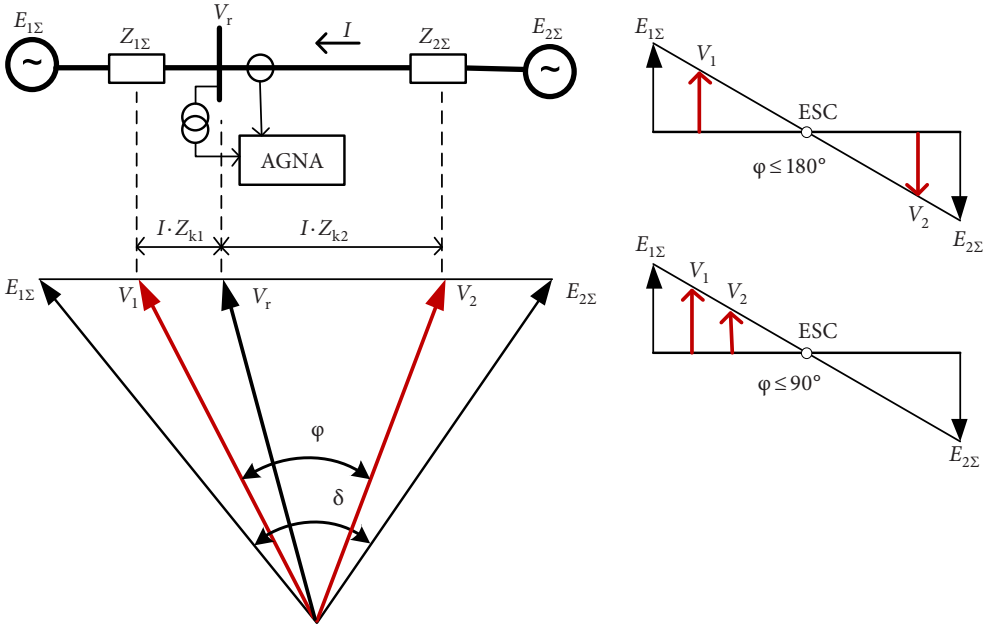

Fig. 2.9. The operating principle of OOS protection AGNA

terminal measures local voltage V_r and line current I and models vectors of two remote voltages V_1 and V_2 according to (2.7).

$$\dot{V}_1 = \dot{V}_r \pm \dot{I} \cdot \dot{Z}_{k1}; \dot{V}_2 = \dot{V}_r - \dot{I} \cdot \dot{Z}_{k2}, \tag{2.7}$$

where $\dot{Z}_{k1}, \dot{Z}_{k2}$ are equivalents of complex impedances, calculated in relation to the location point of AGNA.

AGNA estimates angle φ between two modelled voltage vectors V_1, V_2 as well as calculates the rate of change of the angle, $d\varphi/dt$ [15]. Depending on the location of the device in the network and the values of $\dot{Z}_{k1}, \dot{Z}_{k2}$, the ESC may reside inside or outside the remote voltages modelling zone (Fig. 2.9). Then angle φ will be able to reach 180° or 90°, respectively. A power swing condition is recognised as soon as a number of conditions are met:

- The network is balanced. The negative sequence values of voltage and current are used to detect any unbalanced condition of the network and to block device operation.
- The rate of change of the angle is within the allowed limits (which are determined by the settings) and the increase/decrease of the angle is continuous (the rotation of vectors V_1, V_2 does not change direction).
- The device is not blocked because of a symmetrical fault. A three-phase fault condition is detected using a logical conjunction of maximum allowed current, minimum allowed voltage and the $d\varphi/dt$ constraint (all the parameters are defined by settings).

If all the conditions are fulfilled, the device compares angle φ with the *tripAngle* setting and a line tripping command is issued as soon as the *tripAngle* value has been exceeded.

Two modes of AGNA operation are provided: the first mode – a trip before the generator slips pole ($\varphi < 180°$) (Fig. 2.10 a)) and the second mode – a trip after several (2…9) complete rotation cycles (Fig. 2.10 b)). The angle of vector V_2 is always measured in relation to stationary reference V_1.

In the first mode of operation, two trip angles are provided, each activating a dedicated output relay. If *trip* φ_1 has been exceeded, a signal is sent in an attempt to restore generation/load balance; if after that *trip* φ_2 is exceeded, then a trip line command is sent. If V_2 rotates clockwise with respect to V_1, the *trip* φ_3 angle becomes a trip command threshold. For each *trip* φ angle there are dedicated $d\varphi/dt$ settings associated with it, which define the angle rate of change constraints.

In the second mode of operation, the countdown internal *cycle Timer* starts as soon as the *trip* φ_1 angle has been exceeded (the *trip* φ_1 setting "works" in both rotation directions). When, after a complete rotation cycle, *trip* φ_1 is crossed again and *cycle Timer* has not expired, then *cycle Counter* increases by 1. When *cycle Counter* becomes equal with the *Number of*

cycles setting, the line tripping command is issued. An example of AGNA response to a simulated and replayed OOS scenario is shown in Fig. 2.11.

The main deficiency of the method used by AGNA lies in the necessity to obtain the network's equivalent impedances $\dot{Z}_{k1}, \dot{Z}_{k2}$, which are the settings of the AGNA device. Remote voltage modelling accuracy and,

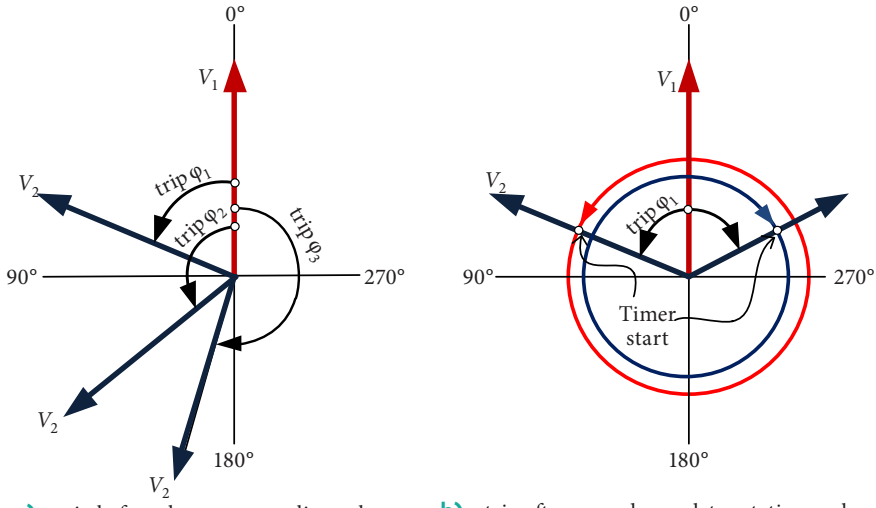

a) a trip before the generator slips pole **b)** a trip after several complete rotation cycles

Fig. 2.10. AGNA operating principle

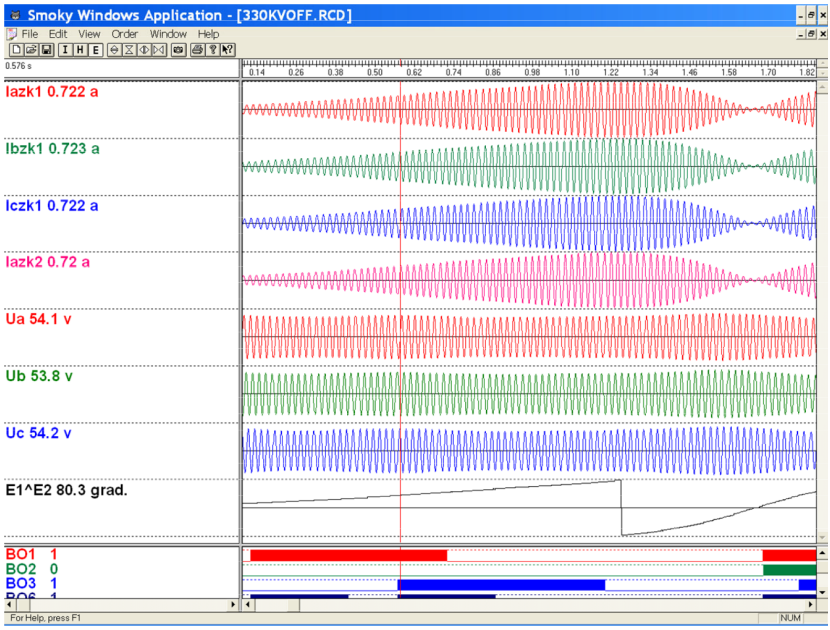

Fig. 2.11. AGNA trip command issued (BO3) at *trip* $\varphi_1 = 80$ el.deg.

consequently, angle calculation accuracy depends directly on the conformity between the device impedance settings and the impedances of the real network. Because of the volatility of the network parameters, the device setting should be chosen as a compromise between reliable detection of OOS in the worst-case scenario and a secured state of the relay for a maximum-load condition. The choice of the particular values of the settings should be confirmed by running stability studies for all the critical regimes of the network and for different network configurations.

To mitigate the uncertainties introduced by the impedance variation, an arrangement based on two terminals has been proposed in [16]. The idea is in placing the AGNA terminals closer (electrically) to the generation sources, thus allowing the equivalent source impedances to be less influenced by network configuration rearrangements and the volatility of the system's regime of operation. At the extreme, the terminals can be placed right at the power station's substation where the generators' currents can be directly measured (Fig. 2.12).

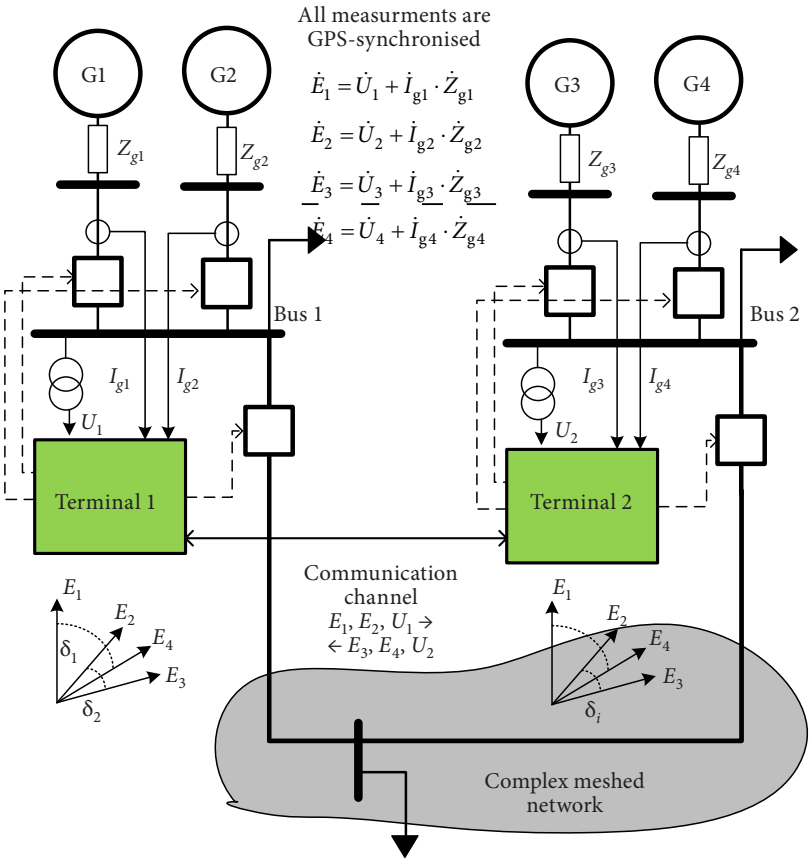

Fig. 2.12. The structure of a two-terminal-based OOS protection system

All the measurements should be GPS-synchronised. Each terminal is modelling the generators' emf vectors $\dot{E}_n$ according to the following:

$$\dot{E}_n = \dot{U}_n + \dot{I}_{gn} \cdot \dot{Z}_{gn}, \tag{2.8}$$

where $\dot{I}_{gn}$ and $\dot{Z}_{gn}$ stand for the generator current and the equivalent impedance of the n^{th} generation source and $\dot{U}_n$ is bus voltage.

Protection *Terminal 1* and *Terminal 2* exchange the modelled emf vectors by using a highspeed communication channel and each terminal calculates the angle difference δ_i between each pair of generators. The operation principle is similar to that of AGNA: the angle difference between any pair of generation sources is compared with the maximum angle settings. The angle differences can be sorted out in ascending order, and the most lagging/most leading source can be chosen as the one suspected to be tripped first. Additional provisions should be made for protection blocking algorithms. In contrast to a single AGNA terminal, blocking of any of the two terminals (if an unbalanced network condition has been detected) leads to blocking of the whole protection system. The advantages of the proposed protection structure are as follows:

- The emf vectors can be modelled with a higher accuracy due to the electrical proximity of the measurement point to the generation sources.
- For the same reason, rearrangements in a meshed network interconnecting generation sources do not degrade the performance of the protection.
- OOS-responsible machines can be detected online by using the most-lagging/most-leading angle principle, thus some degree of flexibility can be provided in choosing the network separation place.

Summarising the deficiencies and advantages of local-measurement-based OOS protection devices, several conclusions can be made.

Power swings represent a system-wide phenomenon with a significant amount of equipment involved and affect almost every measure of the system. Local OOS protection, in turn, uses only the quantities available at the device location point, which are assumed to be the local representation of the system-wide process. In the realm of limited observability, protection is able to successfully detect and correctly respond to unstable power swings only if the real process is similar to the one for which the device settings have been calculated. Because of the inherent variability of power system parameters, calculation of optimal settings becomes a non-trivial task. An extensive stability study is needed to derive and validate the device settings. But even then, we cannot be sure that all the possible scenarios have been anticipated and all the possible contingencies have been considered.

Another important objective which cannot be completely achieved is the choice of the optimal splitting place. The entire system dynamics need to be

considered to cope with the problem, which is not possible in the absence of system-wide information. If local protection is used, a typical approach is to pre-determine the network cutset points. While straightforward, this approach does not always provide an acceptable generation-load balance after network splitting. Some degree of device settings adaptation could be achieved by switching the active settings group depending of network operational regime and configuration. This option is typically externally driven and the number of available groups of settings is limited.

Among the advantages of local OOS protection, a number should be mentioned. Local OOS protection uses traditional approaches to relaying; it is straightforward and is based on well-established principles. Measurements are always available and there is no need for any additional information to take the decision. If the OST function is integrated within the line differential protection terminals, proven and reliable communication links are used. The power swing detection function is an integral part of the distance protection terminal and thus the OST function is readily available for each and every transmission line. Despite all the above deficiencies, the objective of network splitting can be achieved for the majority of the possible OOS scenarios.

3. WIDE-AREA MEASUREMENT SYSTEM

3.1. Phasor

For a steady-state condition of the power system, the voltage and current signals are considered pure sinusoidal waveforms of rated frequency:

$$x(t) = X_{\mathrm{m}} \cdot \cos(\omega t + \varphi), \tag{3.1}$$

where X_{m} – sinusoidal waveform magnitude;
$\omega = 2\pi f$, where f is instantaneous frequency;
φ – angular phase.

Sinusoid (3.1) may be represented by a complex number X, which is also known as the phasor representation:

$$X = \left(\frac{X_{\mathrm{m}}}{\sqrt{2}}\right) \cdot e^{j\varphi} = \left(\frac{X_{\mathrm{m}}}{\sqrt{2}}\right) \cdot (\cos\varphi + j\sin\varphi), \tag{3.2}$$

where $\left(\frac{X_{\mathrm{m}}}{\sqrt{2}}\right)$ is the root-mean-square (RMS) value of the input signal.

A *phasor* is a vector consisting of magnitude and phase angle that corresponds to a sinusoidal waveform at a given frequency. For a steady-state condition, the vector magnitude does not change, whereas the phase depends on the time moment when the signal is sampled. The phase is a relative quantity and two signals sampled at different locations can only be compared if they have been sampled simultaneously. This means that an absolute time stamp should be provided for signal sampling. A phasor that is referenced to an absolute time stamp is termed a *synchrophasor* and can be represented as follows:

$$\bar{X} = \frac{X_{\mathrm{m}}}{\sqrt{2}} \angle\varphi, \tag{3.3}$$

where φ is the instantaneous phase angle of the signal relative to a reference cosine function at nominal system frequency and synchronised to an absolute point in time which is provided by the Coordinated Universal Time (UTC) stamp. The measured angle should be in the range of $\pm\pi$. An alternative representation of a synchrophasor is possible with its orthogonal components:

$$\bar{X} = X_{\mathrm{r}} + jX_i. \tag{3.4}$$

The conventions of synchrophasor representation are explained in Fig. 3.1.

Phasor representation is valid only for a sinusoidal signal with a fixed frequency. The real signals in a power system often also contain components of higher frequencies in addition to those of the fundamental

frequency. It is necessary, in this case, to extract the signal of a single (fundamental) frequency component and then the phasor can be calculated. The classical algorithm for extracting a component of a particular frequency from a complex periodic signal consists in the Fourier transformation. In a digital domain, the input signals are represented by equally spaced samples. Then, the discrete Fourier transform (DFT) can be used to filter out the unnecessary components of the signal. Sinusoidal signal $x(t)$ of frequency f is represented with Fourier series (3.5):

$$x(t) = a \cdot \cos(2\pi ft) + b \cdot \sin(2\pi ft) = \sqrt{a^2 + b^2} \cdot \cos(2\pi ft + \varphi), \quad (3.5)$$

where $\varphi = \tan^{-1}\left(\frac{-b}{a}\right)$ and has a phasor representation:

$$\bar{X} = \sqrt{a^2 + b^2} \cdot e^{j\varphi} = a - jb. \quad (3.6)$$

The RMS value of the phasor is as follows:

$$\bar{X} = \frac{1}{\sqrt{2}}(a - jb). \quad (3.7)$$

For a signal consisting of N samples, the discrete Fourier transform is given by (3.8):

$$X = \frac{1}{\sqrt{2}} \cdot \frac{2}{N} \sum_{n=0}^{N-1} x_n \left[\cos\left(\frac{2\pi n}{N}\right) - j \sin\left(\frac{2\pi n}{N}\right) \right]. \quad (3.8)$$

By defining the sine and cosine sums as follows:

$$X_{\cos} = \frac{\sqrt{2}}{N} \sum_{n=0}^{N-1} x_n \cdot \cos\left(\frac{2\pi n}{N}\right);$$

$$X_{\sin} = \frac{\sqrt{2}}{N} \sum_{n=0}^{N-1} x_n \cdot \sin\left(\frac{2\pi n}{N}\right),$$

the phasor will be given by (3.9):

$$\bar{X} = X_{\cos} - jX_{\sin}. \quad (3.9)$$

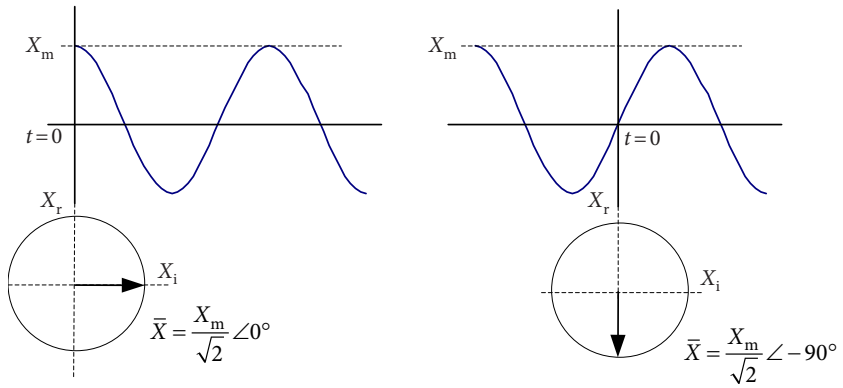

Fig. 3.1. Synchrophasor representation

For the input signal $x(t) = X_{\mathrm{m}} \cdot \cos(2\pi ft + \varphi)$ of frequency f represented with its x_n samples:

$$x_n = X_{\mathrm{m}} \cdot \cos(n\theta + \varphi), \tag{3.10}$$

where $\theta = \dfrac{2\pi}{N}$ is signal sampling angle; $n = 0,1,2\ldots,N-1$.

The sine and cosine sums of the $N-1$-th sample (the last sample taken for phasor estimation) can be calculated as follows:

$$X_{\cos}^{N-1} = \frac{\sqrt{2}}{N}\sum_{n=0}^{N-1} X_{\mathrm{m}}\left[\cos(n\theta+\varphi)\cdot\cos(n\theta)\right] = \frac{X_{\mathrm{m}}}{\sqrt{2}}\cos\varphi; \tag{3.11}$$

$$X_{\sin}^{N-1} = \frac{\sqrt{2}}{N}\sum_{n=0}^{N-1} X_{\mathrm{m}}\left[\cos(n\theta+\varphi)\cdot\sin(n\theta)\right] = \frac{X_{\mathrm{m}}}{\sqrt{2}}\sin\varphi. \tag{3.12}$$

Then the phasor

$$X^{N-1} = X_{\cos}^{N-1} - jX_{\sin}^{N-1} = \frac{X_{\mathrm{m}}}{\sqrt{2}}(\cos\varphi + j\sin\varphi) = \frac{X_{\mathrm{m}}}{\sqrt{2}}e^{j\varphi}. \tag{3.13}$$

Through the DFT-based phasor estimation, the data window is continuously updated by including the newer samples and discarding the older ones (Fig. 3.2). Phasor estimation is performed for each new data window to obtain updated phasors.

The steady-state signals, for which the DFT technique for phasor estimation can be successfully implemented, rarely persist in a real power system. Signals with transients, a decaying DC component, and off-nominal frequency signals are in the realm of power system operation. A transient appears when a transition from one steady-state condition to another steady-state condition occurs. In case of a transient, the data window contains samples from both the transient and the steady-state conditions and phasor estimation will be inaccurate. One should wait until the data window contains only samples of the new steady-state condition. For time-critical applications, this wait time is undesirable and should be avoided.

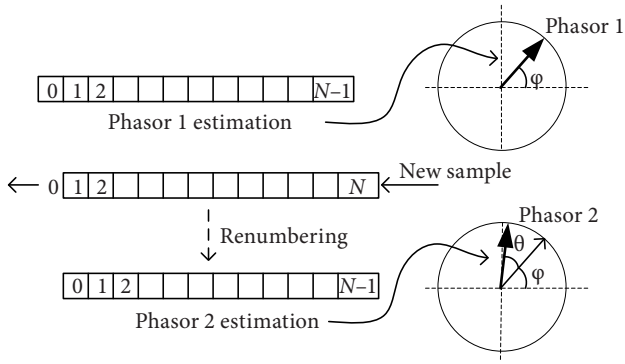

Fig. 3.2. Updating the sample window

A phasor estimation error also appears if the fundamental frequency of the signal deviates from its nominal value. At least several algorithms are known which allow phasor estimation to be carried out faster and/or for off-nominal frequency signals [17]–[24]. The tracking of real frequency accompanied by a signal resampling technique has been proposed in [19] to resolve the problem related to the estimation of the off-nominal frequency phasors. Several non-DFT-based algorithms exist and may be used for phasor estimation: least-square-based methods [23], the Kalman filtering technique [21], the Prony method [24], wavelets [22], and others.

The required phasor estimation accuracy depends on the application. If the estimated phasor is used only locally and is not reported for external applications, then each vendor is free to choose which algorithm to use for each particular application. If the estimated phasor should be available for processing by some external application, then the maximum allowed phasor estimation error should be specified. IEEE Standard C37.118.1-2011 introduces the concept of the total vector error (TVE). The TVE is the measure that combines error evaluation from all error sources, including time synchronisation, phasor angle, and phasor magnitude estimation errors (3.14).

$$TVE(n) = \sqrt{\frac{\left(x_{\mathrm{r}}(n) - x_{\mathrm{r}}\right)^2 + \left(x_{\mathrm{i}}(n) - x_{\mathrm{i}}\right)^2}{x_{\mathrm{r}}^{\,2} + x_{i}^{\,2}}} \cdot 100\%, \tag{3.14}$$

where $\bar{X} = x_{\mathrm{r}} + jx_{\mathrm{i}}$ represents the theoretical phasor value and $\bar{X}(n) = x_{\mathrm{r}}(n) + jx_{\mathrm{i}}(n)$ is the estimated phasor value.

The relationship between the theoretical phasor, the estimated phasor and the maximum allowed TVE error ε is shown in Fig. 3.3.

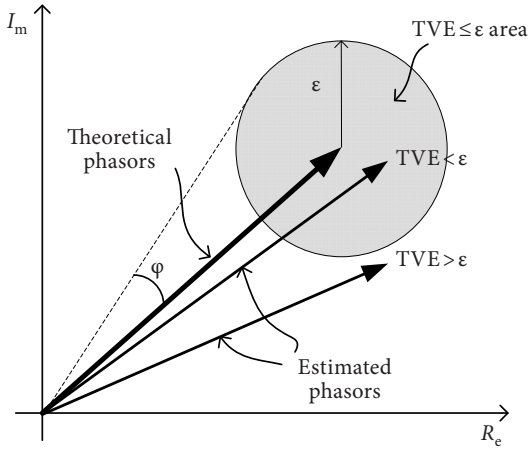

Fig. 3.3. Relationship between theoretical phasor, estimated phasors and maximum allowed error ε

The standard defines the maximum TVE value for a steady-state signal, as shown in Table 3.1.

Table 3.1

Synchrophasor measurement TVE

Phasor estimated for	Reference condition	Range	Deviation from nominal frequency (Hz)	Max. TVE (%)
Voltage signal	100 %	80 %–120 % (for protection application)	+/– 2.0	1
Voltage signal	100 %	10 %–120 % (for measuring application)	+/– 5.0	1
Current signal	100 %	10 %–200 % (for protection application)	+/– 2.0	1
Current signal	100 %	10 %–200 % (for measuring application)	+/– 5.0	1

3.2. Synchronisation of measurements

Global navigation satellite system (GNSS) is a system that is intended to ensure geo-spatial positioning. The best-known examples of a GNSS are the American-owned Global Positioning System (GPS), the European GALILEO system and the Russian GLONASS system. The main part of the GPS navigation system consists of 24 satellites placed into orbit by the U.S. Department of Defence. GPS works at any weather conditions, anywhere in the world, 24 hours a day. The GPS system is free of charge and can be used by anyone. GPS satellites circle the earth twice a day in a very precise orbit and transmit signal information to the earth. GPS receivers take this information and use trilateration to calculate the exact location of the receiver. The receiver compares the time the signal was transmitted by a satellite with the time it was received. The calculated time difference defines the distance of the GPS receiver from the satellite. GPS receivers need to receive GPS signals from at least three GPS satellites to determine the latitude, longitude, and altitude of a position, and to receive signals from one more GPS satellite to determine time. Typical GPS receivers are able to simultaneously track up to 12 GPS satellites. GPS receivers have PRN codes (Pseudorandom Noise Number — a unique code for each satellite) pre-programmed in them that match the codes of the GPS satellites. The receivers use these codes to recover the received signal and synchronise their local clocks with the clocks on the GPS satellites. This gives each GPS receiver the capability to generate a time reference with the same accuracy as that of the atomic clocks used inside each GPS satellite [25]. The time scale to which the GPS receiver time is referenced is the Coordinated Universal Time (UTC) — the

time standard commonly used across the world. The clock accuracy of the commercially available GPS receivers lies within several dozens of nanoseconds.

The main benefits that the knowledge of precise time gives to power system utilities consist in the ability to evaluate the system-wide time-stamped events and synchronise system-wide control actions. Power system utilities rely on GPS-synchronised clocks to synchronise protection and automation devices at substations and control centres. The precise time reference allows utility engineers to perform system-wide condition monitoring, control, and management. The typical applications that require time synchronisation include:

- The wide-area measurement system — a phasor-measurement-unit-based system, which measures the system signals (voltages and currents) at diverse locations of the power system. All measurements are taken synchronously and are time-stamped with respect to a common time reference. When measurements from multiple phasor measurement units (PMUs) are combined within the system control centre, a precise and comprehensive view of state of the entire power system can be provided.
- Disturbance recording — when a power system fault occurs, intelligent electronic devices (IEDs) at diverse locations record the waveforms of the controlled signals. Records from different IEDs may be aligned and used for post-fault evaluation if each record is referenced to a common time source.
- Time-stamped event logging — state changes of the various equipment and apparatus allow reconstructing the sequence of events that have taken place during a contingency.
- Transmission line fault location by using the travelling wave principle requires knowledge of precise time at both ends of the transmission line.
- Multi-terminal-based protection systems use the communication channels for information exchange. Terminal measurement/event synchronisation allows avoiding the communication channel time delay asymmetry problem.
- A substation automation system based on the IEC 61850-9-2 standard assumes that all measurements and events within a substation should be synchronised with a high accuracy.

Commercially available GPS receivers are manufactured as dedicated modules that can be integrated in a user-customised device or as complete functional devices. Some IEDs may be equipped with a dedicated GPS receiver module, but for substation applications, with many devices requiring a common time source, GPS-disciplined substation clocks are used. The substation clock provides a time synchronisation signal, which is distributed

to the IEDs throughout the substation by using a variety of time distribution methods.

Time distribution over a dedicated network (Fig. 3.4 a)) may be implemented by two standardised methods:

1. IRIG-B (inter-range instrumentation group) time codes [26]. IRIG-B transmits 100 pulses per second on an amplitude-modulated 1 kHz sine wave carrier. Information is encoded in the binary coded decimal (BCD) format. The IRIG-B data frame contains information about the day of the year (1–366), hours, minutes, and seconds. A data frame is transmitted every second, and precise synchronisation (within 100 microseconds) can be achieved using the phase-locked loop of the receiver to synchronise the carrier. Twisted-pair wires or coaxial cables can be used for IRIG-B distribution.
2. 1PPS (One Pulse Per Second) is a digital pulse-type signal, which is transmitted every second [26]. The rising edge of the impulse marks the beginning of the new second. If the cable delays occurring during the distribution of the signal are taken into consideration, the achievable accuracy lies within one microsecond. The 1PPS signal itself does not contain any other time information except the new second mark, and additional time information needs to be transmitted to the IEDs via a separate system.

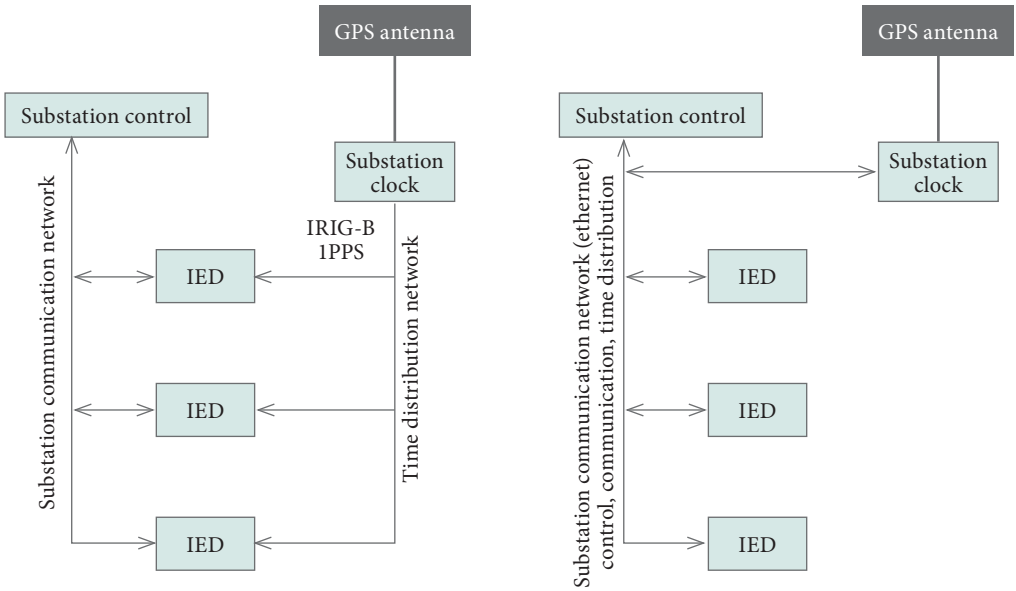

a) using a dedicated network **b)** using the substation's communication network

Fig. 3.4. Time distribution methods within a substation

Time distribution over a LAN (Local Area Network) (Fig. 3.4 b)) synchronises devices via an Ethernet network. Multiple devices can be synchronised through a single Ethernet cable. Time synchronisation information is transmitted along with other data communications over the same communication medium, thus reducing the amount of necessary cabling (Fig. 3.4 b)). The best synchronisation (up to 30–50 ns) can be achieved with the Precision Time Protocol (PTP) [26]. The PTP is a future-proof standard Ethernet protocol described in the IEEE 1588 [27] and IEC61588 standards for time synchronisation. The PTP can be applied on the basis of the existing Ethernet network at a substation. IEEE 1588 uses a master/slave time synchronisation mechanism (Fig. 3.5 a)) and supports hardware-driven time stamps. The master (a GPS clock) sends a data packet to the slave (IED) at time $t_{1(M)}$. The data packet is received by the slave at time $t_{2(S)}$ with time delay t_d. The slave sends the data packet at time $t_{3(S)}$, and the master receives the data packet at time $t_{4(M)}$. All of the time stamps are local and are attached to the data packets sent. If the packet transmission time delay t_d is equal for both packets, then the slave is able to calculate the time difference $\Delta t_{(MS)}$ and then correct for the difference on its own internal clock (Fig. 3.5 a)).

Such a method of time synchronisation is sometimes referred to as the "ping-pong" method. The method is valid only if all the transmitted packets exhibit the same communication path through the network with an equal time delay.

For a switched/multiplexed network it is possible that the data packet transmitted from Master to Slave takes a different path than the data packet

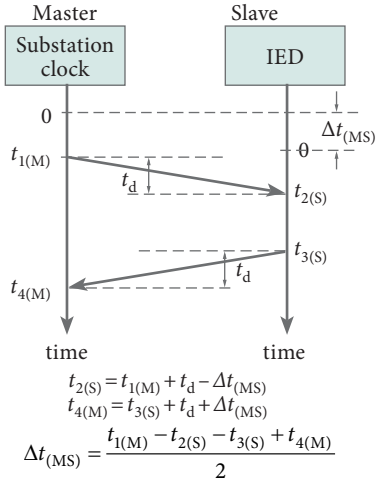

a) Slave synchronisation

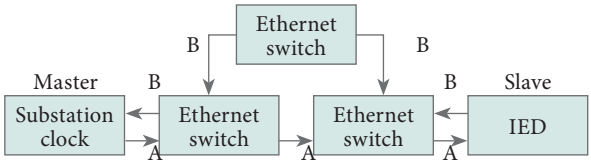

b) master-slave communication time delays

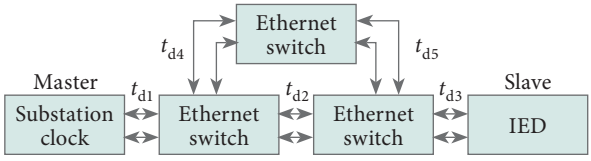

c) P2P mechanism

Fig. 3.5. a) Slave synchronisation; b), c) master-slave communication time delays

transmitted from Slave to Master (Fig. 3.5 b)). The peer-to-peer (P2P) delay calculation mechanism allows getting rid of the problem of different paths. The P2P mechanism uses the same "ping-pong" principle but now time delays between each two consecutive participating elements are calculated: t_{d1}, t_{d2}, t_{d3}, t_{d4}, t_{d5} (Fig. 3.5 c)). Each communication network element between Master and Slave then adds the calculated time delay to the data packet sent by Master. Thus, Slave receives the data packet from Master where all the communication path delays are accumulated. For time synchronisation by using the P2P technique, the special Sync/DelayRequest/DelayResponse data packets are used. A simplified procedure for time synchronisation is shown in Fig. 3.6.

It is assumed that the propagation delay is symmetrical (equal in both directions) for any master-slave pair. Any queuing and buffering delays introduced by the communication equipment along the path may cause variation of the time delay, and this variation inevitably affects the accuracy of the path delay measurements. To account for all queuing and buffering delays, the "*transparent switch*" mode of the communication switch should be used. The transparent switch makes hardware time stamps whenever a Sync message arrives at, or departs from, the transparent clock. The calculated residence time (the time that the packet spends passing through the switch) is then added to the time correction field of the P2P data packet. An example of a multi-segment network with PTP-protocolbased time synchronisation is shown in Fig. 3.7.

Several types of clocks are defined in the IEEE1588 Standard [27]. An *ordinary clock* communicates with the network through a single physical

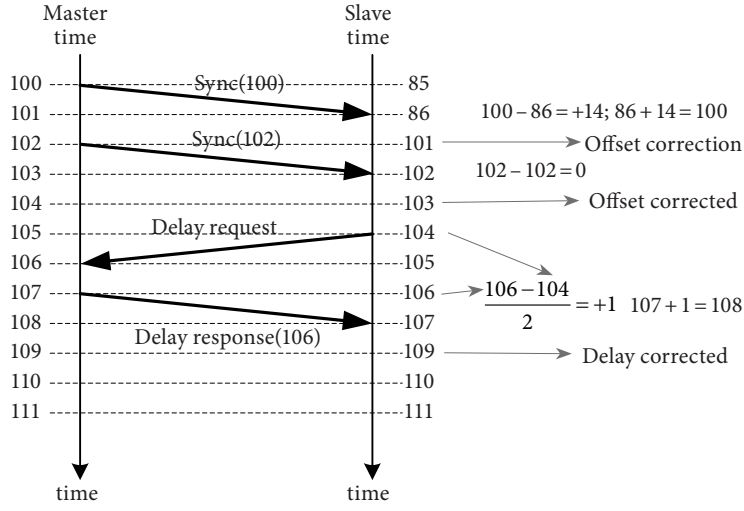

Fig. 3.6. Time synchronisation procedure

port. An ordinary clock can function as a grandmaster clock. A *boundary clock* typically has multiple network connections and can act as a source (master) and as a destination (slave or client) for synchronisation messages. It synchronises itself to the best master clock and synchronises clients through the master ports.

The boundary clock intercepts and processes all PTP messages and passes all other data traffic. A *transparent clock* retransmits all PTP messages like a regular switch but measures the residence time of the packet and communication link delays and then applies a time correction to the PTP message correction field. A *grandmaster clock* serves as a primary reference of the time synchronisation system. It has a highest-precision time source on board (a GPS reference or an atomic clock).

The specific algorithm known as the Best Master Clock Algorithm (BMCA) [27] is used to automatically determine the current best clock, which is then chosen to provide the reference time. This clock becomes the grandmaster clock and all the other clocks synchronise their time to the time of the grandmaster clock. If the grandmaster clock of the network experiences a malfunction, the second-best clock in the network becomes the new grandmaster clock without the need for any special intervention.

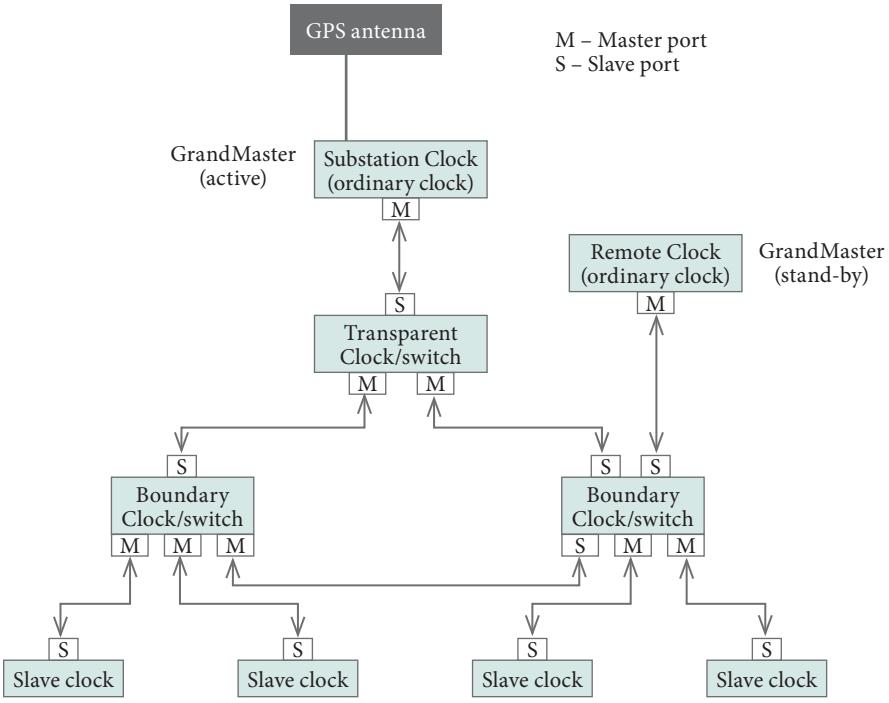

Fig. 3.7. An example of PTP synchronisation network topology

The typical accuracy of the above-described time synchronisation methods is presented in Table 3.2.

Table 3.2

Comparison of time synchronisation methods

Time synchronisation method	Typical time synchronisation accuracy	Distribution method	Limitations
IRIG-B	0.1–10 μs	Dedicated network	One-year overlap
1PPS	0.01–0.1 μs	Dedicated network	No time information
PTP	0.1–1 μs	Ethernet	Special PTP-compatible hardware required

3.3. Phasor measurement unit

Phasor measurement units (PMU) are considered among the most important measuring devices in the future of power systems. A PMU is a microprocessor-based device that produces synchronised-phasor (synchrophasor), frequency, and rate-of-change-of-frequency calculations from voltage and/or current signals and a time-synchronising signal. PMUs are time-synchronised, high-speed measurement units that monitor current and voltage waveforms (sinusoids) in the grid, convert them into a phasor representation and securely transmit phasors in digital form to a centralised server.

A PMU may be a dedicated device, or the PMU function may be incorporated into a protective relay or another device. PMUs provide real-time-synchronised measurements in a power system with a synchronisation accuracy better than one microsecond, which is achieved by using the signals of the Global Positioning System (GPS). PMUs are placed in power system substations and provide measurement of timestamped voltage and current phasors of all monitored buses and feeders. Synchrophasors data are transmitted by PMUs from various substations of the power system to the main monitoring/control centre for further processing. The time stamps assigned to every synchrophasor eliminate the problems related to the inequality of data transmission time delays and thus, a coherent picture of the current state of the power system can be recreated when data from all the PMUs are available in the monitoring/control centre (Fig. 3.8).

The PMU's hardware configuration, features and software algorithms are manufacturer-dependent issues but the generic hardware configuration may be discussed and is presented in Fig. 3.9. The analogue input signals of currents and voltages (U, I) are scaled to an acceptable level by means of an input transducers block. The sampling rate of the analogue signals defines

the required frequency response of the anti-aliasing filter. The sampling rate of modern PMUs can be as high as 256 samples per cycle. A high sampling rate allows more sophisticated algorithms of phasor estimation to be implemented; also the requirements regarding the stability of the analogue anti-aliasing filter parameters could be relaxed because of the possibility to use oversampling and the decimation technique. The phase-locked oscillator with synchronisation from the 1PPS (one pulse per second) signal of the built-in GPS receiver allows precise timing of analogue signal sampling. The accuracy of synchronisation lies within one microsecond, and the data frame with the Coordinated Universal Time (UTC) is provided by the GPS receiver. Along with the analogue signals, the state of the binary input signals is controlled and processed.

The DSP type phasor processor estimates phasors (single-phase, three-phase positive, negative or zero-sequence phasors may be the option) and generates the data frame, which is transmitted further to the communication processor and then transmitted to a higher level in the communication chain. The phasor estimates of the input signals are computed based on a moving sample window. Depending on the algorithm used and the length of the time window, the estimated synchrophasor is assigned with appropriate time indicating the instant of the estimation.

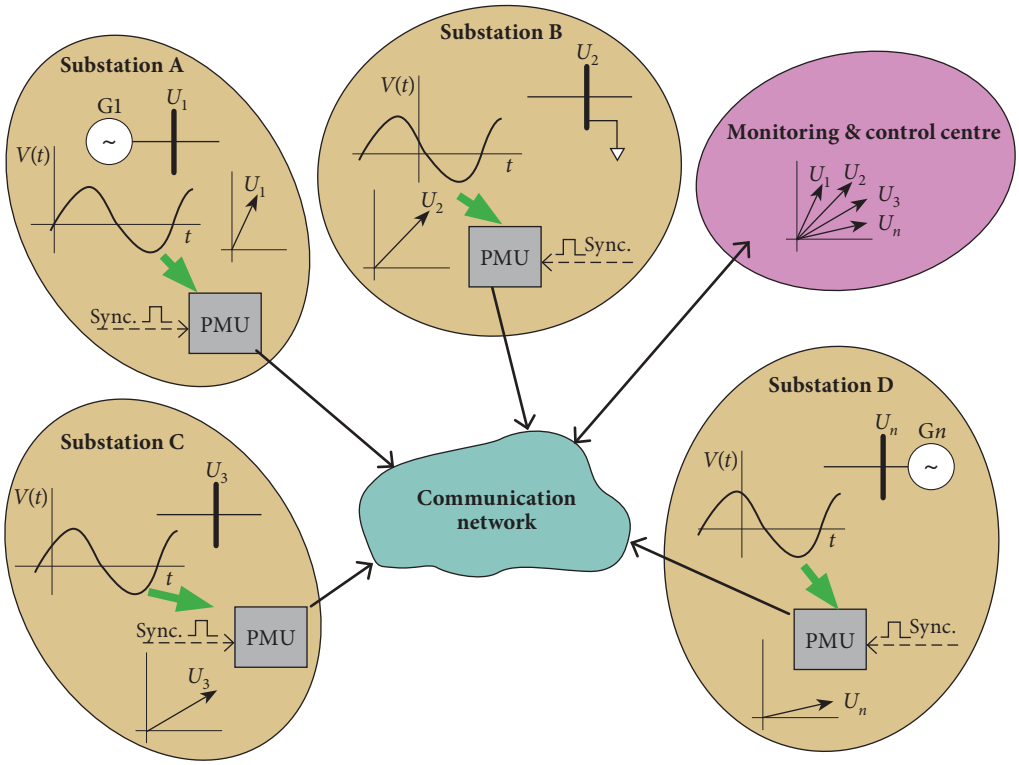

Fig. 3.8. PMU-based monitoring and control of a power system

This time is represented by the time stamp of the synchrophasor. IEEE standard C37.118.1 [28] recommends time-tagging the synchrophasor with the time at the centre of the estimation window. The exact algorithm for phasor estimation is not specified by the standard; however, each PMU vendor should conform to phasor accuracy metrics — the total vector error (TVE). The standard defines the TVE as shown in (3.15):

$$TVE = 100\% \cdot \frac{\left|\vec{x}_{\text{meas}} - \vec{x}_{\text{ideal}}\right|}{\left|\vec{x}_{\text{ideal}}\right|}, \tag{3.15}$$

where $\vec{x}_{\text{meas}}$ is the measured phasor and $\vec{x}_{\text{ideal}}$ is the ideal phasor.
To conform to the standard, the PMU's TVE should not exceed 1%. This translates into a magnitude-only error of <1 %, a phase-only error of <0.573° and a time error of <31.8 μs for a 50 Hz system.

The typical reporting rate of the PMU data frames is a sub-multiple of the system frequency such as 10, 25, 50 frames per second for a 50 Hz system and 10, 12, 15, 20, 30 and 60 frames per second for a 60 Hz system. The communication protocol and the physical media used for PMU communication are not standardised but TCP/IP (Transmission Control Protocol/Internet Protocol) or UDP/IP (User Datagram Protocol/Internet Protocol) is typically chosen. The synchrophasor message structure and data format are defined by the IEEE C37.118.2-2011 standard. Four types of message frames are defined: a data frame, a configuration frame, a header frame and a command frame. Each frame starts with a frame header, which consists of the SYNC word, the FRAMESIZE word, the IDCODE word, and time stamp numbers SOC, FRACSEC followed by the data and the CHK word (Fig. 3.10). The SOC time-tag counts the number of seconds that have

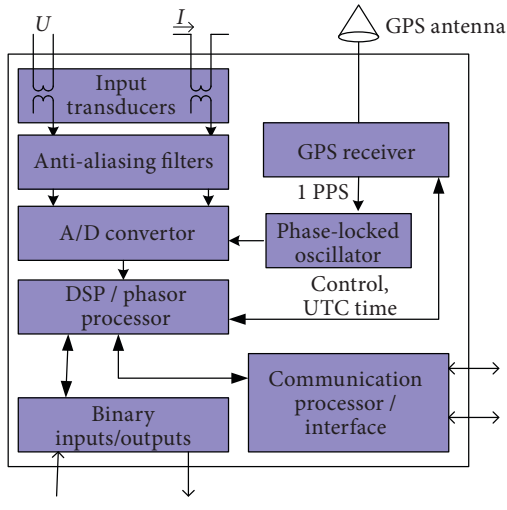

Fig. 3.9. PMU hardware architecture

elapsed since January 1, 1970, and FRACSEC defines the exact time-tag within a second, supplemented with the estimated maximum time error (time-quality flag).

The configuration frame describes how the data frame should be interpreted by the client (including the number of transmitted phasors, the channel names, the data format, the scaling factors, the frame transmission rate and so on). The command frame is intended for the exchange of commands (sending configuration, starting/stopping data transmission) between the

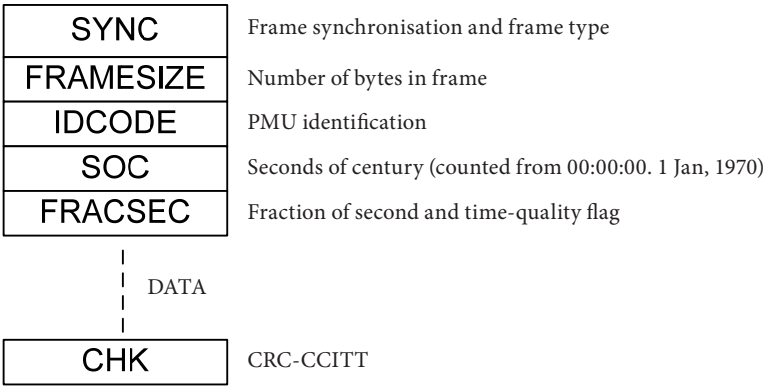

Fig. 3.10. PMU Frame header structure

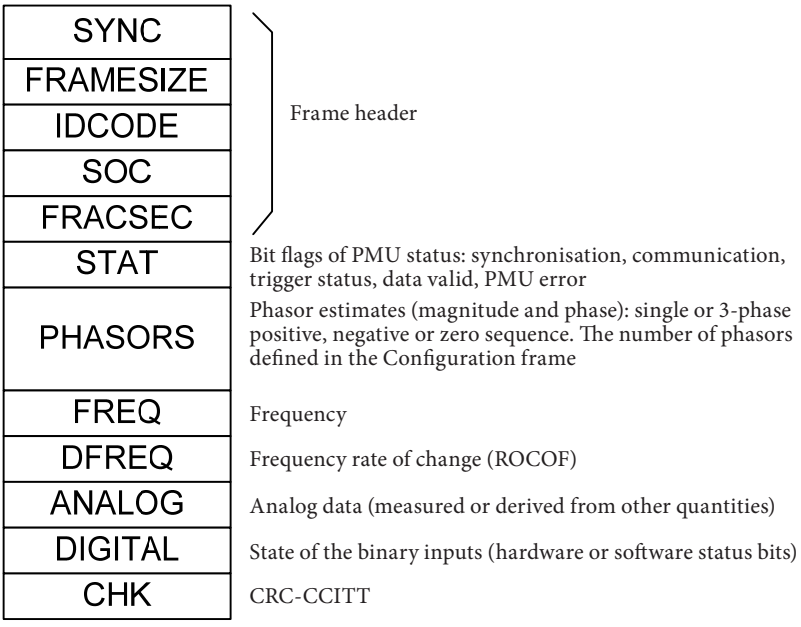

Fig. 3.11. PMU data frame message structure

PMU and the client. The data field in the header frame contains source information such as the MAC address of each input, scaling, filtering, and other algorithms implemented within the PMU. The PMU data frame message structure is presented in Fig. 3.11.

A typical sequence of message exchange between a PMU and client equipment is shown in Fig. 3.12.

3.4. Phasor data concentrator

The phasor data concentrator (PDC) is the next – higher – level in the communication chain of the wide-area measurement system. PDC acquires data from multiple PMUs and outputs a time-aligned data stream in real time. A PDC can exchange phasor data with PDCs at other locations. Through the use of multiple PDCs, multiple layers of data concentration can be implemented within an individual synchrophasor data system (Fig. 3.13). Medium-level and higher-level PDCs collect the information from substation-level PDCs and feed the information to the final application.

A PDC can be implemented as a dedicated microprocessor-based device or as a software-based application installed on a PC-type server.

The main tasks of the PDC can be formulated as follows [29]:

- To receive data frames from multiple PMUs.

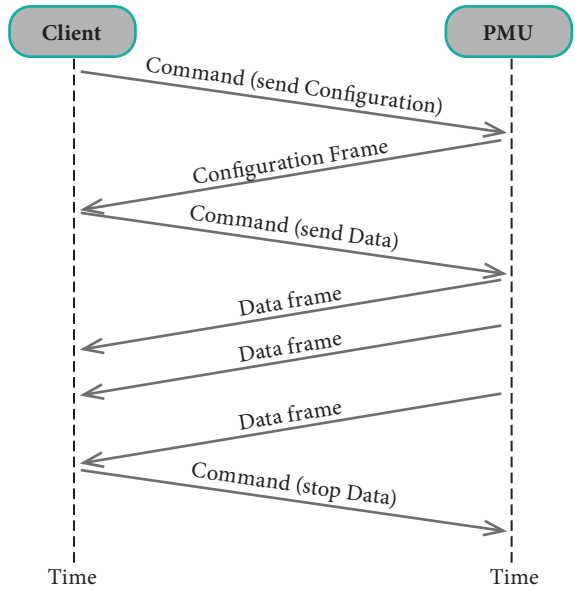

Fig. 3.12. Client-PMU message exchange

- To validate the input data (check the integrity of the input data and the quality of the time stamp).
- To time-align the incoming frames if the data from different PMUs do not arrive at the same time.
- To handle the data from PMUs with different reporting rates.
- To handle multiple synchrophasor data transfer protocols and provide the protocol conversion function.
- To rearrange disordered frames (if the newer data arrive after their predecessor).
- To aggregate data from multiple PMUs and process the acquired information in a unified format (phasor scaling to a common base, unified phasor representation, unified units, etc.).
- To process the output frame, consisting of time-aligned, validated synchrophasor data from multiple PMUs.

The problems regarding the misalignment of data frames are mainly related to communication channel time delay variation and partially related to data latency inequality for various PMUs. There are many reasons that cause the communication channel time delay variation. The transmission delays vary depending on the selected communication protocol: TCP/IP or UDP/IP. The time delay depends on the distance between the PMUs and the PDC and the selected data transmission medium. When a complex switched/multiplexed network is used, each router or switch introduces an additional time delay. The time delay also varies depending of network

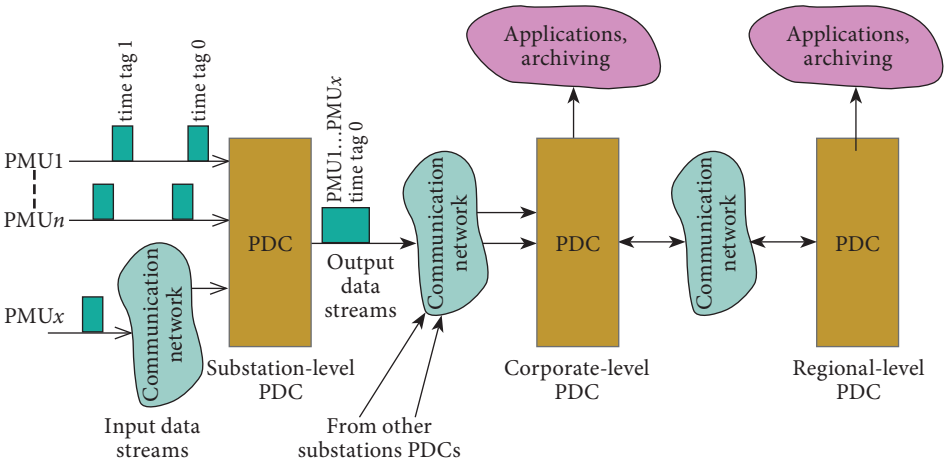

Fig. 3.13. A PDC collecting information from multiple PMUs and exchanging information with other PDCs

traffic and the amount of data in queue. The task of the PDC is to time-align the incoming data streams from various PMUs and form a unified output message (Fig. 3.14 a)). The PDC should be capable of supporting different reporting rates of PMUs, and then the output message is formed using data upsampling (if the PMU has a lower reporting rate than the PDC output rate) or downsampling (if the PMU has a higher reporting rate than the PDC) technology (Fig. 3.14 b)). An extreme case of time delay variation (an abrupt change of the time delay due to sudden changes in the data transmission path) may even lead to a discrepancy in the order of frames. In such case, the new message arrives later than its predecessor (Fig. 3.14 c)). The PDC should be capable of waiting for some time and forming a time-aligned output message if the latecomer has nevertheless been received within acceptable time limits.

The functionality of modern PDCs is not limited only to time alignment of incoming data but some important features may be added: data concentration and local archiving; additional signals may be derived from the PMUs' phasor information; extensive testing of the integrity of the data and the health of the communication channels; data latency calculation. Typically, multiple outputs are available from the PDC, thus providing the information to be fed to multiple applications. Modern PDCs are highly

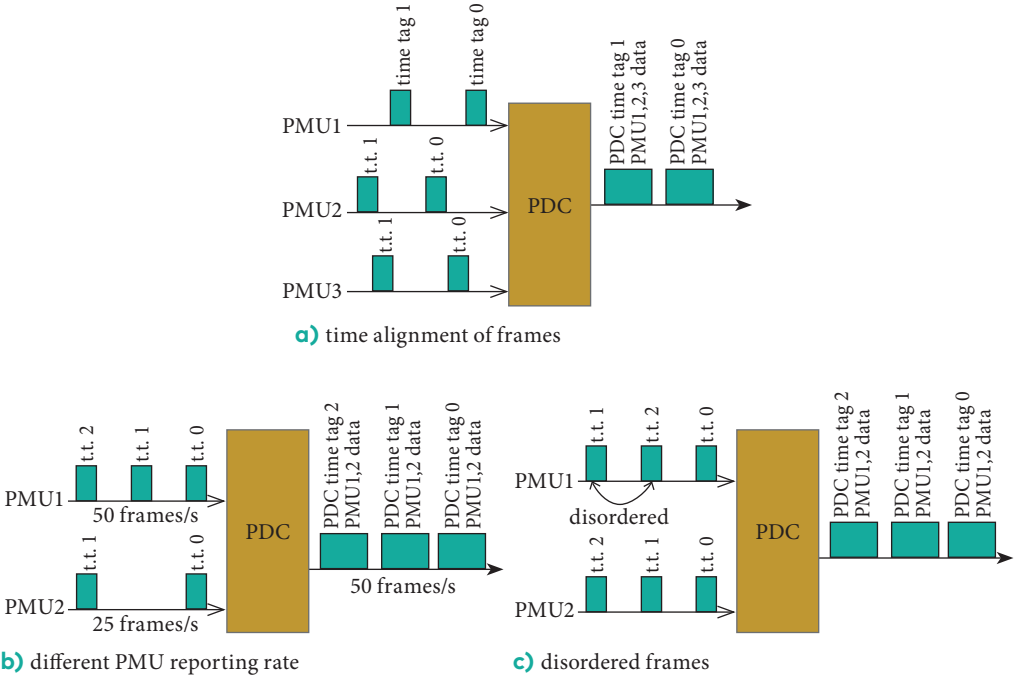

Fig. 3.14. a) Time alignment of frames; b) different PMU reporting rate; c) disordered frames

capable units and the desired PDC functionality is fully configurable. A typical functional block diagram of a PDC is presented in Fig. 3.15.

3.5. Data latency

For an application based on real-time wide-area measurements, the issue of data latency is one of the most critical aspects. Data latency can be defined as follows: the time that has elapsed from the start of data creation to the end of data processing performed by a final application. For the system presented in Fig. 3.16, data latency equals the time difference between the time stamp assigned to the particular PMU measurement and the UTC time at the end of the data processing performed by the application. Depending on the kind of system response it is dealing with, every application has its own specific data latency requirements. Latency is considered not critical for information visualisation, post-event analysis and archiving applications but becomes highly critical for control and emergency applications. The total latency is the cumulative time delay consisting of those introduced by each element in the path from the data source to the destination (Fig. 3.16).

Communication-network-related time delays are comprised of transmission delays, propagation delays, data processing delays, and queuing delays. Communication delay values depend on network structure, the equipment used and data traffic, and these may change over time. For a given network structure, the communication latency can be estimated approximately and then justified experimentally, taking into account the worst-case scenarios.

PMU reporting latency is the time interval calculated as the difference between the time stamp of the reported measurements and the time when the synchrophasor information becomes available at the output of the PMU.

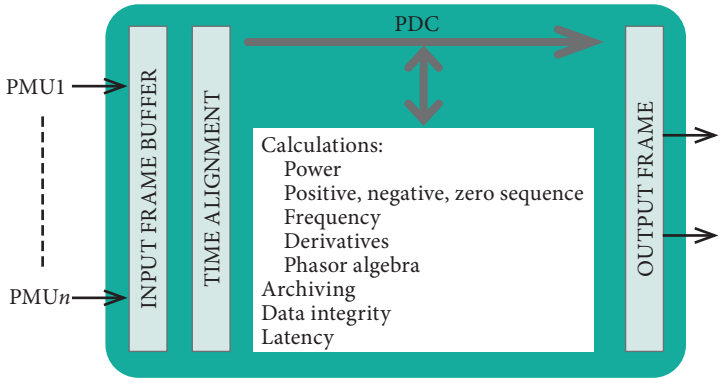

Fig. 3.15. PDC functional block diagram

The PMU latency is comprised of the latencies for the signal acquisition, phasor estimation and data transmission processes. This latency varies depending on the PMU's technical parameters, the number of phasors processed, the algorithms implemented and the PMU reporting rate. IEEE Standard C37.118 [29] introduces two classes of PMU performance. Class P ("Protection") of PMUs is intended for use in time-critical applications like control and protection for which data latency should be minimal. Class M ("Monitoring") of PMUs is intended for applications where a longer latency is acceptable. The synchrophasor standard defines the "maximum PMU reporting latency", which should not exceed 2/(reporting rate) for class P PMUs and 7/(reporting rate) for class M PMUs. Depending on the application, PMU data latency may vary from 20 ms to 140 ms.

PDC latency is comprised of PDC wait time and PDC data processing time. Latency starts counting when the first complete data message with its associated time stamp arrives at the PDC. The PDC waits for a predefined period of time to complete the receiving of data from other PMUs, whereupon the data processing latency starts. Any data that arrive later than the maximum allowed wait time of the PDC will be lost and are not included in the current output frame. Data processing time includes data aggregation, data time-alignment, upsampling/downsampling of data with different reporting rates, computations and message frame forwarding. The PDC manufacturer should clearly specify the impact of PDC data processing in

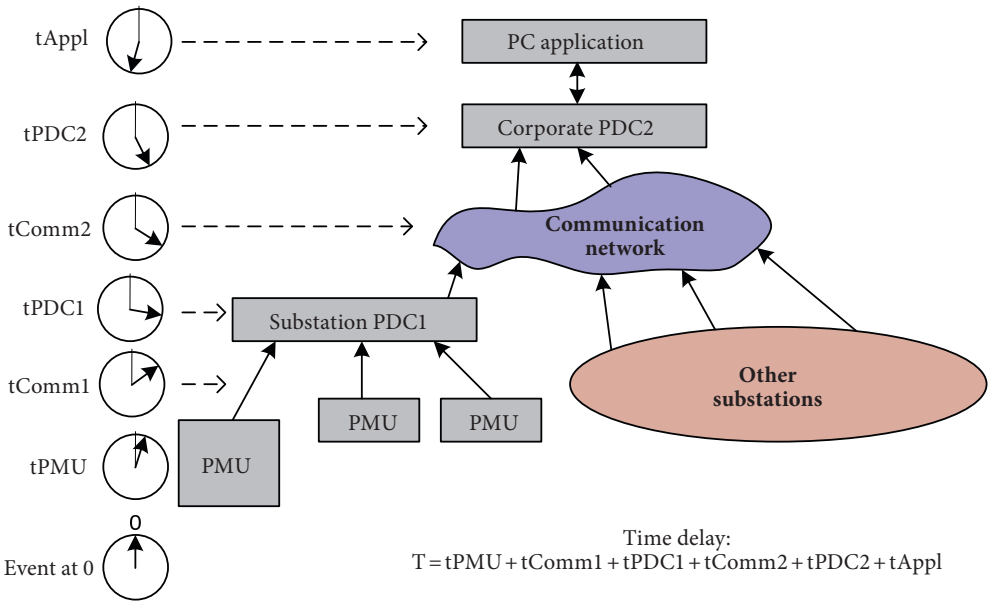

Fig. 3.16. The sources of data latency

terms of maximum magnitude difference, maximum phase difference, and maximum phasor value difference between the input data and the output data. The maximum PDC latency should also be specified for all possible PDC operating modes. The typical range of PDC latency varies from 10 ms to 100 ms.

3.6. Wide-area measurement system structure

The wide-area measurement system (WAMS) is a relatively new but rapidly growing technology, which is now widely accepted by power system utilities around the world. The main reason why WAMSs are becoming more and more integrated with various management and control applications lies in the continuous increase in the power system observability needs. While SCADA systems are still providing the major information for power system operators, the continuous rise in the complexity of interconnected networks calls for the solution of entirely new tasks. Due to various technological and structural reasons, the existing SCADA systems cannot cope with new challenges, which is why the number of WAMS-based applications is growing so fast. The main advantage of using WAMSs lies in the possibility to look through the dynamics of power system processes. Generally, all the processes in a WAMS can be subdivided into three stages: data acquisition, data transmission and data processing. These stages are similar to the ones used in SCADA, but the main difference is in the qualitatively different way of data representation and processing. With the advent of the phasor measurement unit (PMU), the availability of measurement synchronisation and everything that is supported by modern communication technologies, an entirely new level of power system monitoring and control can be achieved. A generalised structure of a WAMS is presented in Fig. 3.17.

At the data acquisition stage, PMUs (or IEDs capable of PMU functionality) synchronously sample electrical signals at different electrically and geographically distant points of the network. The PMU calculates signal phasors and transmits the phasors, along with the frequency and the frequency rate of change, to the PDC, where the data received from multiple PMUs are pre-processed, rearranged and time-aligned. The data are then transmitted to the main control centre by means of a wide-area communication network. As soon as all the necessary information around the network has been centrally collected, the data can be further processed by the control centre equipment and then used for various applications.

The PMU outputs data frames at one of the standardised data rates: 10, 25 or 50 frames per second for a 50 Hz system. Each frame contains time-stamped phasor data derived from synchronously sampled signals.

Synchronisation of the PMUs' measurements is ensured by a GPS-disciplined substation clock up to an accuracy of 1 microsecond.

The final tune and time alignment of the measurements received from remote PMUs/PDCs are held in the control centre. Thus, a continuous stream of wide-area measurements is available at the control centre with each particular set of frames representing a system-wide snapshot of the network signals taken at a specific moment in time.

When comparing with SCADA, the main advantage of WAMS lies in the form of signal representation. The phasor representation used by WAMS preserves the phase and amplitude information of the original signal. Unlike the data polling technique used by SCADA, a WAMS can provide a continuous stream of information in near-real time. Precise synchronisation of measurements allows the system-wide signals to be mutually processed and used to assess the current state of the network.

Among a variety of applications where great progress can be achieved considering WAMSs, several applications should be mentioned as the most important ones:

- Improved observability and control can be achieved in the steady state if traditional SCADA systems are enriched by WAMS

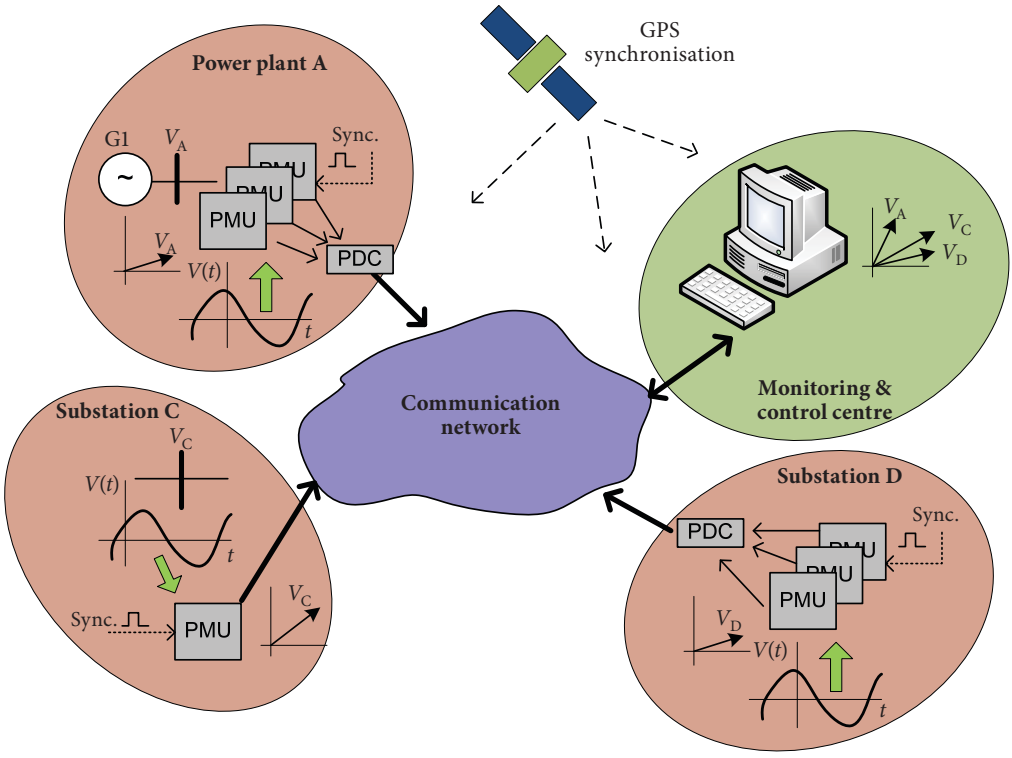

Fig. 3.17. WAMS structure

functionality. Real-time monitoring, state estimation and visualisation applications will all benefit when system-wide information becomes available in real time.

- The possibility to catch the network dynamics allows PMUs' data to be processed online by system stability studies and thus sophisticated situational awareness applications can be created.
- An entirely new level of detail can be achieved in post-fault analysis.
- Given system-wide information, mathematical models of power systems can be verified, corrected and validated.
- The settings of traditional protections can be adapted online, using the knowledge about the current state of the network.
- Availability of system-wide information allows fault location accuracy to be improved.
- System-wide-information-based transient stability assessment allows sophisticated protection schemes to be created with the ability to predict the next power system state in real time.

Over the past twenty years, a generous amount of scientific publications has been devoted to the theoretical and practical issues related to the implementation of WAMS. A comprehensive overview of the articles devoted to existing and future WAMS applications is presented in [30]. Because of the limited scope of the book, only OOS-protection-related WAMS applications will be considered further.

4. OOS PROTECTION. WIDE-AREA-MEASUREMENT-BASED APPROACH

4.1. The objectives of network splitting

The main objective to be achieved by the operation of OOS protection is controlled islanding of the network. The term "controlled" presumes that after splitting, the frequency and voltage profiles within the islands could be supported at an acceptable level. Customers' needs still can be served after controlled islanding, although the quantity, quality and reliability of service may be degraded to some extent. In contrast, uncontrolled islanding may result in unplanned network separation, after which it is impossible to keep the system parameters within acceptable operational limits. In the worst-case scenario, uncontrolled splitting may lead to widespread power outages and blackouts. To successfully solve the controlled splitting task, two main questions should be answered:

- At which particular moment in time does the network splitting become unavoidable? (When to split?)
- Along which particular cutset should the network splitting be done? (Where to split?)

Traditional, local-measurement-based protection devices can answer both questions only partially. The moment when a stable/unstable decision is taken is determined uniquely by the device settings and is the result of a finite amount of simulated stability studies scenarios. An attempt to detect the unstable swings at an early stage may result in a wrong decision since the actual OOS condition may not fit any of the simulated scenarios. This is why the command for network splitting is typically issued when the generators already exhibit the pole slip or even later. The choice of the network-splitting boundary is also somewhat constrained if local OOS protection devices are considered. Typically, the OST function is assigned to critical transmission lines which are the most likely ones to become the weakest links during a contingency. Pre-determination of the splitting boundary, while being a straightforward approach, does not necessarily provide the optimal decision, considering the near-infinite number of contingencies with each of them affecting different parts of the system in different ways. The main deficiency of the local-measurement-based protection devices lies in their inability to adapt their operating conditions to the dynamically changing state of the network.

The possibility of decision-making on the basis of information gathered system-wide is the main area where WAMS-based OOS protection systems clearly outperform the local-measurement-based protection devices. The

decisions of both when to split and where to split could be optimised and taken with a much higher level of confidence if the network dynamical processes are traced in real time. The next chapters will provide an overview of WAMS-based methods and approaches used for OOS detection and controlled splitting. In the following discussion it is assumed that a WAMS in itself is free from any deficiencies related to communication or synchronisation issues and all system-wide measurements are delivered at standardised rates and without significant delays and errors.

4.2. Measurements available from WAMS

The main source of information for a WAMS consists in PMUs or IEDs with PMU functionality. Several quantities are available from the PMU that can be used for OOS protection purposes, namely: single-phase or 3-phase positive-sequence, negative-sequence or zero-sequence phasor estimates (amplitude and phase); signal frequency (FREQ) and rate of change of signal frequency (ROCOF) (see Section 3.3). Since the OOS regime is considered a balanced one, the phasors of positive-sequence voltage and current are the most likely ones to be used for OOS detection while the negative-sequence and zero-sequence phasors could be used for providing protection security for all unbalanced conditions. When negative-sequence and zero-sequence phasors are used to discern unbalanced/transient conditions, it has to be considered that the PMU's report rate (10, 25 or 50 frames per second) may be insufficient to detect fast transients by means of collecting the PMU's data in a centralised manner. The possible decision consists in detecting transients locally at a much higher signal sampling rate of PMU/IED and then attaching the result (balanced/unbalanced state) as supplementary information to a regular data frame. Then the centralised decision-making logic will be able to sort out the measurements affected by transients and thus decision-making under transient conditions will be avoided.

The positive-sequence voltage and current phasors provide both the amplitude and phase information of the signal and, while amplitude is important, the relation between the phases of signals sampled system-wide becomes paramount for angular instability detection. Voltage phasors synchronously sampled at different network locations provide a snapshot of system-wide angles and it then can be directly used to assess the network stability. The derivatives of angles can be estimated, providing a view of the system processes over time. Voltage and current phasors can be used to estimate the power flows, thus allowing the root of angular instability phenomena — the power mismatch — to be assessed. System frequency and frequency rate of change are two additional quantities that clearly indicate how fast and in which direction the processes are deviating from the steady-state condition.

4.3. Coherence of generators

One of the most important aspects to be considered when implementing controlled islanding is that after network splitting each island should contain generators that remain in synchronism with one another. Only when this condition is fulfilled and the generators within the island operate synchronously, does it become possible to avoid further cascaded splitting within the island and finally achieve an acceptable power balance.

It is known that there is a tendency in the behaviour of generators in response to a contingency when a number of machines swing in a similar fashion. This tendency can be explained by the fact that the interaction of machines depends on how strongly these machines are interconnected within the network. A strong electrical interconnection will result in the generator rotors swinging together, while weakly connected machines tend to diverge from one another. In order to be sure that the islanded part of the network contains only generators that will continue to operate synchronously, it is necessary to investigate the behaviour of generator rotors after the system has been exposed to a severe disturbance. The generators that exhibit similar behaviour are called coherent, and the objective is to sort out coherently swinging machines and then choose the islanding boundary such that all the coherent generators remain within one island. For two perfectly coherent generators *i* and *j* the following can be stated:

$$\Delta\delta_i(t) - \Delta\delta_j(t) = 0, \tag{4.1}$$

where $\Delta\delta_i(t) = \delta_i(t) - \delta_i(t_0)$; $\Delta\delta_j(t) = \delta_j(t) - \delta_j(t_0)$ are the deviations of the generators' rotor angle from the steady-state point at t_0.

A group of generators can be called coherent if each pair of generators within the group is coherent. It is unlikely that two absolutely coherent generators can be found in real life, but the degree of coherence can be determined and then the generators could be grouped depending on the degree of coherence. The idea of grouping coherent generators is based on the assumption that there exist two modes of generator rotor angle oscillations after a disturbance [31]. Fast oscillations between the generators within some area are superimposed on slow oscillations between groups of generators in different areas of the network. As soon as the fast oscillations decay, the slow oscillations between the generator groups in different areas remain and these slow inter-area oscillations define how the dynamical processes of the system are developing. In a real power system, the dynamics of which is highly nonlinear, numerous oscillation modes are presented, each with its own time scale. The slow-mode-coherence-based approach assumes that oscillations of the lowest modes (with the largest time scale) constitute an indication of a weak interconnection between network areas, and thus the grouping of the generators should be established based on the oscillations

of the lowest mode. A detailed description of the slow coherence theory is provided in [32]–[34].

Initially, the slow-coherence-based approach was implemented to reduce the power system model for the purpose of transient stability studies. Then, the procedure for forming coherence-based dynamic equivalents consists of three stages [35]:

1. Identification of groups of coherent generators.
2. Network reduction. The terminal buses for each group of coherent generators are replaced by a single equivalent bus.
3. The generator models are aggregated into a single equivalent generator model.

The theory of slow coherence can be successfully applied to OOS relaying in fulfilment of the requirement regarding the synchronicity of intra-island generators. The technique used for the identification of coherent groups differs depending on the data source used. The analytical approach assumes that a power system is represented by linear state space equations and then the coupling between machines can be derived from the state matrix [36]. The model-based approach assumes that multiple dynamic simulations should be carried out, followed by data analysis. Modern computer-aided programs allow simulating any possible contingency scenario, and then generators' coherence can be investigated just by observing the time response of the generators' terminal bus angles (Fig. 4.1). For a small power system with few generation sources that are interconnected by means

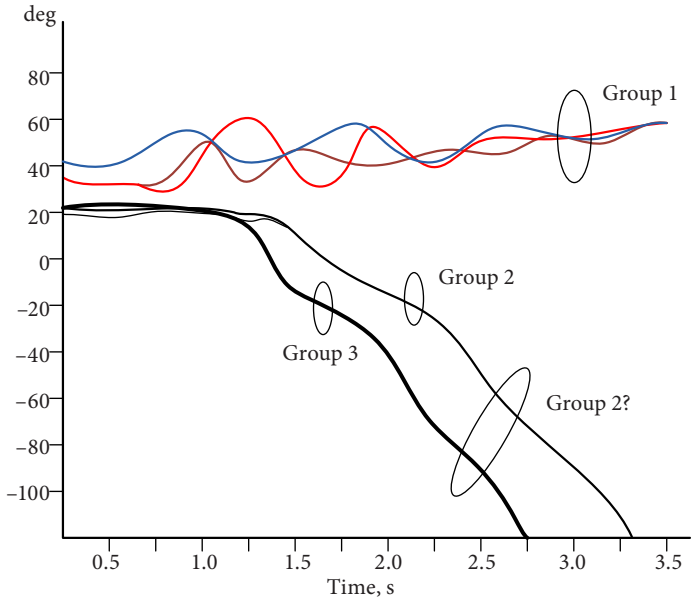

Fig. 4.1. Generators' angle trajectories after a disturbance

of several lines, it is feasible to detect the possible groups of coherent generators offline. OOS scenarios should be simulated for several predominant network configurations and power transfer regimes. The number of groups and the number of islanding solutions will typically be limited to 1–3 cut-sets, and then the OST function could be delegated to relays belonging to the chosen transmission lines.

For large interconnected power systems with hundreds of generators and thousands of interconnecting lines, the number of possible splitting solutions increases rapidly and the offline approach becomes unacceptable. Detection of groups of coherent generators could be successfully implemented online when WAMS capabilities are considered. The measurement-driven techniques will always be advantageous over the model-based techniques because of the ability of the former ones to capture the dynamics of the real system and because there is no need to know the power system parameters. Having the snapshots of system-wide angles in real time, the only question remains as to which coherence identification algorithm to choose.

There are several items in the bibliography that are dedicated to measurement-driven coherence identification methods. The fast Fourier transform (FFT) method, applied to generator speed to extract the dominant nonzero component of the oscillation frequency, is proposed in [37]. The coherence is then identified by comparing the phases of the dominant component for all the generators. A spectral-analysis-based technique is also used in [38]. Methods that take into account the non-stationary and non-linear nature of system dynamical processes have been proposed in [39]. Empirical mode decomposition (EMD) followed by the Hilbert transform is used in [39] to derive the instantaneous phase of the dominant oscillation modes. Instantaneous phase differences are then used to detect the coherence between machines. The principal component analysis (PCA) method as applied to the data of generator speed and bus angles is proposed in [40]. PCA is a clustering method where a set of presumably correlated random variables are transformed into a new set of uncorrelated variables (principal components), which represent the linear combination of the originals. Then the impact produced by the variation of the original data on the principal components is explored. An artificial-neural-network-based method is proposed in [41], particle-swarm and k-means techniques are described in [42]. The partitioning-around-medoids (PAM) method is proposed in [43]. This method is based on the calculation of dissimilarity indexes followed by an iterative search for groups for which the sum of dissimilarities is minimised. Hierarchical clustering and self-organising feature map methods are used in [44] and [45], respectively. [46] explores the similarities between the trajectories of the angles by calculating four weighted indexes each representing a distinct property: angle deviation, direction of swing, speed deviation, and change of swing direction. A simple

and computationally efficient algorithm based on Pearson correlation coefficients is presented in [47].

An example of Pearson-correlation-coefficient-based generator grouping will be further illustrated using the model of the Latvian power system [48]. A simplified structure of the Latvian 330 kV network with five major generation sources *G1…G5* is presented in Fig. 4.2. The Latvian power system has interconnections with the Estonian (*EE*), Lithuanian (*LT*), and Russian (*RU*) power networks.

Groups of coherent generators can be identified online according to the methodology described in [48]. The method is based on generators' angle control. The correlation coefficient CR_{ij} of generators i and j is calculated according to Formula (4.2):

$$CR_{ij} = \frac{\sum_{n=1}^{N}\left(\varphi_i - \overline{\varphi}_i\right)\left(\varphi_j - \overline{\varphi}_j\right)}{\sqrt{\sum_{n=1}^{N}\left(\varphi_i - \overline{\varphi}_i\right)^2 \sum_{n=1}^{N}\left(\varphi_j - \overline{\varphi}_j\right)^2}}, \tag{4.2}$$

where φ_i and φ_j stand for the generators' voltage vector angles and $\overline{\varphi}$ is the average of the N samples. The correlation coefficients range from –1 (the strongest negative correlation) to +1 (the strongest positive correlation). The observation time is defined by a sliding window T (data buffer), in which the oldest sample is discarded as soon as a new sample becomes available.

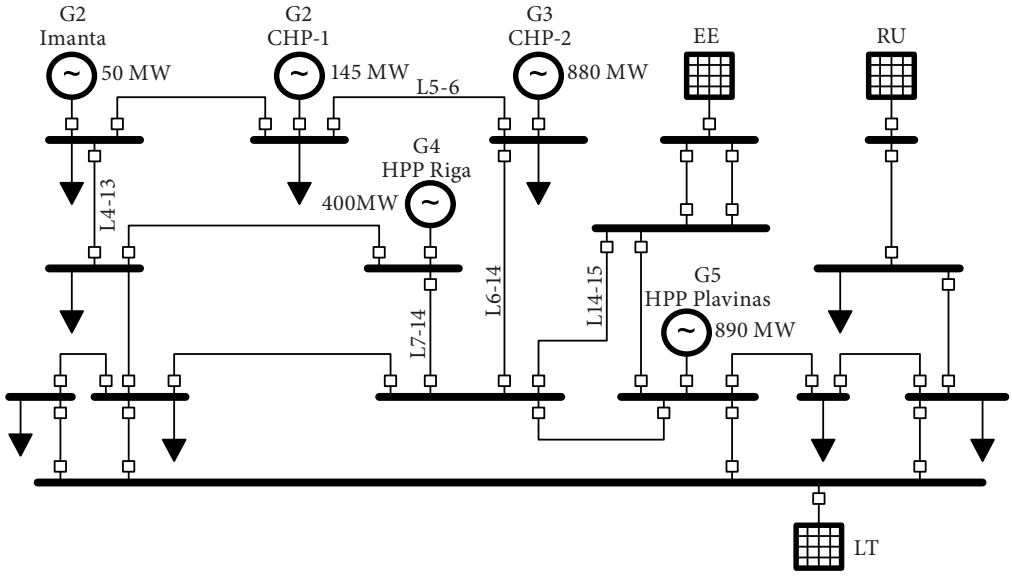

Fig. 4.2. The 330 kV network of the Latvian power system (simplified) [48]

The coherence determination procedure uses the data from the history data buffer, which will be "frozen" as soon as the angle difference between any pair of generators exceeds the maximum allowed limit *C1* (Fig. 4.3).

Two conditions indicate the generators' coherence; the value of the correlation coefficient of the generator pair CR_{ij} is close to its maximum value (1.0) and the correlation coefficient does not change significantly during observation. The groups of coherent generators are formed by comparing the values of the correlation coefficients with constant *C2* and comparing the standard deviation of the correlation coefficient, S_{ij} (4.3), with constant *C3* (Fig. 4.3).

$$S_{ij} = \sqrt{\frac{\sum_{n=1}^{N}\left(CR_{ij} - \overline{CR}_{ij}\right)^2}{N}}, \tag{4.3}$$

where $\overline{CR}_{ij}$ is the average of the N calculated correlation coefficients.

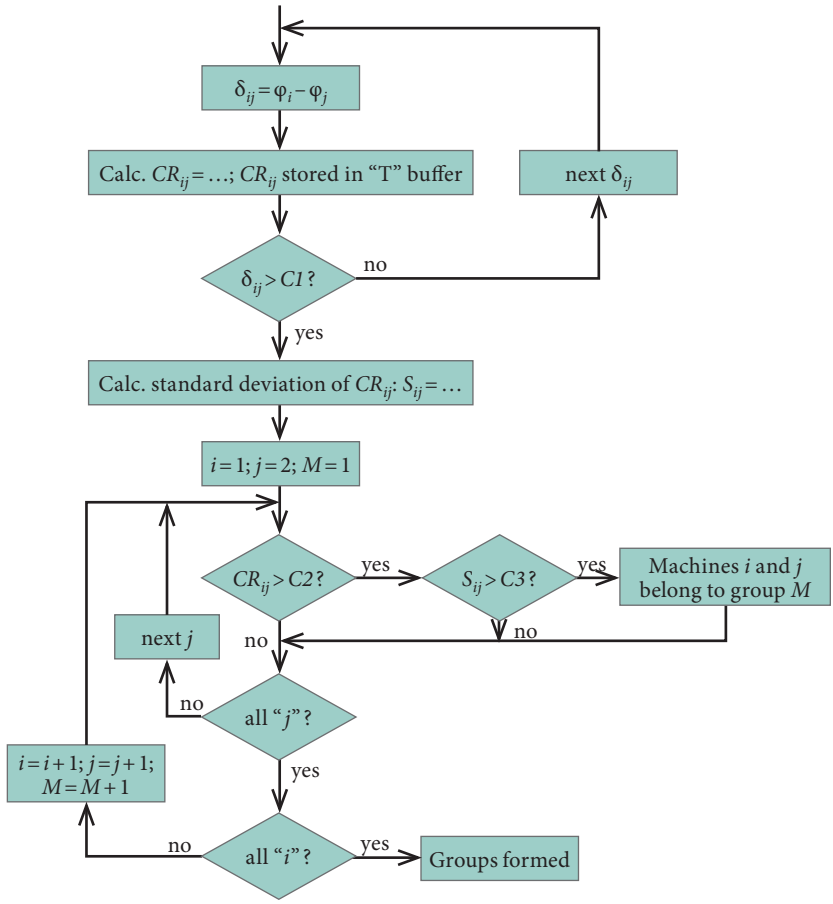

Fig. 4.3. Flowchart for grouping coherent generators

Coherent generators groups' identification time window length T was set to 1 second for all simulated scenarios, which corresponds to 50 data samples. The maximum allowed angle difference between any pair of generators' angles (*C1*) was set to 360 electrical degrees. The generator grouping constants *C2* and *C3* were set to $C2 = 0.8$ and $C3 = 0.1$.

OOS regimes were created as a result of short circuit applied to one of the critical transmission lines, followed by tripping of the circuit breakers of the faulted line. The results of OOS regime simulation for several scenarios are presented in Figs. 4.4–4.8. Each scenario is presented with two charts; the first chart shows the generators' angle variation after the contingency has been applied, and the second chart shows how the correlation coefficient, calculated for a one-second sliding window, changes in time. The correlation coefficient for the pre-fault regime may have a meaningless value (the denominator in (4.2) may have zero value); this is why the correlation coefficient charts start from the 1 s time point.

The first scenario is a short circuit applied to line *L14–15* (Fig. 4.2). The purpose of this simulation was to create a condition in which all the machines of the Latvian power system swing together relative to the neighbouring networks (the Estonian and Lithuanian ones). While the maximum angle setting *C1* was not reached in this case (Fig. 4.4), the correlation coefficient chart shows that CR_{ij} for all pairs of generators asymptotically approaches 1 at the time moment of 2 s. This indicates that all the generators will form one large group and there is no asynchronous operation between the generators of the Latvian system. In this case, islanding should be done by tripping the lines that interconnect the Latvian network with the Estonian and Lithuanian networks.

The second scenario is a short circuit applied to line *L7–14*. Power transfer from the Estonian side was intentionally limited for this scenario (one of the two parallel lines from the side of the Estonian network was not in operation). Generators *G1*, *G2,* and *G4* swing together with respect to other machines and *G1* and *G2*, finally running out of synchronism (Fig. 4.5). The maximal angle setting value was reached at approximately 1.2 s. The correlation coefficient of generator pairs *G1*, *G2*, and *G4* has the highest value (close to 1.0), indicating that generators *G1*, *G2,* and *G4* form a group that is operating asynchronously with respect to other machines. Generator *G4* finally settles down after the first complete rotation circle. This fact is observed in the correlation coefficient chart, where *CR(G1,G4)* and *CR(G2,G4)* diverge from 1, starting from 1.5 s. The correlation coefficient *CR(G1,G2)* remains almost constant with the standard deviation not exceeding $S_{12} = 0.005$, while the standard deviation of the correlation coefficients for all the remaining pairs exceeds the *C3* threshold. If the decision was made at the time moment of 2.0 s, then only generators *G1* and *G2* constitute the asynchronously operating group.

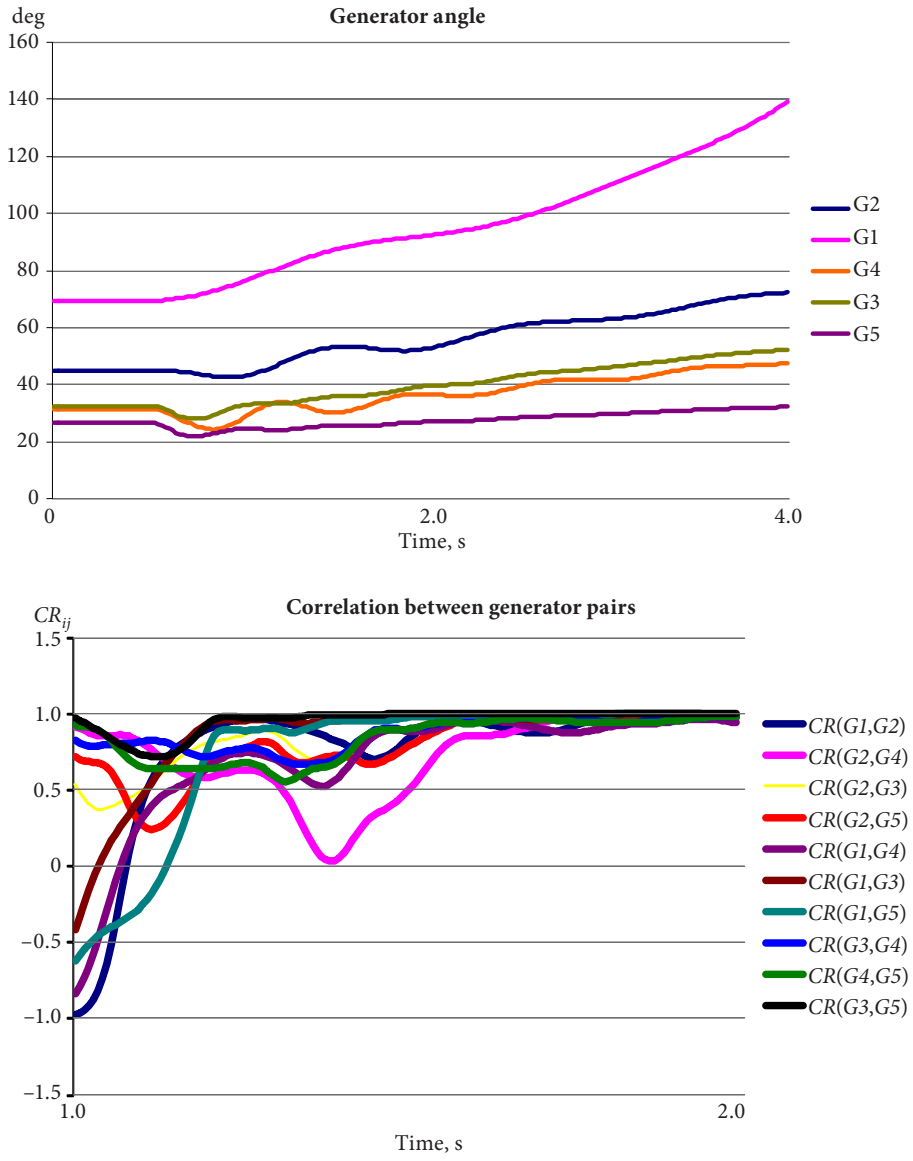

Fig. 4.4. Scenario with the Latvian network generators forming one group

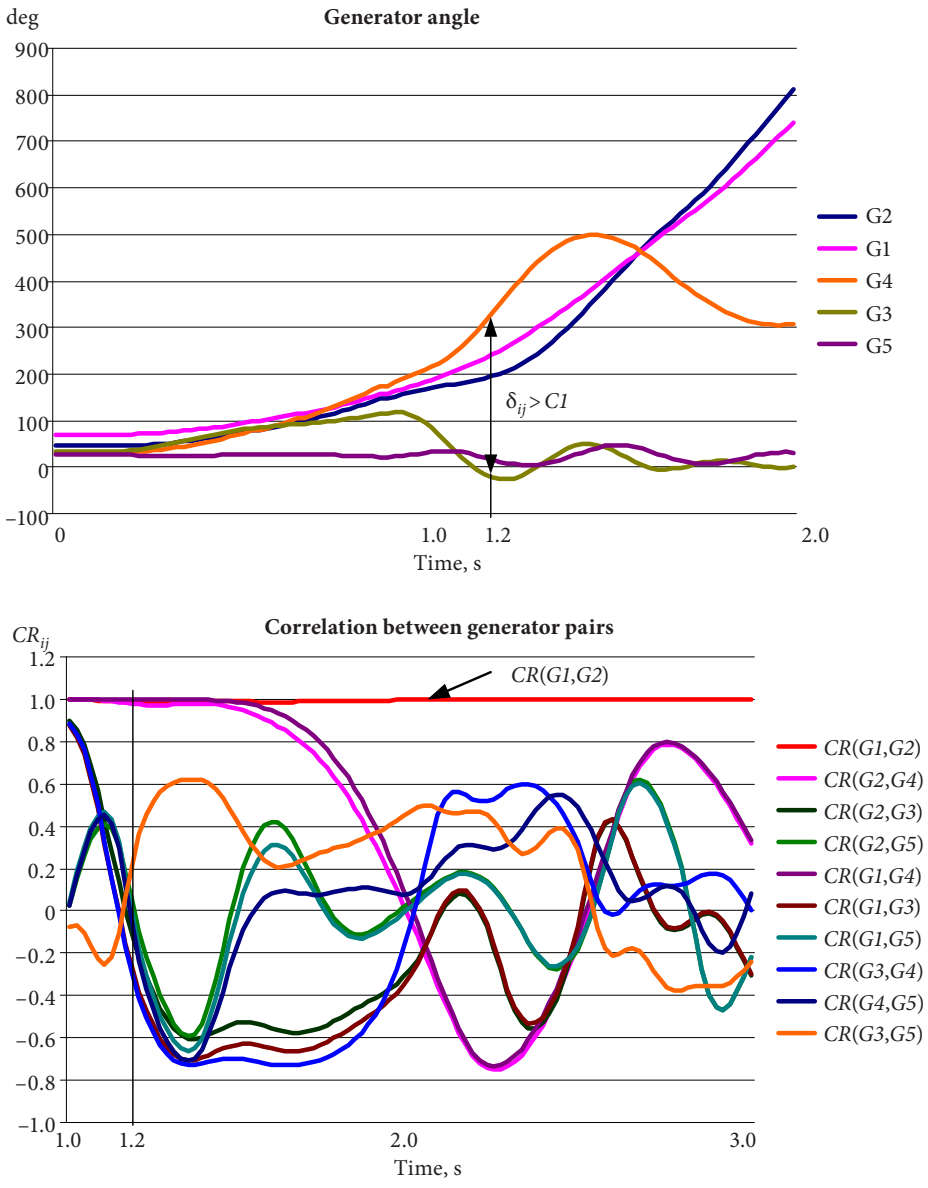

Fig. 4.5. Scenario with *G1* and *G2* going out of step

The well-damped behaviour of the remaining machines is observed after splitting the network by means of tripping lines *L5–6* and *L4–13* (Fig. 4.6).

In the third scenario, short circuit was applied to line *L6–14*. Two generators, *G3* and *G1*, are running out of synchronism (Fig. 4.7).

The correlation coefficient *CR(G1,G3)* is close to 1.0 and remains almost constant (the standard deviation of *CR(G1,G3)* does not exceed $S_{13} = 0.02$), while the correlation coefficients of all the other pairs significantly diverge, starting from 1.3 s. The maximum angle constant *C1* was exceeded at the time moment of 1.2 s, but reliable grouping of generators can be made at the time moment of approximately 1.5 s.

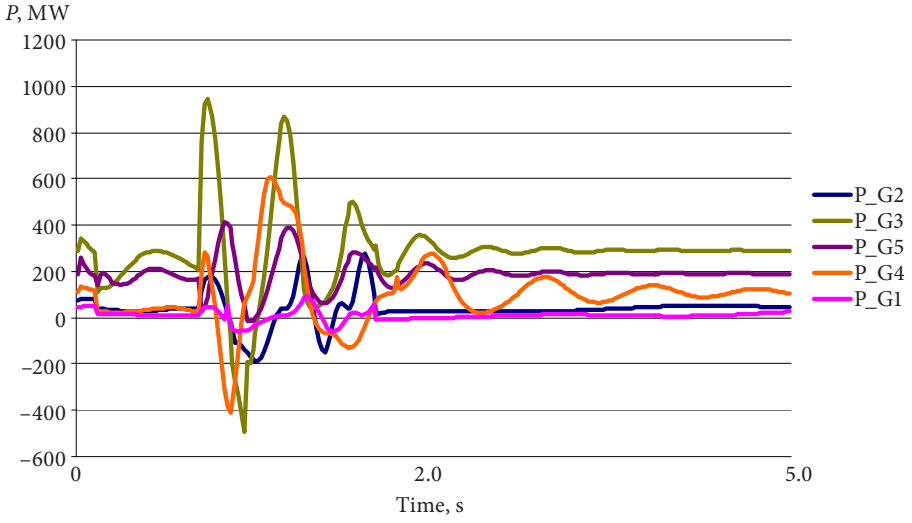

Fig. 4.6. Electrical power of generators after tripping lines *L5–6* and *L4–13*

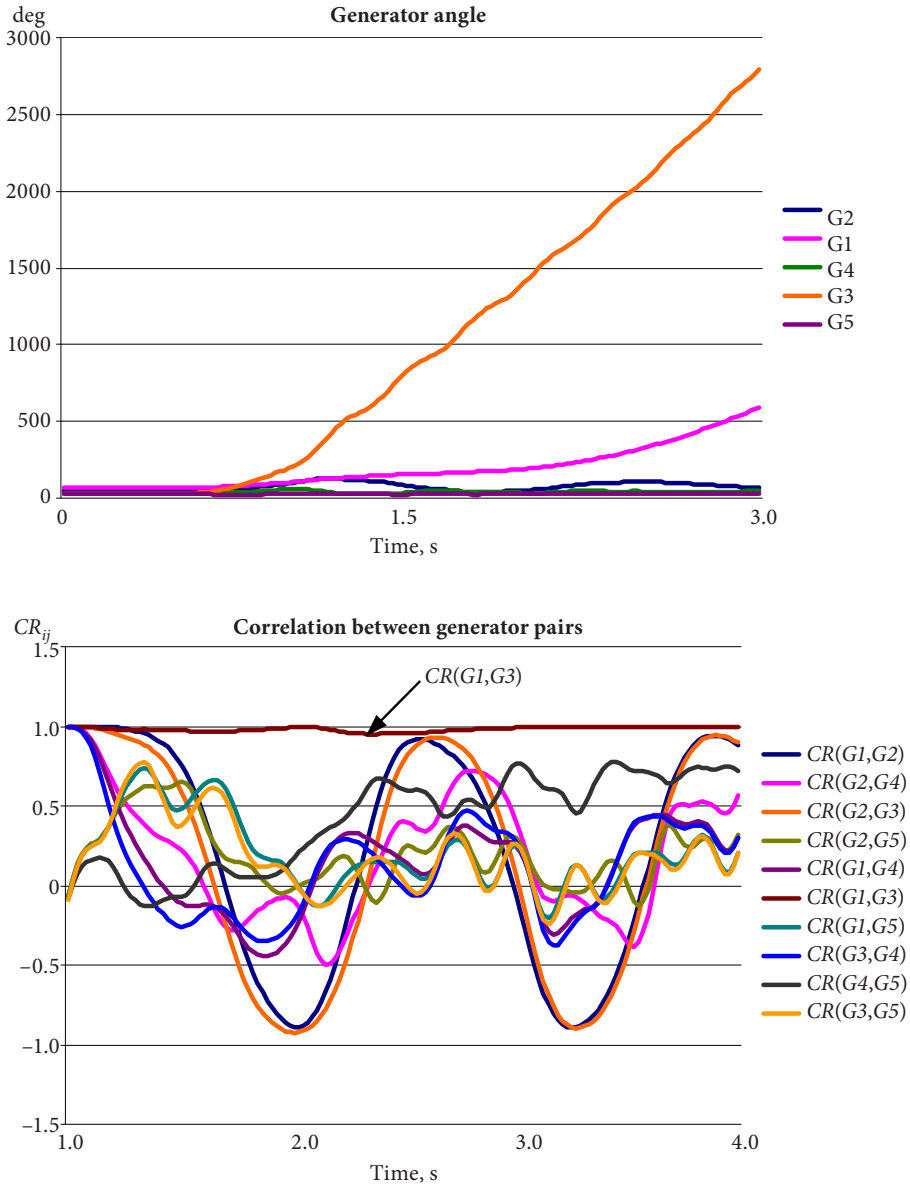

Fig. 4.7. Scenario with *G1* and *G3* going out of step

Despite the fact that *G1* and *G3* both operate asynchronously with respect to the remaining network, the only suitable splitting decision is the tripping of line *L5–6*, which only disconnects the *G3* generator. In this case, generator *G1* needs to be shut down separately. The result of such splitting at the time moment of 1.8 s is presented in Fig. 4.8.

The examples above reveal an inherent contradiction in controlled splitting. The confidence in correctly conducted grouping increases with the increase of observation time, but the effectiveness of the network-splitting action decreases with the passing of time after the disturbances. The preferences given to one or another method of generator grouping will generally depend on the answer to the following question: can coherent groups be reliably formed before the time period when the splitting decision needs to be taken expires? The answer to this question may become a nontrivial task and can probably be found as a result of an acceptable compromise between both objectives. In such case, two approaches are possible.

The first approach assumes that islanding must be applied as soon as the OOS condition detection threshold has been exceeded. For this case, the group of generators (or just one generator) which has already been formed by the time point of OOS detection should be separated first. This initial splitting will affect the behaviour of the remaining machines and thus new rearrangements of the remaining generators are possible. Then the OOS detection procedure will be applied to newly formed groups.

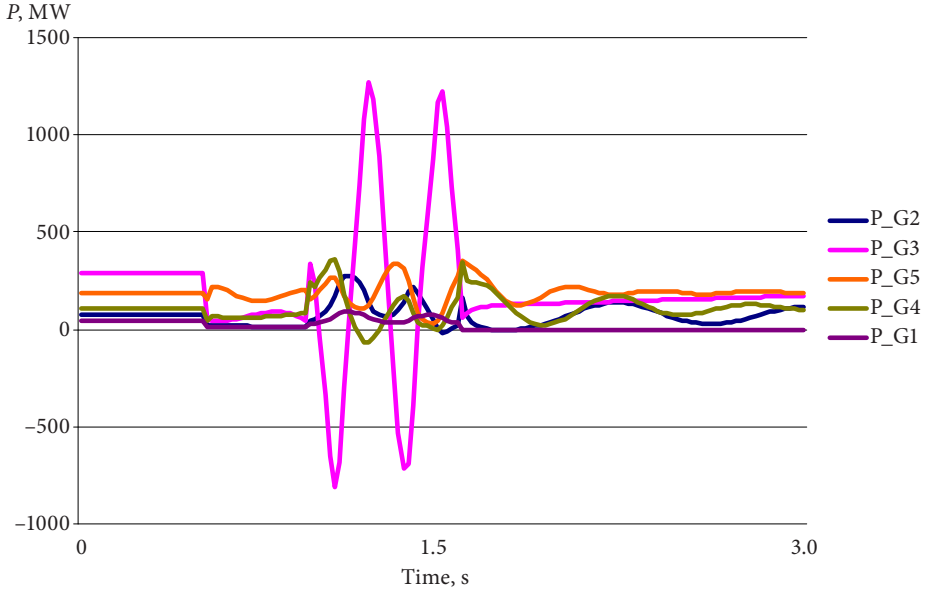

Fig. 4.8. Electrical power of generators after tripping line *L5–6* and switching off *G1*

Straightforward implementation of such an approach may result in cascaded network-splitting, which may or may not be acceptable depending on the network topology and the mode of operation. In the worst-case scenario, the entire network may be separated into an unacceptably high number of islands, and then self-healing of some islands becomes questionable. Two improvements could be made to avoid the above-described situation. The number of possible islands can be intentionally limited in advance. The maximum number of possible islands for a given network can be derived as a result of network stability studies and should be proved by the knowledge and practical experience of the power system operator. The second improvement is related to the recognition of acceleration/deceleration trends for different groups. As soon as an OOS condition has been detected between two groups, the trends of acceleration or deceleration for all the other groups have to be analysed. The "closest" groups of accelerating generators can be treated as an accelerating cluster, and a similar approach can be applied to decelerating groups. Then, the splitting decision separating the clusters should be initially found and only after splitting should the behaviour within the cluster be analysed further. The closeness rating between two groups can be obtained as a result of estimating the aggregated acceleration/deceleration for each group and then sorting out the groups with the closest trends in acceleration/deceleration.

The second approach to resolving the contradiction between the time needed for confident grouping and the time of splitting consists in assisting the online grouping procedure by offline, model-based information. The tendencies in the behaviour of generators in response to various contingencies can be identified offline and then used as references for the online-measurement-based technique. If the results of online grouping are in good agreement with the scenario simulated offline, the grouping can be considered proven and the splitting decision can be taken immediately. If no similarities are found, the time of splitting can be extended until the classification has been done or until the critical OOS threshold has been reached. Presumably, this approach can be implemented as an online technique, which is assisted by an offline-built decision tree.

In conclusion, WAMS-based generator grouping techniques allow the very important objective of controlled splitting to be achieved. The formation of islands in accordance with the generator slow coherence principle allows the preliminary islanding decision to be made. The risk of intra-island asynchronous operation is significantly reduced if the splitting decision relies on the coherence of the generators, and thus the potential of island self-healing increases. These objectives cannot be fully achieved by using traditional, local-measurement-based methods, and this is why the system-wide-measurement-driven approach provides much more confidence in finding a proper splitting solution.

4.4. Islanding strategies

Coherence-based generator grouping helps in deciding between which groups of generators the network-splitting should be done. Typically, for a large-scale power system there are several ways of how groups of asynchronously operating generators can be separated. Depending on the particular choice of the transmission lines to be tripped, the islands formed will differ in configuration as well as in the power balance within the islands. A successful strategy of controlled splitting implies that an acceptable generation-load balance should be achieved within each island, while it is accepted that the level of services to the customers may deteriorate. It is rarely the case that a network is separated into perfectly balanced areas. Naturally, load-rich and generation-rich areas will emerge after splitting. The under-frequency load shedding scheme (UFLS) will be applied to load-rich areas while generation regulation/rejection is a typical method for providing the balance within generation-rich areas. The successful islanding strategy is aimed at reducing the power imbalance in the post-islanding configuration, thus allowing less load to be shed or excessive generation to be tripped. Assuming that generator groups have been established, the remaining objectives of controlled islanding can be formulated as follows:

1. The splitting boundary should be chosen between groups of coherent generators.
2. The cutset of the transmission lines should be chosen in such a way that load-generation imbalance within the islands should be minimised.
3. If the splitting boundary is intruding into the networks of different transmission system operators (TSO), the TSOs should prove/coordinate the chosen cutset beforehand.
4. Transmission lines and associated facilities within each island should not be overloaded after splitting.
5. Each of the islands formed should be capable of black start.

Immediate fulfilment of all these conditions is a challenging task. Some of the objectives are in contradiction with each other, and thus an optimal decision cannot be achieved if each task is considered separately. Nevertheless, some reasoning can be applied that may help in arranging the tasks according to their importance.

Fulfilment of the first condition seems to be mandatory because only synchronous intra-island operation will preserve the island formed from further fragmentation. Only if there are no asynchronously operating areas within the island could all actions to maintain island self-healing be successfully performed. The second task consists of choosing the optimal cutset to form the island with coherent machines while providing the minimal

generation-load imbalance within the islands. The minimal imbalance could be achieved by attaining more or less load depending on the generation capacities of the presumable island. The decision as to which load buses should remain within the islanded part of network may be affected by several constraints. Typically, bulk power transfer between large interconnected networks is dictated by various economical and structural reasons. Power is transferred from the areas with a large generation capacity to the areas with an energy deficit, and these areas often belong to different TSOs, and they may even belong to the networks of different countries. When an OOS condition occurs between large areas, one with generation capabilities and the other with an energy deficit, then the native constraints of different TSOs' networks should be considered. Typically, every TSO has its own plan of defence against network collapse. The particular defence strategy is a result of the TSO's comprehensive knowledge about the network equipment performances, the customer types and the protection systems in use. Often the defence plans of different TSOs are not entirely coordinated; the UFLS settings may be different, as may the generation rejection/regulation capabilities; the priorities in load shedding differ depending of the region. If the minimal generation-load imbalance criterion does not account for these aspects, then the island formed may include parts of the network of which each has its own, often incompatible and contradictory, properties. In such a situation island self-healing becomes problematic and the approach involving splitting along the boundary between TSOs may be preferable over the minimal imbalance objective.

The fourth and fifth objectives are both intended to help island survival after network-splitting. The most problematic part is the self-healing of the deficient islands. Efficient UFLS actions should be implemented to support the frequency and voltage profiles within acceptable margins, thus providing generation-load balance without overloading the generation and transmission capabilities of the network. While it is acceptable that island generation and transmission capacities could be used at ratings higher than normal, a long-term overload may result in the tripping of the corresponding protection devices, and thus the generation-load balance will be further stressed. The worst-case scenario of unsuccessful UFLS/defence actions should also be considered. If the power supply collapses completely, generator units should be available that are capable of re-energising the network (black-start-capable generators).

Several methods are described in literature that are dedicated to finding the optimal splitting decision. The majority of the methods are largely based on the graph theory and use various graph manipulation techniques. The main idea lies in representing the entire network by a weighted graph where the network buses are represented by the graph vertices and the transmission lines are represented by the graph edges. Then, a power system with n buses can be described as a connected undirected weighted graph

$G=(V, E, W_v, W_e)$, where $V=\{v_1, v_2, \ldots v_i\}$ is a set of indexed vertices, $E=\{E_{12}, E_{13}, \ldots E_{ij}\}$ is a set of edges interconnecting vertices, $W_v=\{w_{v1}, w_{v2}, \ldots w_{vi}\}$ is the set of weights assigned to the vertices, and $W_e=\{w_{e12}, w_{e23}, \ldots w_{eij}\}$ is the set of weights assigned to the edges. Then, the network topology is described by a set of binary values: $e_{ij}=0$ if there is no interconnection between bus i and bus j, or $e_{ij}=1$ if an interconnection exists. The vertex weight W_{vi} equals the active power injection at a given bus and may have a positive or negative value. The edge weight W_{eij} equals the absolute value of the averaged real power transmitted through the line. It is assumed that reactive power compensation after the islanding can be provided locally. A graph representation of a 3-generator 9-bus system is shown in Fig. 4.9, with the bus weights shown in blue and the transmission line weights shown in red.

As soon as the network graph has been derived, graph minimisation rules can be applied, which effectively reduce the network while retaining all the useful information. The principles of network graph reduction are illustrated in Fig. 4.10.

The vertices with zero weight can be eliminated (Fig. 4.10 a)). A vertex that has only one edge can be combined with the adjacent vertex (Fig. 4.10 b)). Vertices belonging to one coherent group and the associated edges can be collapsed (Fig. 4.10 c)). The network reduction can be implemented online after groups of coherent machines have been detected.

Given a graph representation of the network, the network-splitting problem is transformed into a graph-partitioning problem with several restrictions to be met and several objectives to be fulfilled. Then, the network-splitting problem can be formulated as follows. Given a graph $G=(V, E, W_v, W_e)$, a set of edges $E_{cut} \in E$ has to be found, by removing which the

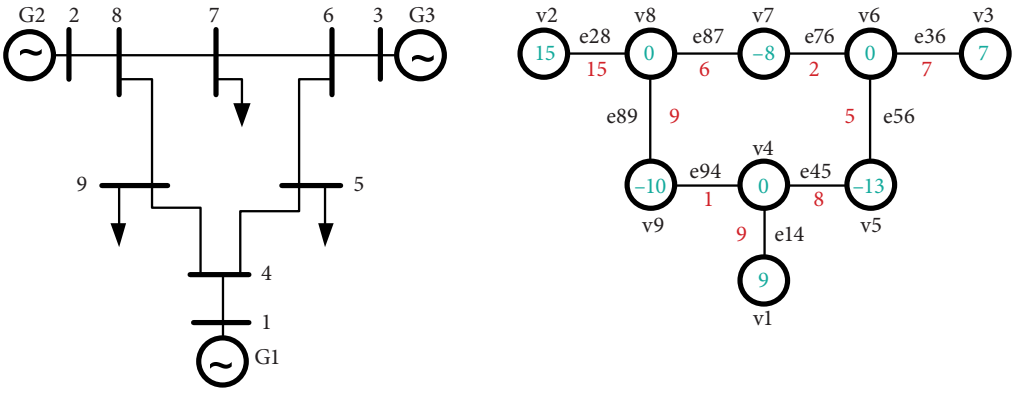

Fig. 4.9. 3-generator 9-bus network and corresponding graph representation

graph will be partitioned into two sub-graphs $G_1 = (V_1, E_1, W_{1v}, W_{1e})$ and $G_2 = (V_2, E_2, W_{2v}, W_{2e})$ with the following conditions satisfied:

1. Each of the sub-graphs G_1, G_2 is a connected graph.
2. Each of the sub-graphs G_1, G_2 contains only vertices that are coherent.
3. The total weight of the vertices for the sub-graphs G_1 and G_2 is minimised:
   $\min(|\sum_{v_i \in V_1} w_i|)$ and $\min(|\sum_{v_i \in V_2} w_i|)$.
4. The weights of the edges for each sub-graph should not exceed thermal/stability limits: $w_{eij} \leq k_{ij}$ for all $e_{ij} \in E_1$ and $e_{ij} \in E_2$. This condition can be checked only after the power flow has been calculated, and thus power flow analysis for the presumed islands becomes the last step to single out the optimal splitting decision from non-optimal ones.

Exploring the entire strategy space of all the possible splitting decisions by using brute-force search methods is not suitable here because the number of candidates will explode exponentially as the size and complexity of the network increases [49]. The computation time needed to check all the candidates then quickly exceeds the limitations of a system operating in real time.

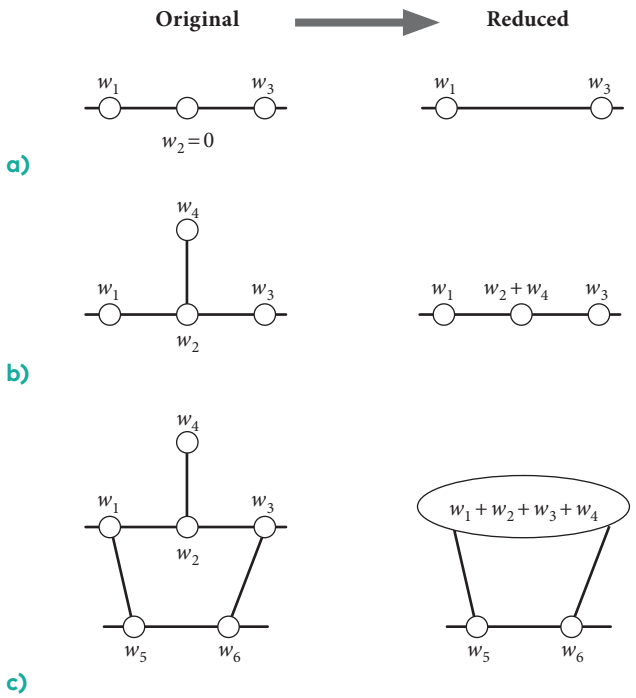

Fig. 4.10. Network graph reduction techniques

Thus, the majority of methods strive to reduce the searching space and to decrease the computational burden.

Most recently, a real-time approach using the graph theory and a searching method based on an Ordered Binary Decision Diagram (OBDD) has been presented in [49]–[51]. OBDD is a directed acyclic graph representation of a Boolean function [52]. The main idea lies in transforming the network-splitting problem into a satisfiability-checking problem for the Boolean function, which can then be solved by an OBDD-based model-satisfiability-checking tool, such as a symbolic model verifier [50]. As soon as the network is represented by a graph, the network topology can be described with a matrix where each element is a Boolean variable b_{ij}, which only takes a value of 0 or 1. An example of an adjacency matrix created for the network graph in Fig. 4.9 is presented below.

$$A = \begin{bmatrix} 0 & 0 & 0 & b_{14} & 0 & 0 & 0 & 0 & 0 \\ 0 & 0 & 0 & 0 & 0 & 0 & 0 & b_{28} & 0 \\ 0 & 0 & 0 & 0 & 0 & b_{36} & 0 & 0 & 0 \\ b_{14} & 0 & 0 & 0 & b_{45} & 0 & 0 & 0 & b_{49} \\ 0 & 0 & 0 & b_{45} & 0 & b_{56} & 0 & 0 & 0 \\ 0 & 0 & b_{36} & 0 & b_{56} & 0 & b_{67} & 0 & 0 \\ 0 & 0 & 0 & 0 & 0 & b_{67} & 0 & b_{78} & 0 \\ 0 & b_{28} & 0 & 0 & 0 & 0 & b_{78} & 0 & b_{89} \\ 0 & 0 & 0 & b_{49} & 0 & 0 & 0 & b_{89} & 0 \end{bmatrix} \tag{4.4}$$

$b_{ij}=1$ if there is an edge between vertices i and j or $b_{ij}=0$ otherwise. All the possible paths from vertex v_i to vertex v_j can be described by a Boolean expression. Referring to Fig. 4.9, the interconnection between vertices v_8 and v_3 will be described as follows:

$$A_{83} = b_{89} \cdot b_{49} \cdot b_{45} \cdot b_{56} \cdot b_{36} + b_{87} \cdot b_{76} \cdot b_{36}, \tag{4.5}$$

where "·" and "+" denote logical operators AND and OR, respectively.

To separate vertices v_i and v_j is to decide upon a b_{ij} such that the above expression becomes equal to 0. The constraint of splitting between groups of synchronous generators can also be formulated in the form of a Boolean expression. For instance, if generators *G1*, *G3* constitute a coherent group and should be separated from *G2* (Fig. 4.9), this will be described with the following Boolean expression (4.6):

$$A_{13}\left[A_{14}A_{34} \oplus A_{24}\right]\left[A_{15}A_{35} \oplus A_{25}\right]\left[A_{16}A_{36} \oplus A_{26}\right]\left[A_{17}A_{37} \oplus A_{27}\right]\left[A_{18}A_{38} \oplus A_{28}\right]\left[A_{19}A_{39} \oplus A_{29}\right] \tag{4.6}$$

where $\oplus$ is the logical "Exclusive OR" operator and "·" is omitted.

The constraint of minimal power imbalance after network separation can be converted into a satisfiability-checking problem if the weights of the vertices are represented by Boolean variables. To do this, the vertex weight

is scaled up and rounded, thus yielding an integer value with minimal loss of accuracy. Then, these integer values (including negative ones) are binarily encoded and the further mathematical operations are translated into equivalent logic operations. After the problems of coherent groups and minimal imbalance have been converted into Boolean representation, the OBDD of each problem can be constructed and suitable splitting decisions are searched for, using the OBDD's manipulation techniques. A comprehensive description of the manipulation of symbolic Boolean functions with OBDDs is provided in [52], [53]. At the last stage, a simplified power flow analysis is performed on the islands to discard splitting decisions that violate the operating constraints, e.g., transmission line limits and the ratings of the transformers.

Another theoretical approach that uses slow coherence and graphs is described in [54], [55]. The method of network splitting is treated as a network graph partitioning problem. In providing the islanding strategy with minimal imbalance after splitting, the following considerations are provided. Once the groups of coherent generators have been formed, the power flows through transmission lines interconnecting groups of generators will indicate the amount of power deficiency in the load-rich area and the amount of excessive power in the generation-rich area. Then the net flow between areas becomes a clear indicator of power imbalance within each area. Therefore, the objective of power imbalance minimisation is converted into searching for the cutsets with a minimal net flow between islands (minimal cutset) while providing separation of the slow-coherence-based groups. The formulation of the minimal-cutset problem with the application of power network partitioning in mind is provided in [56]. Before minimal-cutsets-based graph partitioning is applied, the network graph undergoes an extensive simplification process. In addition to the graph reduction principles presented in Fig. 4.10, the closed loop removal technique is applied to the network graph. A closed loop is then replaced with a single node (Fig. 4.11 a)) [54]. The minimum spanning tree (MST) of the network graph containing coherent generators is built and then a tree collapse algorithm is applied to replace the MST with a single node. To construct the MST, the breadth-first searching (BFS) algorithm is used, followed by a specific trimming procedure to remove irrelevant nodes (Fig. 4.11 b)). All the transformations that the nodes undergo during the processes of spanning tree building and collapsing are recorded in a spanning tree creation history. As a result of graph simplification and MST collapse, the size of the original graph is reduced several times. The reduced graph is then partitioned using the METIS graph-partitioning software [57]. Typical examples of METIS software implementation are large-scale numerical simulations on parallel computers, which require distribution of the finite element mesh between the processors. The aim of this distribution is to balance the computations among the processors while minimising

the communication resulting from the placement of adjacent elements to different processors [57]. METIS can partition an unstructured graph into a user-specified number of parts, using either the multilevel recursive bisection or the multilevel k-way partitioning paradigm [58]–[60]. The cutset obtained corresponds to a simplified graph of the network and may thus fail to designate the particular lines to be tripped. To recover the lines of the original network which corresponds to the cutset, the history of spanning-tree creation is analysed and then the lines that belong to the cutset can be found out.

Network graph partitioning by using some of the basic provisions of the spectral graph theory has been proposed in [61]. The spectral graph theory is the study of graph properties by means of analysing the eigenvectors and eigenvalues of the matrices associated with the graph. Given a graph $G=(V,$

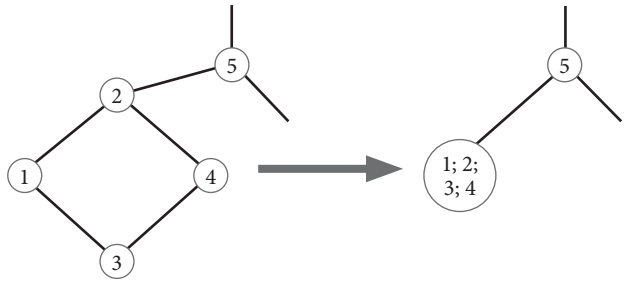

a) Removal of closed loops

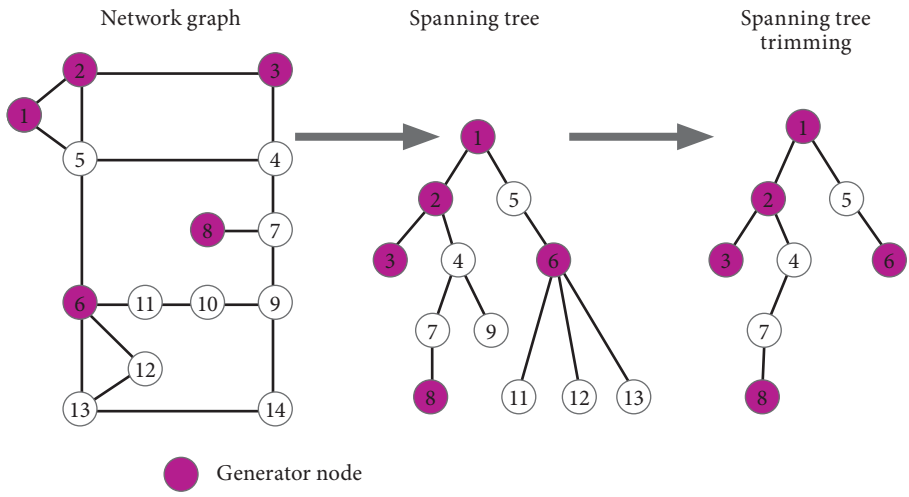

b) building and trimming a spanning tree

Fig. 4.11. a) Removal of closed loops; b) building and trimming a spanning tree (Adopted from [54])

E), multiple matrices can be defined from it. The adjacency matrix of G, $A=(a_{ij})$ is defined such that

$$a_{ij}=\begin{Bmatrix}1,(i,j)\in E\\0,(i,j)\notin E\end{Bmatrix}. \tag{4.7}$$

The degree matrix of G, $D=(D_{ij})$ is defined such that

$$d_{ij}=\begin{Bmatrix}d_i,(i=j)\\0,(i\neq,j)\end{Bmatrix}, \tag{4.8}$$

where degree d_i of vertex i corresponds to the number of edges that are incident with the vertex.

Then the Laplacian matrix of graph G is the matrix

$$L=D-A. \tag{4.9}$$

Given a square matrix $A\in\mathbb{R}^{n\times n}$ and vector $z\in\mathbb{R}^n$, the product $A\boldsymbol{z}$ is another vector in $\mathbb{R}^n$.

Special vector $\boldsymbol{v}$ for which it is true that $A\boldsymbol{v}=\lambda\boldsymbol{v}$ is called the eigenvector of A. This vector has the same direction as $\boldsymbol{v}$ but is scaled by scalar factor λ; $\boldsymbol{v}$ is called an eigenvector of A and λ is the eigenvalue corresponding to eigenvector $\boldsymbol{v}$. An $n\times n$ matrix will have at most n of eigenvector-eigenvalue pairs. To calculate the eigenvalues of an $n\times n$ matrix A, let us find all the possible solutions λ of the equation

$$\det\left(A-\lambda I_n\right), \tag{4.10}$$

where I_n is the $n\times n$ identity matrix.

Then the eigenvector corresponding to the eigenvalue λ can be calculated from

$$\left(A+\lambda I_n\right)\boldsymbol{v}=\mathbf{0}, \tag{4.11}$$

where $\mathbf{0}$ is the vector of an appropriate size (here – of length n) where every entry is 0.

Referring to the problem of network graph partitioning, the procedure looks as follows. Given a network graph $G=(V, E)$, let us construct Laplacian $n\times n$ matrix L, calculate the eigenvector-eigenvalue pairs of L, label eigenvalues in increasing order such that $\left\{\lambda_1=0,\leq\lambda_2\leq,\ldots\leq\lambda_n\right\}$. An important property of the Laplace matrix of the graph with non-negative weights is that L is positive semidefinite, symmetric and singular and has non-negative eigenvalues. The set of eigenvalues $\left\{\lambda_1,\lambda_2,\ldots\lambda_n\right\}$ of the Laplacian $n\times n$ matrix is referred to as the Laplacian spectrum of the graph. Analysis of graph spectra can tell us how well the graph is connected. The strength of graph connection reflects the graph connectivity properties in terms of number of nodes, number of paths and path lengths needed to reach from a given vertex to any other vertex of the graph. It is known from the spectral graph theory that the eigenvector-eigenvalue pair (v_2, λ_2), with the second smallest eigenvalue λ_2 exhibits the connectivity properties of the graph.

This eigenpair was termed by Fiedler the *algebraic connectivity* of the graph [62], [63].

The eigenvector $\boldsymbol{v}_2$ that corresponds to the second-smallest eigenvalue λ_2, is known as the Fiedler vector and is used to partition the vertices into two subsets. Let $n = |V|$ and each vertex be assigned with a unique number {1,2, …*n*}. Considering that $L \in \mathbb{R}^{n \times n}$ and $\boldsymbol{v}_2 \in \mathbb{R}^n$ vertex *i* corresponds to a single entry *i* of $\boldsymbol{v}_2$. Then graph *G* can be partitioned into two graphs *G1* and *G2* by means of examining the sign of $\boldsymbol{v}_{2i}$ for each vertex *i*. All vertices *i* with $\boldsymbol{v}_{2i} < 0$ will constitute graph *G1* and all the remaining vertices constitute graph *G2*. The graph minimal cut optimisation problem can be formulated as follows. Let $G = (V, E)$ be a graph. Given a set $S \subseteq V$ of the vertices of G, let $\overline{S} = V \setminus S$ be the complement of *S* in *V*. Let $|S|$ and $|\overline{S}|$ denote the number of vertices in *S* and $\overline{S}$, respectively. Let $e(S) = e(\overline{S})$ denote the number of edges between *S* and $\overline{S}$. The cut ratio ϕ of cut S–$\overline{S}$ can be defined as follows:

$$\phi(S) = \frac{e(S)}{\min\left(|S|, |\overline{S}|\right)}. \tag{4.12}$$

Then the cut of a minimum ratio is the cut that minimises ϕ(*S*):

$$\phi(G) = \min_{S \subseteq V} \phi(S). \tag{4.13}$$

The cut ratio (4.13) is aimed at minimising the number of edges across the cut while penalising cuts with a small number of vertices within *G1, G2*. In [61], the cut ratio is defined as follows:

$$\phi(S) = \frac{e(S)}{d(S)d(\overline{S})}, \tag{4.14}$$

where $d(S) \equiv \sum_{u \subset V} d_u$, $d(\overline{S}) \equiv \sum_{u \subset V \setminus S} d_u$ are the sums of the degrees of vertices $d(u)$. This approach strives to minimise the number of edges to be cut, while stimulating the degree of connectivity within *G1* and *G2*.

The slow-coherence-grouping-based method of network-splitting which considers the objective of imbalance minimisation is described in [64]. After preliminary identification of the groups of coherent generators, the passive boundary area between these groups is explored. The passive boundary consists of non-generator buses which may belong to one or another coherent group. The main idea lies in the minimisation of the power imbalance by means of attaching the load buses of the boundary area to one or another coherent group (Fig. 4.12). Each bus of the boundary network is represented by a spanning tree and all the branches of the spanning tree, except generator-connected buses, are considered as candidates for the imbalance minimisation problem. The depth of search penetration into the network can be determined by the dimension of the matrix of electrical distances between each boundary bus and the generator bus [64]. A spanning-tree-based breadth-first search algorithm is used to determine all the possible combinations of buses which can be interchanged between areas. Then the

best solutions could be found that satisfy the minimal imbalance constraint. The optimal solution can be singled out as a result of finding an equilibrium between the maximum allowed imbalance and the maximum number of lines allowed to be cut. A similar approach has been described and evaluated in [65].

A decision-tree-assisted controlled splitting strategy has been evaluated in [66]. The goal of this approach is to avoid uncontrolled separation of the network by means of arming the out-of-step relays for the feasible cutsets while blocking all the other relays that may respond inadequately and trip undesired lines (Fig. 4.13). This approach does not entail online evaluation of the splitting boundary but helps preventing uncontrolled network separation at undesirable points. The DT uses the generator rotor angles and speeds as predictors and produces the "stable"/"unstable" decision for each scenario as well as states the degree of confidence for the decision. The splitting strategy consists of two stages. At the offline stage the DT is trained, using data regarding the angle and speed of the generators obtained from a dynamic processes simulation program. At this stage, scenarios with various degrees of the system stability should be simulated, starting from "extremely stable" towards "critically stable" and ending with "unstable" conditions. Generators' coherence along with preferable splitting decisions for each case should also be examined at this stage. A set of trained DTs is obtained as a result of extensive simulations, and the DTs are then inputted with real system measurements obtained online from the WAMS to produce the splitting decision in real time.

All of the above-described methods and approaches have been tested by the corresponding authors using standardised IEEE power system models,

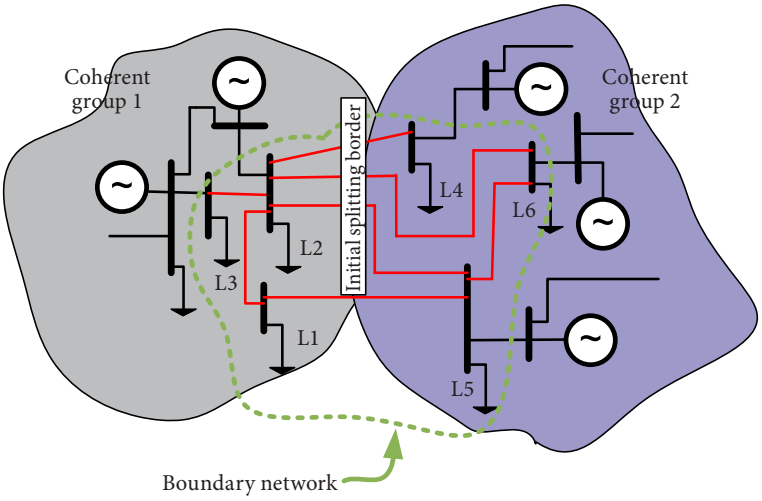

Fig. 4.12. A boundary network between two coherent areas. *L1–L5* could be "moved" between the groups to achieve a better balance within the groups (Adopted from [64]).

and some of the authors have also tested models of real power systems. The high level of confidence, the computational efficiency, and the applicability to each particular method were proved by the results of simulations. The computational complexity of the methods varies, and OBDD and spectral-theory-based methods require the largest computational resources. The computational burden can be significantly reduced if some parts of the complex task can be implemented offline or if several natural restrictions are taken into account in advance. For example, the huge search space can be efficiently limited by excluding those transmission lines which are not intended to be cut because of regional/environmental restrictions or simply because they do not have any effect on network partitioning. Similarly, the search space may be limited by including only those lines which interconnect large parts of networks that belong to different TSOs. The evaluation of the power system model dynamics for all feasible steady-state conditions and at various stressed conditions helps delineating the boundaries of the presumable search spaces, thus further reducing the computation time.

While the majority of the above-described methods are aimed at finding the splitting decision for a large-scale power system, a simplified approach can be efficiently used in the case when relatively small networks of different TSOs are interconnected by means of several high-capacity transmission lines. It is often the case that exactly these lines become the weak links between neighbouring networks. If this proposition has been confirmed by online analysis of generator grouping, then the transmission corridor will be the best candidate to cut the networks even though the compliance with

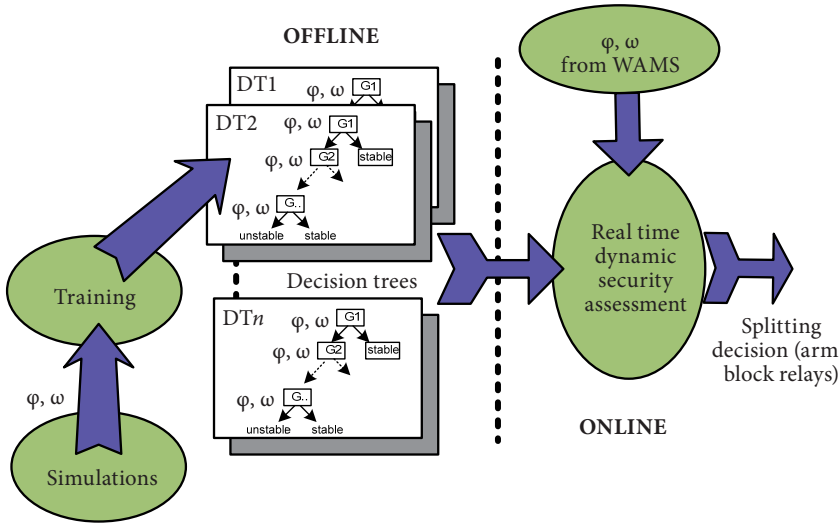

Fig. 4.13. Decision-tree-assisted network separation

the minimal imbalance criterion will not be optimal. It has already been mentioned above that every TSO should have a strategy plan to protect themselves against network collapse should the external interconnections be lost. Such a simplified approach is implemented within the interconnected networks of the Baltic States where the Latvian, Estonian, Lithuanian as well as Russian networks have a few interconnections that are considered the most probable candidates for network-splitting.

5. WAMS-BASED OOS DETECTION METHODS

All of the local-measurement-based OOS detection methods have a common distinct feature: the moment in time when a power swing is classified as unstable is determined solely by a set of predetermined constants (the settings of the protection terminals). Angular instability is a system-wide phenomenon that may affect large areas of the network, and the way the angular instability is evolving will be highly dependent on the particular configuration of the network, the pre-fault parameters, the network topology and the severity and location of the fault. Typically, protections of the local type are unable to adapt their settings in real time to all the possible network mode variations and to all the possible contingency scenarios. This is why in attempting to provide the highest dependability and security, protection settings are chosen in a very conservative manner. For blinder-and-timer-based schemes, the OOS condition is typically declared when the locus of apparent impedance crosses the left blinder, i.e., when the generators already exhibit pole slip. Moreover, the trip signal could be further delayed to avoid the peak currents resulting from the difference between the generator rotor angles being close to 180°. Line current differential-protection-based and SCV-based principles also exhibit a similar deficiency. The method of controlling the angle of the modelled vectors (implemented in AGNA, see Section 2.5), while allowing tripping before the generator pole slip, is still subjected to decision-confidence-related problems. AGNA settings are chosen as a result of extensive simulation of the power system dynamics and cannot be adapted to network state variations in real time. Thus, the conservative approach in the determination of settings would also be preferable here. As a generalisation about the methods used by local protections, it has to be said that they all lack the ability to predict with a high degree of confidence whether or not a power swing will be unstable. Attempting to predict an OOS condition by using solely local measurements, the protection security may be lost, which is unacceptable. The main reason for this inability to predict is that local protection only responds to the dynamical behaviour of the controlled parameter but is unable to analyse the instability phenomenon itself. In contrast, a much clearer view of the stability phenomenon will be provided if system-wide information is available. Knowing the initial state of the system and having in hand suitable models of the system elements, it is possible to forecast the system behaviour after changes in the system state have taken place.

Conventionally, the transient stability phenomenon is assessed by using various time-domain programs. Eurostag, ETAP, MATLAB, ETMSP, and EMTP are only a few examples of transient stability assessment (TSA) software packages. The main task of the TSA is the evaluation of the power

system behaviour in response to various disturbances. Two parts of the evaluation can be singled out for which the TSA should provide credible answers. The first part requires an answer to the following question: would the system be able to reach a new state of equilibrium after the disturbance? The second part requires an answer to the following question: what will be the new parameters of the power system after the system has reached the post-fault equilibrium state? From the OOS protection system point of view, the first question is of importance; namely, whether the system will lose stability after a disturbance. To answer this question, the system's response has to be evaluated.

Time-domain methods evaluate the power system's dynamical response using a power system model, which in turn is comprised of models of each individual component. In general form, the model of the power system dynamics can be represented with two sets of non-linear Equations (5.1) and (5.2):

$$\dot{x} = f\left(x, y, p\right); \tag{5.1}$$

$$0 = g\left(x, y, p\right). \tag{5.2}$$

Set of differential equations (5.1) is intended to describe the dynamics of the rotational elements of the system (generators and motors with the associated control units). Set of algebraic equations (5.2) describes the network and the loads. The dimension of vector x is defined by the required degree of accuracy of the model. Typically, the number of state variables required to accurately model a generator with an excitation system, a turbine and a governor exceeds ten. Static load does not introduce additional state variables and the dynamic load model may be represented sufficiently with two state variables. If needed, the models of static VAR compensators, FACTS and other equipment can be presented. The dimensionality of vector y depends on the number of nodes in the network. Vector p represents those parameters of the system which may influence the stability of the power system (the power of the generators, the amount of load, the transmission line loading and changes in network topology, disturbances, etc.). Considering WAMS-based stability assessment, the parameters described by vector p can be available online. Time-domain methods analyse the transient behaviour of the system by means of finding the solution of (5.1) and (5.2) in the time domain. The computation starts from the pre-disturbance condition and continues until it is decided that each of the synchronous machines maintains or loses synchronism with respect to the remaining network. Among the different system models, the one should be chosen that is most suitable for a given system state (pre-fault state, state during fault and post-fault state) and which most accurately describes its behaviour. Specific transient stability models are intended to evaluate the behaviour of the system when subjected to perturbations.

5.1. Dynamic security assessment

The analysis used to investigate a system's performance at the planning stage or shortly after the system state has been changed is known as the dynamic security assessment (DSA). The main goal of the DSA is to ascertain whether the existing or planned configuration of the power system is adequate to withstand the prescribed set of disturbances without loss of stability. This question can be answered after carrying out a dozen of simulations of various transients. A quantitative result can be obtained in the form of critical clearing time – the maximum time for which a fault may exist before the system loses stability. Extensive simulation also allows deriving various stability indices which designate how close to instability the system resides.

The possible concept of DSA, which relies on the availability of system-wide information, is shown in Fig. 5.1. Measurements gathered from the WAMS represent the actual state of the system which is refreshed in real time and compared with the previous state. The information required contains the actual condition of the generation/load balance, the electrical topology of the network and also information about network faults should be available from the protection systems. As soon as the state of the system changes for any reason (switching on or off of transmission lines, significant changes in the power balance, upon reporting the fault from the protection relays), the new state of the system is compared with the scenarios contained in the "instability library". At the initial stage, the "instability library" contains a set of scenarios modelled offline in the form "pre-fault state/applied contingency" for which it has previously been evaluated that the system becomes unstable. If the current state matches one from the "instability library", then system instability can be declared. Otherwise, the network model is refreshed to match the actual state of the system and then DSA studies are conducted by applying a set of prescribed contingency scenarios. Each contingency scenario is formulated in terms of fault type, location and duration, including the fault clearing sequence as well as the presumable switching actions that may be taken after the fault has been cleared. The system's security may be evaluated by considering various constraints like thermal overload limits, bus voltage limits, active and reactive power produced, permissible generators' angles difference, frequency deviation and so on. If a new scenario of instability has been found, the "instability library" is updated and thus, after some time, the library will contain the bulk of all the probable scenarios that may push the system into instability. This approach would be preferable to a purely offline DSA approach because the "instability library" can be updated online with those system states that have not been discovered by offline simulations but nevertheless exist in a real network.

While the DSA is a very powerful tool in providing the power system operators with a detailed view of the degree of system stability, the implementation of the DSA concept for online detection of angular instability will be seriously compromised because of several major drawbacks.

The first drawback is related to the excessive computation time needed to solve a huge set of differential equations describing the system dynamics. The time needed for each time-domain simulation is highly dependent on the network size, the number of active elements (rotating machines, non-linear loads, FACTS), the degree of modelling detail, the particular

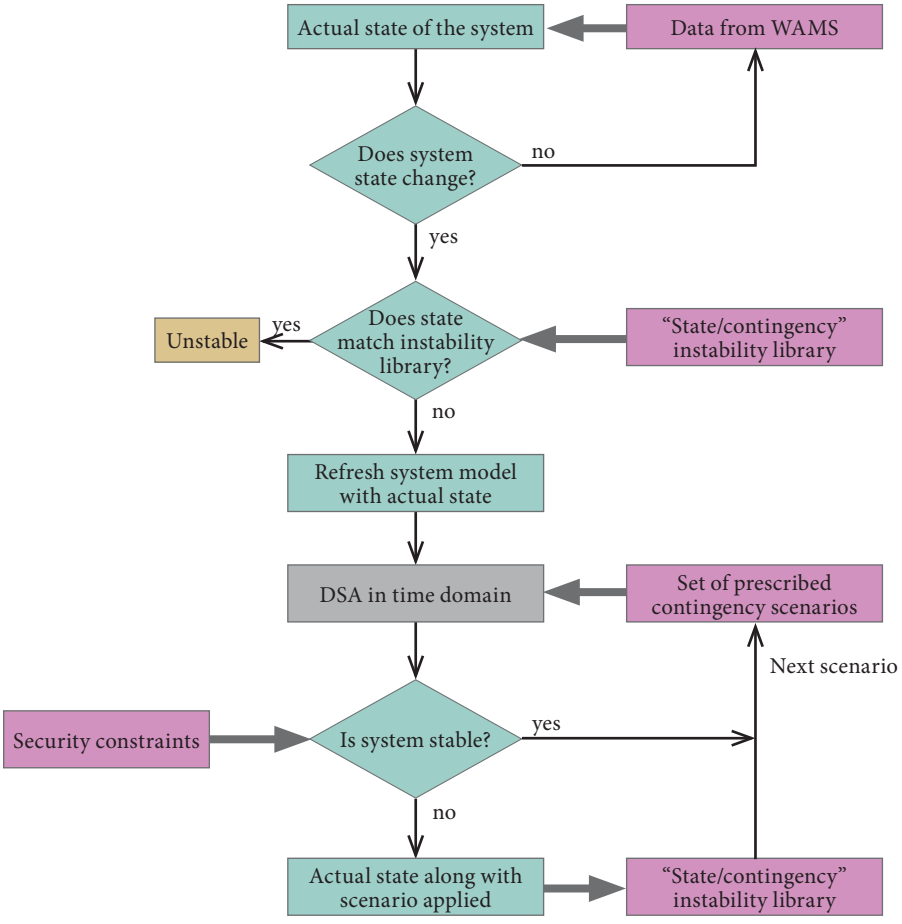

Fig. 5.1. WAMS-measurement-based DSA concept

scenario of the applied contingency and the computational efficacy of algorithms and hardware. Typically, it takes several hundreds of milliseconds to detect instability for a small-scale power system that has been severely stressed, whereas it may take up to several minutes for full-scale modelling of a large power system with hundreds of generators and thousands of buses. The typical way of improving the computational efficacy is the implementation of distributed computing architecture [67]. When system dynamics is evaluated in response to a large number of prescribed contingencies, each particular simulation is assigned to a dedicated computer, thus a set of contingencies is evaluated simultaneously. An additional way of improving the computational efficacy is the reduction of simulation time. Generally, it is considered that instability, if it exists, will manifest itself within 10–15 seconds after the beginning of the contingency. Angular instability typically manifests itself within a much shorter period of time. Therefore, the time of simulation needed to identify angular instability can be reduced to 3–5 seconds. Referring back to the concept presented in Fig. 5.1, a huge amount of state/contingency scenarios still need to be generated to cover the entire space of all probable cases. Besides, we will never be guaranteed that the real-life scenario perfectly fits the one from the library. Thus, implementation of online DSA to predict an OOS condition within a real-time operating environment still remains disputable and questionable.

Several methods are mentioned in literature [68]–[73] that are intended to provide near-real-time stability assessment. Basically, these methods represent an attempt to reduce the computational burden by implementing more sophisticated and faster algorithms to solve the system equations; besides, they also attempt to linearise the system models while still providing an adequate accuracy.

5.2. Energy-function-based methods

The attractiveness of using the concept of energy for power system stability studies lies in the very principle of power system operation, that is, the energy of the prime mover is converted into electrical energy. In a steady-state condition there should always be a balance between the energy gained from the prime mover and the energy consumed. Stable operation of the system is maintained as long as the energy balance persists in the system, whereas a significant mismatch of the above-mentioned energies may occasionally lead to the loss of stability. Thus, evaluation of power system stability from the viewpoint of how energy is converted from one form to another will be rationalised by the very physics of power system operation.

Energy-based methods are often called “direct methods” for stability assessment; they are direct in the sense that there is no need for the entire

evaluation of the post-fault system trajectory to make a conclusion about the system stability. Instead, these methods attempt to predict system behaviour by analysing how the process of energy conversion evolves and thus, it becomes possible to predict the final state of the system before this state has been reached naturally. Theoretically, system stability or instability could be decided on as soon as the fault has been cleared. The origins of energy-based methods lie in Lyapunov's theory of stability which states the following: if the total energy of the system is dissipating, then the system must be stable. Therefore, by looking at how an energy-like function (Lyapunov function) behaves, we can conclude that a system is stable, asymptotically stable or unstable, without the need to solve nonlinear differential equations.

Referring to Fig. 5.2 a), an equilibrium state $x^* = 0$ of an autonomous system is stable (in the sense of Lyapunov) if for any $\varepsilon > 0$ there exists $\delta(\varepsilon) > 0$ such that

$$\left\| x_0 - x^* \right\| < \delta \Rightarrow \left\| x(t, x_0) - x^* \right\| < \varepsilon, \forall t \geq t_0. \tag{5.3}$$

An equilibrium state $x^* = 0$ is asymptotically stable (Fig. 5.2 b)) if it is stable by (5.3) and there exists $\delta(\varepsilon) > 0$ such that

$$\left\| x_0 - x^* \right\| < \delta \Rightarrow \lim_{t \to \infty} x(t) = x^*. \tag{5.4}$$

An example of an unstable equilibrium point is presented in Fig. 5.2 c).

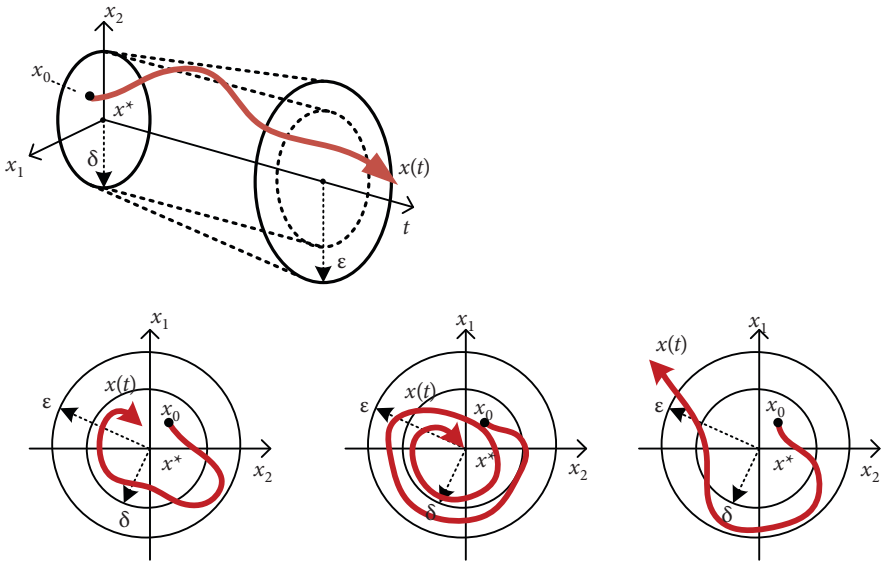

a) stable in the sense of Lyapunov **b)** asymptotically stable **c)** unstable

Fig. 5.2. Equilibrium point

From the power system stability point of view, the task can be formulated as follows. Suppose the system's behaviour is described by a set of two differential equations: during fault (5.5) and after fault (5.6).

$$\dot{x}(t) = f_{\text{fault}}\left(x(t)\right); \tag{5.5}$$

$$\dot{x}(t) = f_{\text{post-fault}}\left(x(t)\right), \tag{5.6}$$

where $x(t)$ is a system state variable.

If we assume that the initial pre-fault conditions are known, then, by solving (5.5) up to the time moment when the fault was cleared $x(t_0)$, the initial conditions for (5.6) will be provided. If we suppose that the solution of (5.6) has a stable equilibrium point x^*, then the question to be answered is whether the trajectory $x(t)$ converges to x^* as $t \to \infty$. Considering practical implementation, we need to construct Lyapunov function $V(x)$ which describes the system's motion in the post-fault state, and then, knowing the initial conditions at the moment of fault clearing, determine the value that the function will take on the boundary of stability V_{cr}. If this value does not exceed V_{cr}, the system is stable; otherwise, the system loses stability. A suitable function should satisfy several conditions:

- $V(x)$ should be a continuous scalar function of system state variables (angular positions, velocities, accelerations, etc.);
- $V(x) > 0$ for all $x \in S, x \neq x^*$, where S is the region of stability defined by $V(x) < b$ where b is a positive constant;
- $\dot{V}(x) < 0$ for all $x \in S, x \neq x^*$, and $\dot{V}(x) = 0$ for $x = x^*$;
- there may be many equilibrium points of the system, thus the previous condition should satisfy the entire set of possible equilibrium points $X^*, x^* \in X^*$.

The problem of finding a suitable function and defining the stability boundary has been addressed by many authors [74]–[80]. Unfortunately, there are no general, straightforward rules of how to construct the Lyapunov function for the particular dynamical system. It has been shown by several authors that a Lyapunov-like function obtained by using power system state variables is an equivalent to the transient energy function (TEF) initially developed in [81], [82]. A simplified mathematical model which describes the motion of the i-th generator in an n-machine system is presented in (5.7).

$$M_i \dot{\omega}_i = P_i - P_{ei}; \tag{5.7}$$

$$\dot{\delta}_i = \omega_i, \; i = 1, 2, \ldots, n;$$

$$P_i = P_{mi} - E_i^{\,2} \cdot G_{ii}; \tag{5.8}$$

$$P_{ei} = \sum_{\substack{j=1 \\ j \neq i}}^{n} \left[C_{ij} \cdot \sin\left(\delta_i - \delta_j\right) + D_{ij} \cdot \cos\left(\delta_i - \delta_j\right) \right], \tag{5.9}$$

where for machine *i*:

$C_{ij} = E_i E_j B_{ij}$;
$D_{ij} = E_i E_j G_{ij}$;
P_{mi} – mechanical power input;
M_i – moment of inertia;
ω_i, δ_i – rotor angular speed, rotor angle;
E_i – constant voltage behind transient reactance;
G_{ii} – driving-point conductance;
B_{ij}, G_{ij} – transfer susceptance and transfer conductance.

This simplified model does not take into account system damping and also machine mechanical input, machine inertia and the voltage behind machine transient reactance are assumed to be invariant. These simplifications can be accepted, considering the short time period for which stability is evaluated (first-swing stability). All the variables of (5.7) are referenced to an arbitrarily chosen synchronous reference frame. In principle, any machine can be chosen as a reference, but the standard practice is to use the centre-of-angles (COA) reference. COA is intended to represent the "mean motion" of the system and for a *n*-machine system is defined as follows:

$$\delta_0 \equiv \frac{1}{M_T} \sum_{i=1}^{n} M_i \cdot \delta_i; \tag{5.10}$$

$$M_T = \sum_{i=1}^{n} M_i;$$

$$\dot{\delta}_0 = \omega_0,$$

where δ_0, ω_0 are, respectively, the angle and the angular speed of the COA reference.

Then the motion of the COA is described by (5.11):

$$M_T \dot{\omega}_0 = \sum_{i=1}^{n} (P_i - P_{ei}) \equiv P_{COA}. \tag{5.11}$$

Equation (5.7) for the *i*-th machine can be rewritten for COA coordinates.

$$M_i \dot{\tilde{\omega}}_i = P_i - P_{ei} - \frac{M_i}{M_T} P_{COA}, \tag{5.12}$$

where $\tilde{\omega}_i = \omega_i - \omega_0 = \dot{\theta}_i$; $\theta_i = \delta_i - \delta_0$.

Then, the TEF was derived in [74] as

$$V=\frac{1}{2}\sum_{i=1}^{n}M_i\tilde{\omega}_i^2-\sum_{i=1}^{n}P_i\left(\theta_i-\theta_i^s\right)-$$
$$-\sum_{i=1}^{n-1}\sum_{j=i+1}^{n}\left[C_{ij}\left(\cos\theta_{ij}-\cos\theta_{ij}^s\right)-\int_{\theta_i^s+\theta_j^s}^{\theta_i+\theta_j}D_{ij}\cos\theta_{ij}\,\mathrm{d}\left(\theta_i+\theta_j\right)\right], \quad (5.13)$$

where:

$\frac{1}{2}\sum_{i=1}^{n}M_i\tilde{\omega}_i^2$ – the change of the rotor's kinetic energy relative to the kinetic energy of the COA;

$\sum_{i=1}^{n}P_i\left(\theta_i-\theta_i^s\right)$ – the change of the rotor's potential energy relative to the potential energy of the COA;

$C_{ij}\left(\cos\theta_{ij}-\cos\theta_{ij}^s\right)$ – the change of the magnetic energy of branch *ij*;

$D_{ij}\cos\theta_{ij}\,\mathrm{d}\left(\theta_i+\theta_j\right)$ – the change of the energy dissipated in branch *ij* due to transfer conductance.

All these changes in energy are in relation to the post-fault stable equilibrium point (denoted with a superscript "*s*"). Energy functions similar to (5.13) have also been obtained in [75], [76], [79], [83]. The last-listed term, which represents transfer conductance, is a path-dependent integral which cannot be predicted accurately from the fault-on mode data. The extended Lyapunov function has been proposed in [84] to cope with the problem of transmission losses.

In general, the TEF is comprised of two types of energies (5.14): the kinetic energy $V_k(\omega)$, which is a function of the rotor's angular speed, and the potential energy $V_p(\omega)$, which is a function of the relative angular positions of the generators.

$$V\left(\omega,\delta\right)=V_k\left(\omega\right)+V_p\left(\delta\right). \quad (5.14)$$

At the next step, the stability boundary V_{cr} should be defined, upon exceeding which the system becomes unstable. A region enclosed by the stability boundary is known as the stability region or the region of attraction (Fig. 5.3).

Calculation of V_{cr} is not a trivial task. The stability boundary will depend on the severity of the fault (the system trajectory during the fault), the fault clearing time as well as the post-fault configuration of the network. Several approaches have been proposed to estimate V_{cr} and the associated unstable equilibrium point (u.e.p.) (Fig. 5.3). Generally, all of these methods can be classified into three groups:

1. Among all the unstable equilibrium points that constitute the stability boundary, the one is taken which has the minimal value, $\min V_{cr}$. The assumption is made that the stable equilibrium point (s.e.p.) for the post-fault configuration will be close to the pre-fault s.e.p. [79]. Then the machine that has the largest accelerating-power-to-momentum ratio is chosen as the starting point, and by applying the

minimisation technique, the u.e.p. is chosen that is closest to the post-fault s.e.p.

2. $V_{cr} = V(x_u)$ where x_u is the u.e.p. closest to the point where fault-on trajectory $x(t)$ exits the stability region – the controlling u.e.p. [74], [85], [86].
3. $V_{cr} = \max\{V_p(x)\}$ – the stability boundary is equal to the local maxima of the potential energy component along the system trajectory; this method is referred to as the principal energy boundary surface (PEBS) method [87], [88]. PEBS represents the surface for which the total energy of the system is completely converted into potential energy. Thus, at the PEBS the potential energy is at its maximum and the system maintains stability if the kinetic energy has been fully converted to potential energy before reaching a particular point on the PEBS.

To conclude, the TEF-based transient stability assessment is performed by comparing two values of transient energy. The transient energy injected into the system during disturbance $V(\omega,\delta)|_{cl}$ is evaluated at the fault-clearing moment, and then $V(\omega,\delta)|_{u.e.p.}$ is evaluated at the u.e.p. to obtain the maximum energy V_{cr}that the system is able to absorb. The system is stable when $V(\omega,\delta)|_{cl} \le V_{cr}$; it is unstable otherwise.

Unlike Equation (5.13), which is a TEF of the total system energy, the individual machine's TEF is of more interest for OOS protection applications. It would be desirable to know which particular machine loses synchronism. A TEF of individual machine V_i with respect to COA (5.15) has been obtained in [76].

$$V_i = \frac{1}{2} M_i \omega_i^2 + \int_{\theta_i^s}^{\theta_i} \left(-P_i + P_{ei} + \frac{M_i}{M_T} P_{COA} \right) d\theta_i. \tag{5.15}$$

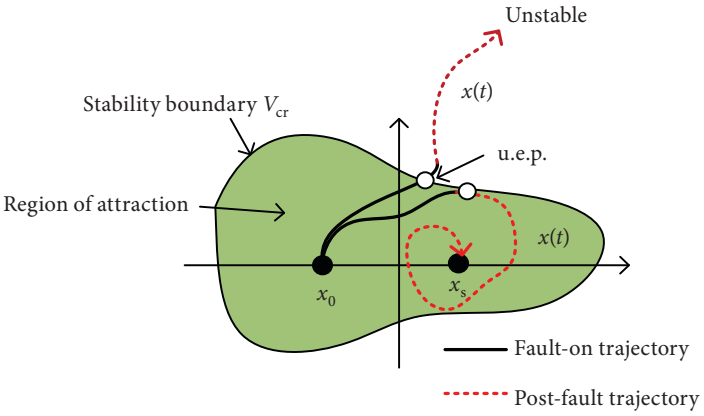

Fig. 5.3. The region of attraction and the stability boundary

The stability boundary of the individual machine is then found as the maximum of potential energy along the post-fault trajectory [76].

Considering the practical implementation of a Lyapunov-like energy function, particularly for a wide-area-measurement-based OOS operating in real time, several comments can be made.

- Originally, the energy-based TSA approach was aimed at reducing the time expenditure of the conventional time-domain methods. Great progress has been achieved here. The approach is a system-model-based one and, consequently, the best accuracy can be achieved when models preserving the system integrity are used. This may significantly increase the computational burden and limit the attractiveness of the method for real-time emergency control applications (like OOS protection). Even a simplified form of Equation (5.13) without taking into account damping and with an approximated transfer conductance term may present significant difficulties when implemented within a real-time environment.
- On the other hand, system-wide measurements allow a significant part of complexities to be replaced with the actual response of the system. For instance, calculation of the system trajectory during fault can be replaced with real-time measurements, and thus, the initial conditions for the post-fault regime will be explicitly defined. In addition, the post-fault configuration of the network can be accessed in real time, and then the system model can be adjusted accordingly.
- Typically, the emergency state resulting from angular instability is a result of a combination of events which can hardly be predicted in advance. Even if the system does not lose stability after the initial fault clearing, it is possible that post-fault transients (caused by auto-reclosing actions, tripping of other lines) may push the system into instability. Thus, we cannot rely on the assumption that the post-fault trajectory will be unaffected by various switching events. This makes challenging the prediction of the final state of the system (stable/unstable) by relying solely on the fault-on trajectory and the initial conditions at fault clearing. The system's response to changes in the post-fault configuration will be of great importance for correct OOS detection and should be traced in real time.

5.3. Equal-area-criterion-based methods

5.3.1. Single-machine equivalent (SIME) method

A set of methods that use the energy concept similarly to the Lyapunov-function-based approach but are more suitable for real-time emergency control applications are known as equal-area-criterion-based methods.

Unlike the Lyapunov-function-based approach, these methods evaluate the system trajectory for both the fault-on and post-fault periods. The classical representative of this approach can be seen in the EAC method in and of itself. The classical EAC is an energy-based method but has a significant drawback: it can be successfully applied to a one machine infinite-bus system but cannot be directly used for multi-machine networks. Substantial attempts have been made to tackle the classical EAC deficiency, and these attempts have resulted in the development of several hybrid time-domain-EAC-based methods. The general idea of these methods lies in the transformation of a multi-machine system into a two-machine system and then into a one-machine infinite-bus equivalent system (OMIB). After such transformations, the classical EAC can be applied to assess the stability of the OMIB system. Therefore, the main objective of this approach lies in obtaining a correct two-machine equivalent of the multi-machine system. To do this, a heuristic statement is made that is based on the observation of the generators' behaviour when the system loses synchronism. The statement relies on two propositions [89], [90]:

1. Irrespective of how complex the loss of synchronism of a multi-machine system is, it originates from irrevocable separation of all the machines into two clusters: the cluster of critical machines (CM) is composed of the generators which are supposed to be responsible for the loss of synchronism, and the remaining generators compose the cluster of non-critical machines (NM) [89]. The generators that belong to each particular cluster exhibit similar behaviour during an out-of-step condition.
2. Therefore, two clusters can be replaced by a two-machine equivalent and then by an OMIB. The stability of the relevant OMIB can be assessed by using the classical EAC method.

The first proposition has been confirmed by a huge amount of time-domain simulations as well as proved by real-life scenarios.

Two general methods are known which rely on the above propositions: the Extended Equal Criterion (EEAC) method and the Single Machine Equivalent (SIME) method. A generalised flowchart of the methods is shown in Fig. 5.4.

Both methods use the same EAC energy-based principle but differ in the way the OMIB equivalent is obtained.

The EEAC method relies on a time-invariant OMIB, that is, the parameters of the OMIB are obtained at the beginning of the transient and remain "frozen" during the entire process of system stability evaluation. The $P-\delta$ curve of the OMIB is supposed to be sinusoidal, like in the classical EAC method. To sort the generators out into CM and NM, the initial acceleration of the generators is analysed and the generators with the largest acceleration form the CM cluster candidate. Then, the critical clearing time (CCT) is calculated for all the candidates, and the cluster with the smallest CCT is

chosen as the actual CM cluster [90]. The drawback of the method lies in the assumption that the OMIB is invariant. The OMIB, once defined, does not consider the behaviour of generators after the fault has been cleared and thus, the after-fault system dynamics is not taken into account.

It is supposed that the SIME method is free of the deficiencies characteristic of the EEAC method. A detailed description of the SIME method can be found in [89]. SIME relies on a time-varying OMIB for which the post-fault dynamics of generators are taken into account. The mathematical formulation of the multi-machine/OMIB transformation is presented below as derived in [89].

The COA δ_{CM} of the CM cluster and the COA δ_{CM} of the NM cluster are obtained as follows:

$$\delta_{CM}(t) \equiv \frac{\sum_{k \in CM} M_k \delta_k(t)}{M_{CM}}; \tag{5.16}$$

$$\delta_{NM}(t) \equiv \frac{\sum_{j \in NM} M_j \delta_j(t)}{M_{NM}}, \tag{5.17}$$

where: $M_{CM} = \sum_{k \in CM} M_k$;

$M_{NM} = \sum_{j \in NM} M_j$;

δ_k, δ_j – the angular position of the generators' rotors;

M_k, M_j – the generators' inertia constants.

The rotor speed of the CM and NM clusters is defined as follows:

$$\omega_{CM}(t) \equiv \frac{\sum_{k \in CM} M_k \omega_k(t)}{M_{CM}}; \tag{5.18}$$

$$\omega_{NM}(t) \equiv \frac{\sum_{j \in NM} M_j \omega_j(t)}{M_{NM}}, \tag{5.19}$$

where ω_k, ω_j – the speed of the generators' rotors.

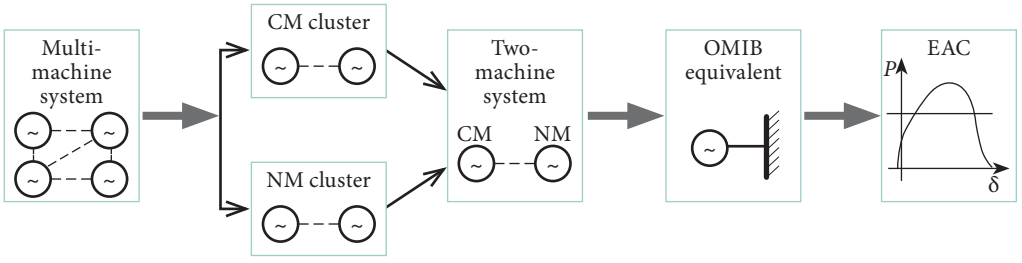

Fig. 5.4. Flowchart of the transformation from a multi-machine system to OMIB

Then, the rotor angle and the rotor speed of the OMIB is defined as follows:

$$\delta(t) \equiv \delta_{\mathrm{CM}}(t) - \delta_{\mathrm{NM}}(t); \tag{5.20}$$

$$\omega(t) \equiv \omega_{\mathrm{CM}}(t) - \omega_{\mathrm{NM}}(t). \tag{5.21}$$

The inertia coefficient of the equivalent OMIB:

$$M = \frac{M_{\mathrm{CM}} M_{\mathrm{NM}}}{M_{\mathrm{CM}} + M_{\mathrm{NM}}}. \tag{5.22}$$

The mechanical power of the equivalent OMIB:

$$P_{\mathrm{m}}(t) = M\left(\frac{\sum_{k\in \mathrm{CM}} P_{\mathrm{m}k}(t)}{M_{\mathrm{CM}}} - \frac{\sum_{j\in \mathrm{NM}} P_{\mathrm{m}j}(t)}{M_{\mathrm{NM}}}\right). \tag{5.23}$$

The electric power of the equivalent OMIB:

$$P_{\mathrm{e}}(t) = M\left(\frac{\sum_{k\in \mathrm{CM}} P_{\mathrm{e}k}(t)}{M_{\mathrm{CM}}} - \frac{\sum_{j\in \mathrm{NM}} P_{\mathrm{e}j}(t)}{M_{\mathrm{NM}}}\right). \tag{5.24}$$

If only the first-swing stability is evaluated, the mechanical power can be considered invariant and equal to the electric power immediately before the contingency. The first-swing stability of the OMIB equivalent is assessed in the same way as in the classical EAC method. That is, the total area A consisting of acceleration and deceleration areas is calculated from the moment of fault inception δ_0 and until the unstable equilibrium angle $\delta_{\mathrm{u.e.p.}}$ is reached (5.25).

$$A = \int_{\delta_0}^{\delta_{\mathrm{u.e.p.}}} \left(P_{\mathrm{m}} - P(\delta)\right) \mathrm{d}\delta. \tag{5.25}$$

If the system angle reaches $\delta_{\mathrm{u.e.p.}}$ and there still exists excessive accelerating energy $A > 0$, the system loses stability. An example of an unstable scenario (simulated on the model of the Latvian power system; see Section 4.3) is shown in Fig. 5.5. Two generators *G1* and *G4* constitute the CM group with the remaining generators forming the NM group. The first two plots of Fig. 5.5 show the generators' angles, the COA angles of the CM and NM clusters as well as the angle of the equivalent OMIB. The last plot shows the power-angle curve of the OMIB equivalent for an unstable case ($A > 0$).

The generators' angles, the COA for both groups and the OMIB power-angle plot for a stable scenario are shown in Fig. 5.6. It is supposed that for a stable scenario there are no CMs, still, for demonstration purposes, generator G1, which has the largest angular excursion, was chosen as the CM.

In this case, the accelerating area is lower than the decelerating area ($A < 0$) and the system swings back after reaching angle δ_{return}.

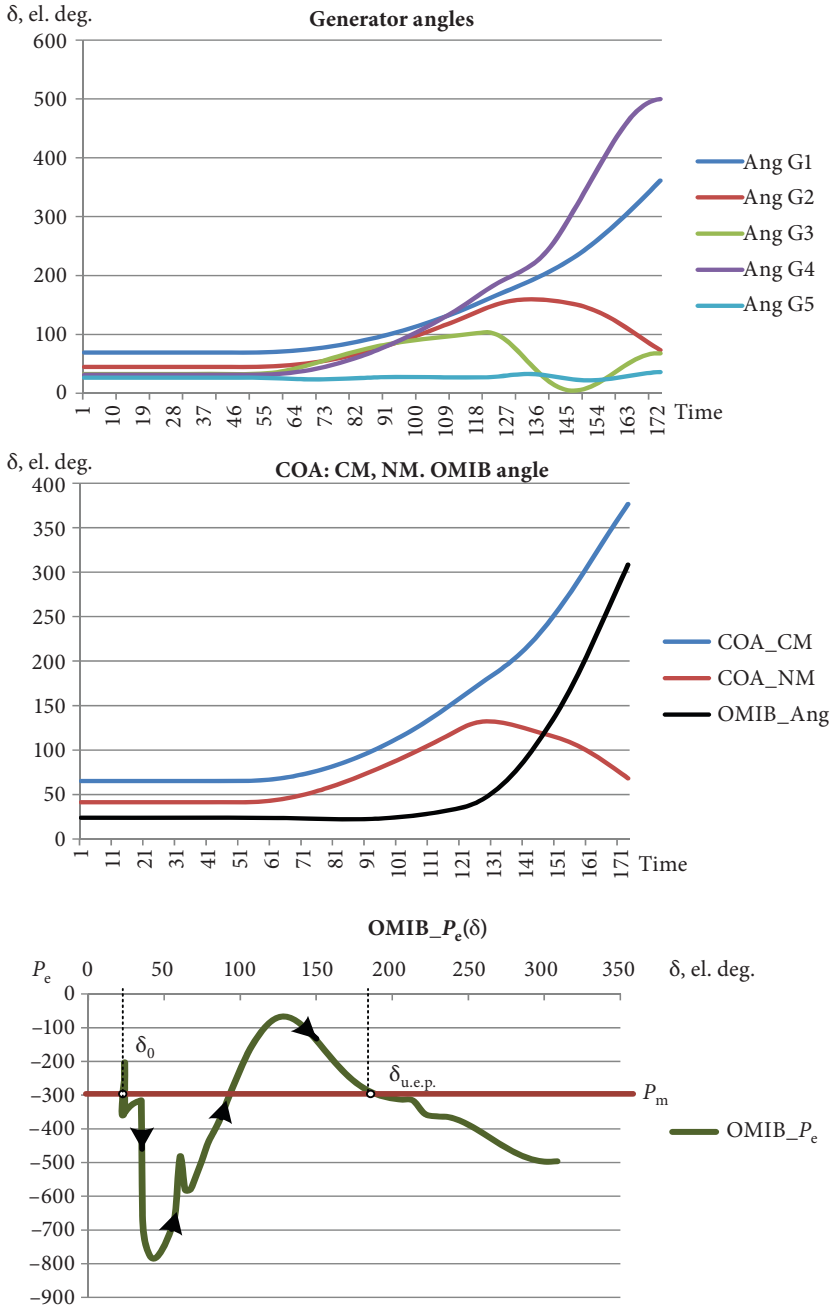

Fig. 5.5. Generators' angles, OMIB angle, and OMIB power-angle curve for an unstable scenario

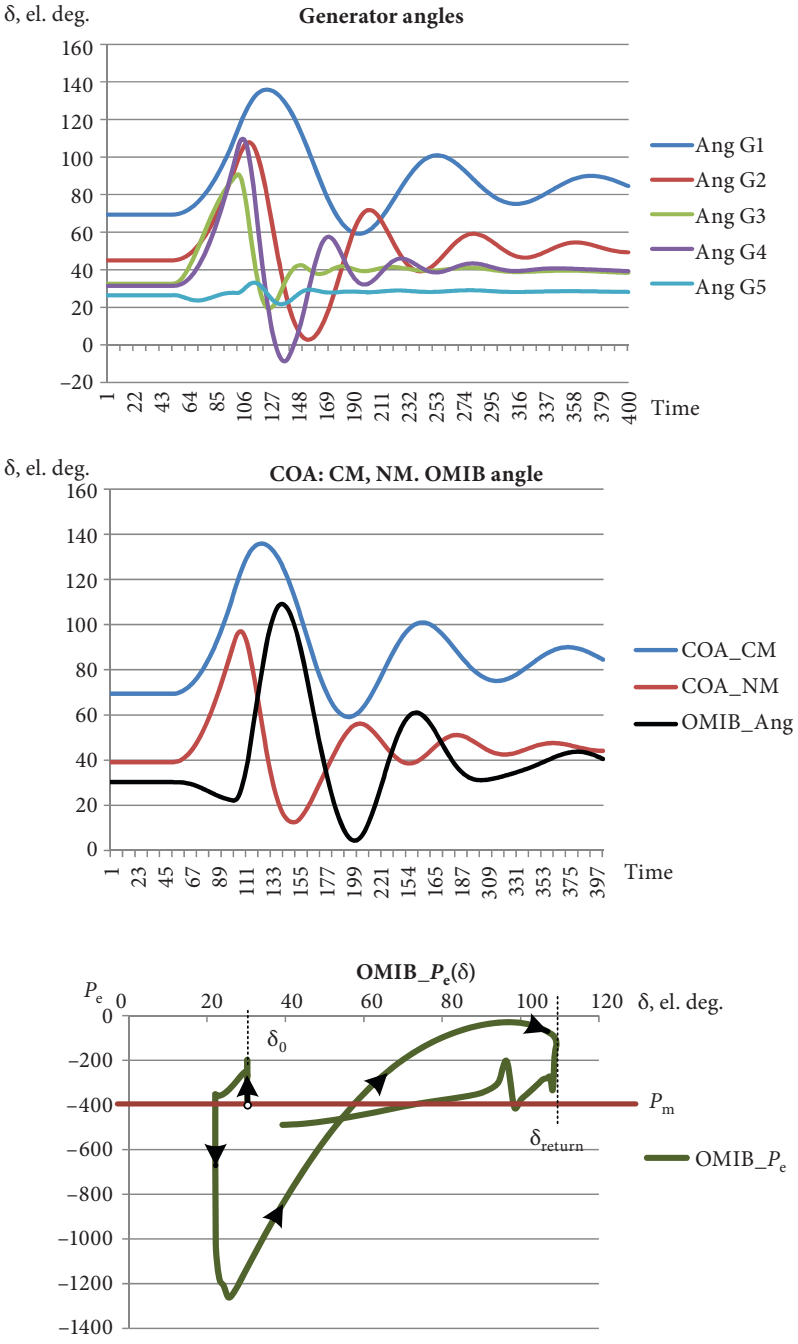

Fig. 5.6. Generators' angles, OMIB angle, and OMIB power-angle curve for a stable scenario

The system which is first-swing stable may lose stability as a result of various switching and network rearrangement events which may happen after the initial clearing of the fault. An example of a first-swing stable system losing stability because of unsuccessful auto-reclosing of the faulted line is presented in Fig. 5.7. A detailed look at the power-angle curve (the last plot in Fig. 5.7) shows that the OMIB angle stops increasing at δ_{return} and swings back but then auto-reclosing action (*AR*) drives the system into instability.

As had been expected, the SIME-EAC method allows the detection of an OOS condition during the first swing but is not intended to cope with more complex scenarios. Some other technique should be used in addition to the SIME-EAC method that allows covering all the possible OOS scenarios.

Regarding the practical implementation of the SIME method, several other questions arise. SIME provides correct OMIB representation of the system if the CMs are properly identified. It is easy to classify generators into CM and NM groups by observing the evolution of the generators' angles when the system has already lost synchronism. But it is not so evident if we want to identify CMs at the early stage of the post-fault process. In particular, generators which initially seem to constitute the CM group may diverge significantly and may drop out of the CM group. This means that generators' membership in the CM cluster may vary over time and should be traced in real time. Real-time clustering of generators can be implemented using the generator coherence detection technique (described in Chapter 4). Time-varying CM and NM clusters suggest that different candidate OMIBs can be formed at different stages of the evolution of the system trajectory. Therefore, EAC-based stability assessment should be applied continuously to each candidate OMIB and the candidate that first becomes unstable is supposed to be the correct representative of the actual system stability. The flowchart of the suggested algorithm is depicted in Fig. 5.8.

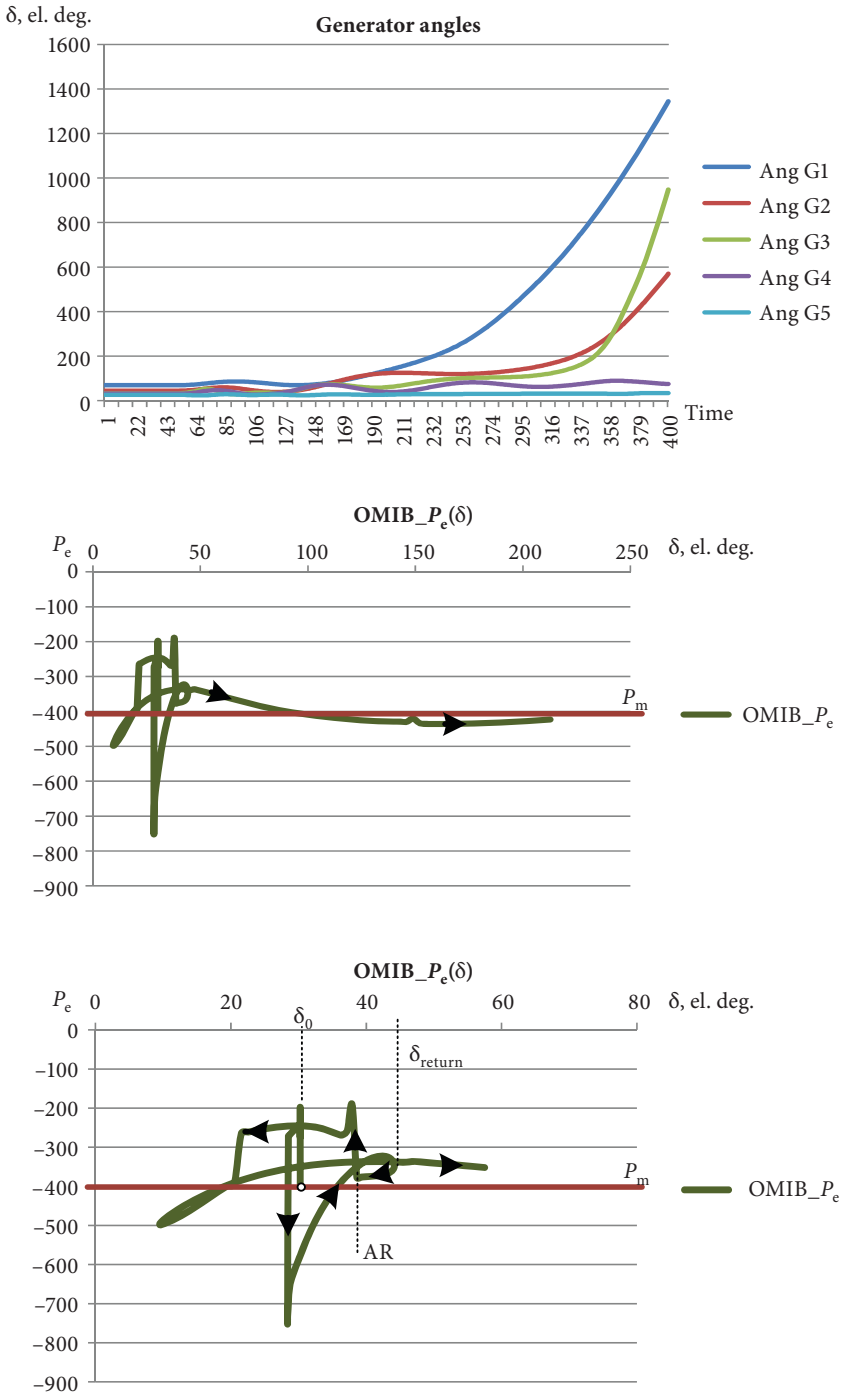

Fig. 5.7. Generators' angles, OMIB angle, and OMIB power-angle curve for an unstable scenario

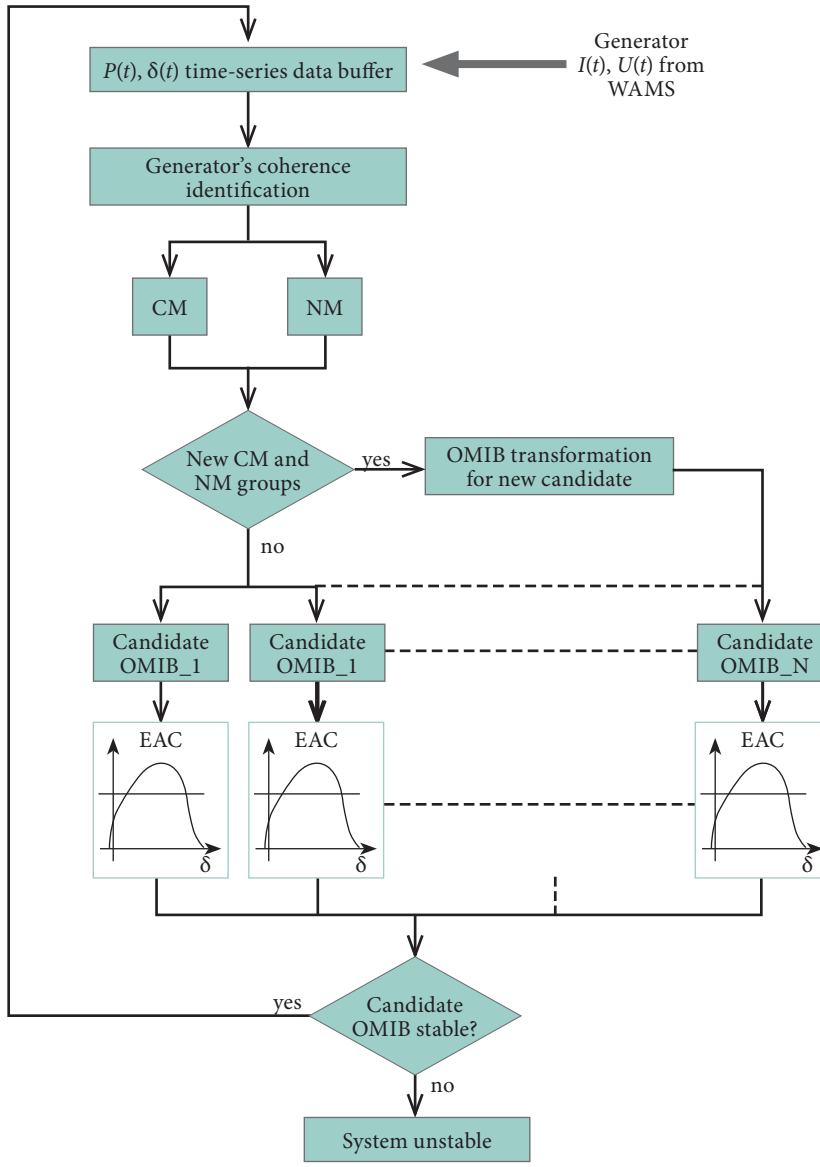

Fig. 5.8. SIME-EAC algorithm flowchart

Another important question is the determination of the unstable equilibrium angle $\delta_{u.e.p.}$. The OMIB enters an unstable condition as soon as the OMIB's trajectory reaches $\delta_{u.e.p.}$ with a positive acceleration energy ($A > 0$). Graphically, $\delta_{u.e.p.}$ corresponds to the point where curve $P_e(\delta)$ and line P_m intersect in such a way that $P_e(\delta) > P_m$ before the intersection and $P_e(\delta) < P_m$ after the point has been crossed (Fig. 5.5). The most straightforward method to detect the u.e.p. then consists of only the two above conditions that need to be fulfilled. The accuracy of the detection will depend on the sampling rate of the power-angle curve; the higher the sampling rate, the better the detection accuracy. The u.e.p. can also be predicted by using extrapolation methods. In [88], the weighted least square (WLS) method is used to predict the power-angle curve of the OMIB. The curve is approximated by solving (5.26) for *a, b, c* for at least three consecutive measurements taken with sampling interval Δt.

$$P_a(\delta) = a\delta^2 + b\delta + c, \tag{5.26}$$

where $P_a = P_m - P_e$ is the accelerating power of the OMIB.
Then the u.e.p. can be determined as the point for which conditions (5.27) are satisfied [89].

$$P_a(\delta) = 0; \dot{P}_a(\delta) > 0. \tag{5.27}$$

The last question that needs to be considered is the existence of the u.e.p. The concept of u.e.p. is valid only for cases when there exists the decelerating area, that is, the area for which $P_e(\delta) > P_m$. Otherwise, the u.e.p. is not defined at all and cannot be estimated. An example of such a scenario will be presented in the next Section.

5.3.2. EAC-in-time-domain method

Classical EAC assesses stability by means of exploring the $P - \delta$ curves of the system at fault and post-fault conditions. The idea of the EAC-in-time-domain method was proposed by several authors in [91]. The method relies on the same energy equilibrium principle as the classical EAC method but is implemented in the time domain. The stability is assessed by observing the trajectory of generator power evolution over time (the $P - t$ curve) and by comparing the energy that accelerates generator (*A1*) with the energy that decelerates the generator (*A2*) (Fig. 5.9).

A generator is stable if the total energy *A* satisfies (5.28).

$$A = A1 + A2 = \int_{t_0}^{t_{max}} \left(P_m - P_e(t)\right) \mathrm{d}t \le 0, \tag{5.28}$$

where: P_e – generator electric power;
P_m – generator mechanical power (assumed to be invariant during the first swing and is equal to P_e immediately before the contingency);
t_0 – time of fault;
t_{max} – the time when the integration is terminated.

Two classical scenarios of a stable generator and an unstable one are presented in Fig. 5.9. The EAC-in-time-domain approach seems to be very attractive from the point of view of practical implementation because all the information needed to decide about stability is the generator's real power. An algorithmically straightforward approach can be used with minimum amount of data required and minimal computational efforts involved. A flowchart of the proposed algorithm is presented in Fig. 5.10. The calculation of acceleration area *A1* and deceleration area *A2* relies on the detection of the $P_m > P_e(t)$ and $P_m < P_e(t)$ transition moments. Acceleration area *A1* is calculated from the moment of fault inception t_0 and until the $P_m < P_e(t)$ transition occurs. Then deceleration area *A2* is calculated by the moment when the $P_m > P_e(t)$ transition occurs (the t_{max} point).

The algorithm was tested for several OOS scenarios simulated on the model of the Latvian power grid and shows reliable results, except for several scenarios (sometimes unrealistic) for which it was discovered that the algorithm had deficiencies.

The first scenario is a short circuit of a very long duration (0.4 s) which was applied to transmission line *L4–13* (Fig. 5.11).

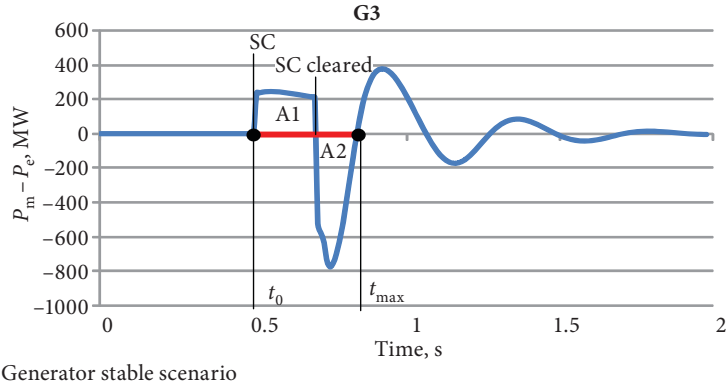

a) Generator stable scenario

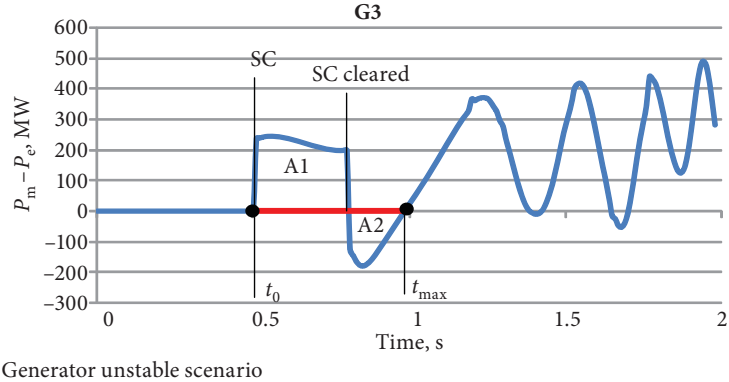

b) Generator unstable scenario

Fig. 5.9. Generator stable (a) and unstable (b) scenario (taken from [93])

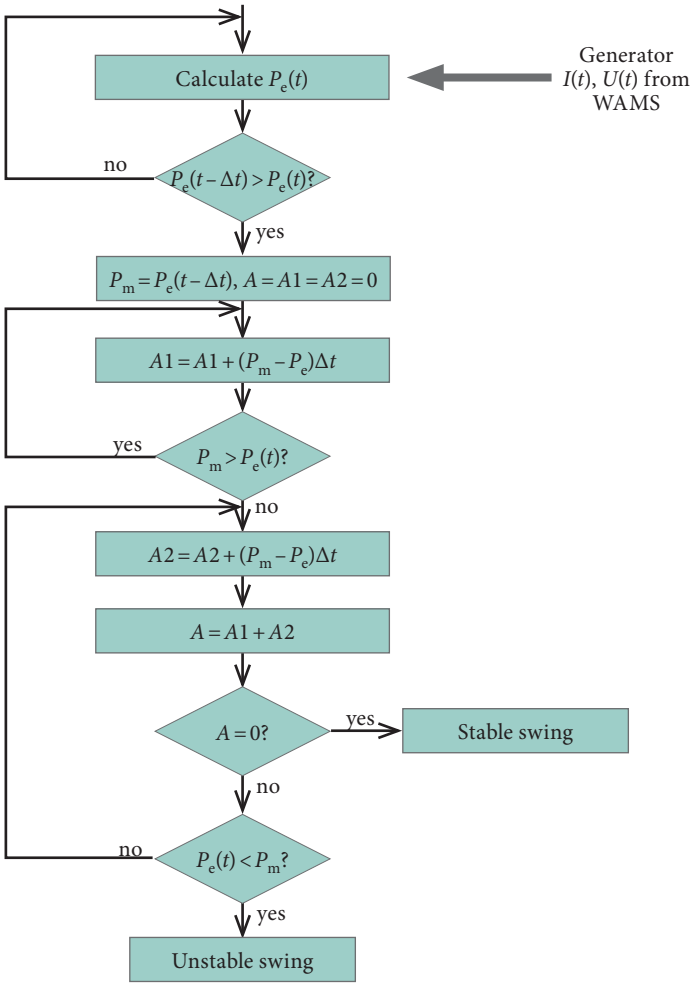

Fig. 5.10. EAC-in-time-domain algorithm

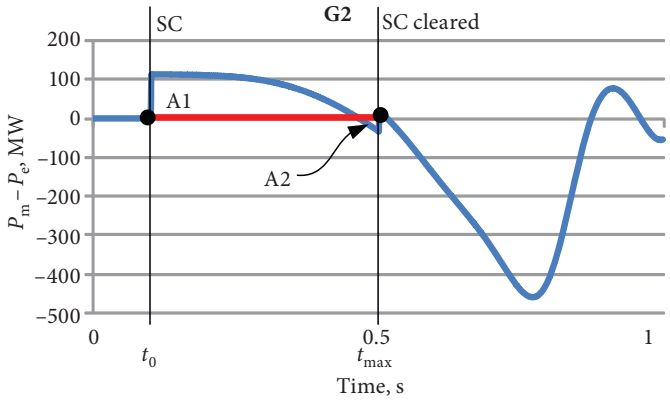

Fig. 5.11. Scenario with long-lasting short circuit (taken from [93])

Generator G2 does not lose stability, but the algorithm detects generator instability ($A1 > A2$ at t_{max}) because at the moment when the fault was cleared the generator was already in the deceleration mode. The algorithm misinterprets the discontinuity (which results from fault clearing) as the fulfilment of integration termination criterion $P_m > P_e(t)$. As a result of such misinterpretation, deceleration area $A2$ was underrated and generator instability was declared incorrectly.

A scenario of severe instability is presented in Fig. 5.12. The short circuit was cleared only at one side of line *L6–14*. Generator G2 is running out of step but there is no deceleration area at all and the criterion for terminating integration is absent in this case. Thus, the algorithm fails to detect generator instability.

Several scenarios were simulated for which a first-swing stable generator ($A2 > A1$) finally runs out of step (Fig. 5.13). This scenario corresponds to the case when a u.e.p. does not exist.

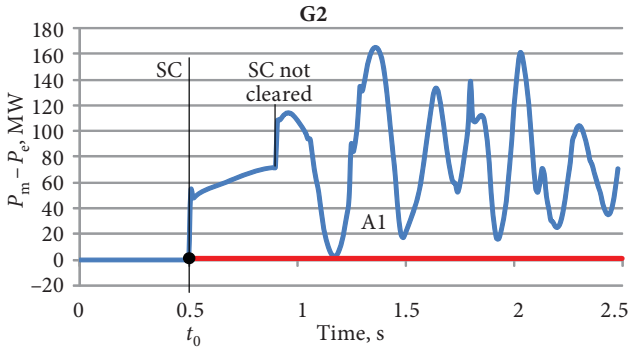

Fig. 5.12. Scenario of severe instability (taken from [93])

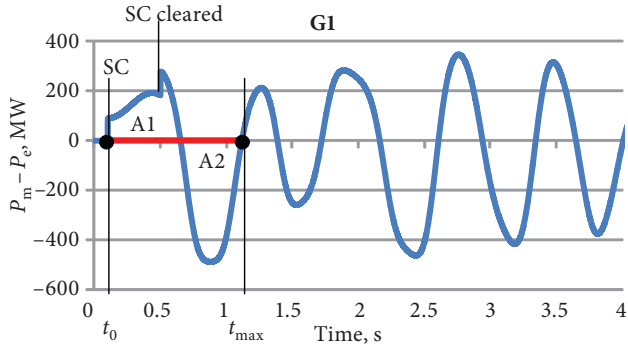

Fig. 5.13. First-swing stable generator ($A2 > A1$) is running out of step

Summing up the results of the above simulations, several conclusions can be made. Unlike the SIME approach, which evaluates the stability of the entire network, the EAC-in-time-domain method evaluates the stability of the particular generator or a group of generators which are tightly coupled within the framework of a power station. The method does not require any network reduction technique and can be implemented for a multi-machine system. The method requires only the real power of generators to be known and is very efficient computationally. At the same time, two deficiencies of the algorithm were identified by simulations. The first deficiency has to do with the algorithm's inability to correctly detect the integration termination moment t_{max}; that is, the time moment when acceleration and deceleration areas should be compared may be incorrectly recognised due to network rearrangements in the post-fault mode. Thus, some other integration termination criteria should be used instead of $P_m > P_e(t)$. Another deficiency is dictated by the very principle of EAC, which is not intended for detecting multi-swing instability. This means that some other method should be used in addition to EAC to detect multi-swing instability.

5.3.3. EAC-in-time-domain method supplemented by angle control

The deficiencies of the EAC-in-time-domain method can be resolved considering that generator terminal voltage angle measurements are available from the WAMS. The protection operation algorithm may be improved if two approaches are used simultaneously [92]:

1. The EAC in-time-domain approach should be implemented for first-swing instability detection.
2. An angle-control-based method should be used for multi-swing instability detection.

The EAC-in-time-domain algorithm (Fig. 5.10) should be modified to take into account the deficiencies identified by the simulations. The modified algorithm should be able to cope even with complex scenarios for which several transitions between $P-\delta$ curves persist during the post-fault stage. An example of such a scenario is presented in Fig. 5.14, where the system trajectory jumps several times between different $P-\delta$ curves with each curve representing a new state of the network. The unmodified algorithm, which is based on $P_m > P_e(t)$ transition, does not take into account the extra acceleration and deceleration energies which arise due to line autoreclosing followed by line tripping (Fig. 5.14). The correct points on the $P-\delta$ curve, for which the acceleration and deceleration area comparison will be valid, are the ones that correspond to unstable equilibrium angles (δ_{cr1}, δ_{cr2}, δ_{cr3} in Fig. 5.14). The system will definitely lose synchronism as soon as the trajectory reaches δ_{cr} with the acceleration energy being positive. The value of δ_{cr} depends on the actual $P-\delta$ curve of the post-fault stage and thus may vary when transitions between different $P-\delta$ curves occur. The actual δ_{cr}

can be calculated in real time, assuming that the $P-\delta$ curves are piecewise sinusoidal (5.29)…(5.31).

$$P_e(t) = P_{max} \cdot \sin(\delta(t)); \tag{5.29}$$

$$\sin(\delta_{cr}(t)) = \frac{P_m}{P_{max}}; \tag{5.30}$$

$$\delta_{cr}(t) = 180° - \sin^{-1}\left(P_m \frac{\sin\delta(t)}{P_e(t)}\right). \tag{5.31}$$

For practical reasons, the calculated critical angle should be bounded within $100° < \delta_{cr} \leq 180°$. $P-\delta$ curve 4 in Fig. 5.14 is a special case, for which there is no deceleration area and, consequently, a u.e.p. does not exist. There are two ways how this case of severe instability could be handled. The first method is to decide that the u.e.p. is equal to the following:

$$\delta_{cr1} = 180° - \delta_0, \tag{5.32}$$

where δ_0 is the stable equilibrium point of the pre-fault curve (Fig. 5.14). This approach unavoidably delays the moment when instability can be detected, which is highly undesirable in the presence of a severe instability condition.

Another approach lies in the calculation of the remaining "theoretically possible deceleration" area. That is, starting from the moment of fault

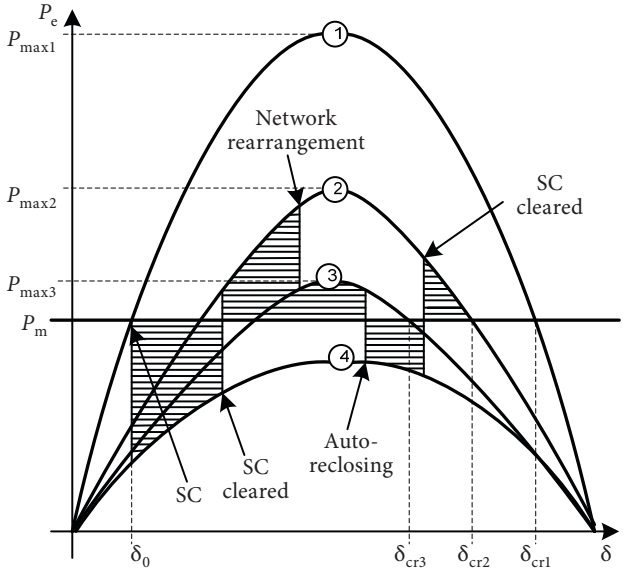

Fig. 5.14. Scenario with several network rearrangements in the post-fault stage (taken from [92])

inception at δ_0, the remaining theoretically possible deceleration area D of the pre-fault $P-\delta$ curve is calculated according to (5.33).

$$D = \int_{\delta(t)}^{\delta_{cr1}} \left(P_{max1} \cdot \sin\delta(t) - P_m\right) d\delta. \quad (5.33)$$

Assuming that the pre-fault regime will be restored in the best-case scenario, instability could be definitely declared as soon as acceleration area *A1* becomes larger than the remaining theoretically possible deceleration area *D* (Fig. 5.15).

A modified algorithm is presented in Fig. 5.16. The value of "*thr1*" defines the beginning of the transient energy computation. At each new circle $\delta_{cr}(t)$ is computed. Instead of calculating acceleration and deceleration areas separately, the total cumulative energy A is calculated. An instability condition is declared as soon as $\delta(t)$ reaches $\delta_{cr}(t)$ with the acceleration energy being positive ($A > 0$) as well as in the case when $A > D$.

The algorithm was tested for several OOS scenarios applied to the model of the Latvian power system network (Fig. 4.2). The behaviour of generators G1–G5 (Figs. 5.17–5.23) is a result of a short circuit on transmission line *L7–14* (applied at 0.5 s and cleared at 0.6 s), which is followed by unsuccessful autoreclosing (applied at 1.0 s and cleared at 1.2 s). Three generators – G1, G2, G3 – go out of step, and generators G4, G5 remain stable (Fig. 5.17).

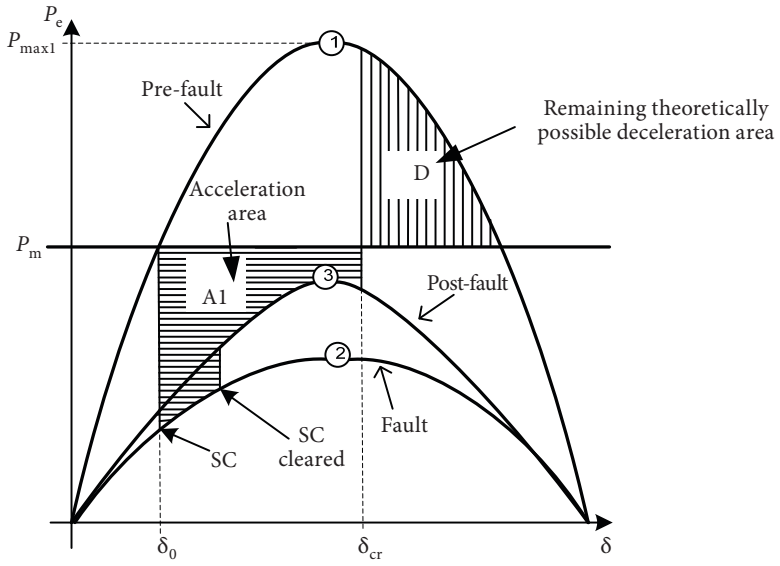

Fig. 5.15. Severe instability scenario (acceleration area *A1* > theoretically possible deceleration area *D*)

The algorithm, based on the $P_m > P_e(t)$ transition criterion, has identified that generator G1 is stable ($A < 0$ at the red dot in Fig. 5.18), which is not correct. The modified algorithm takes the decision at the time moment when the calculated $\delta_{cr}(t)$ curve (*UEP G1*) crosses curve *Ang G1* (point *b* in Fig. 5.18). At this point (1.7 s) the cumulative area $A > 0$, which indicates that G1 will lose stability.

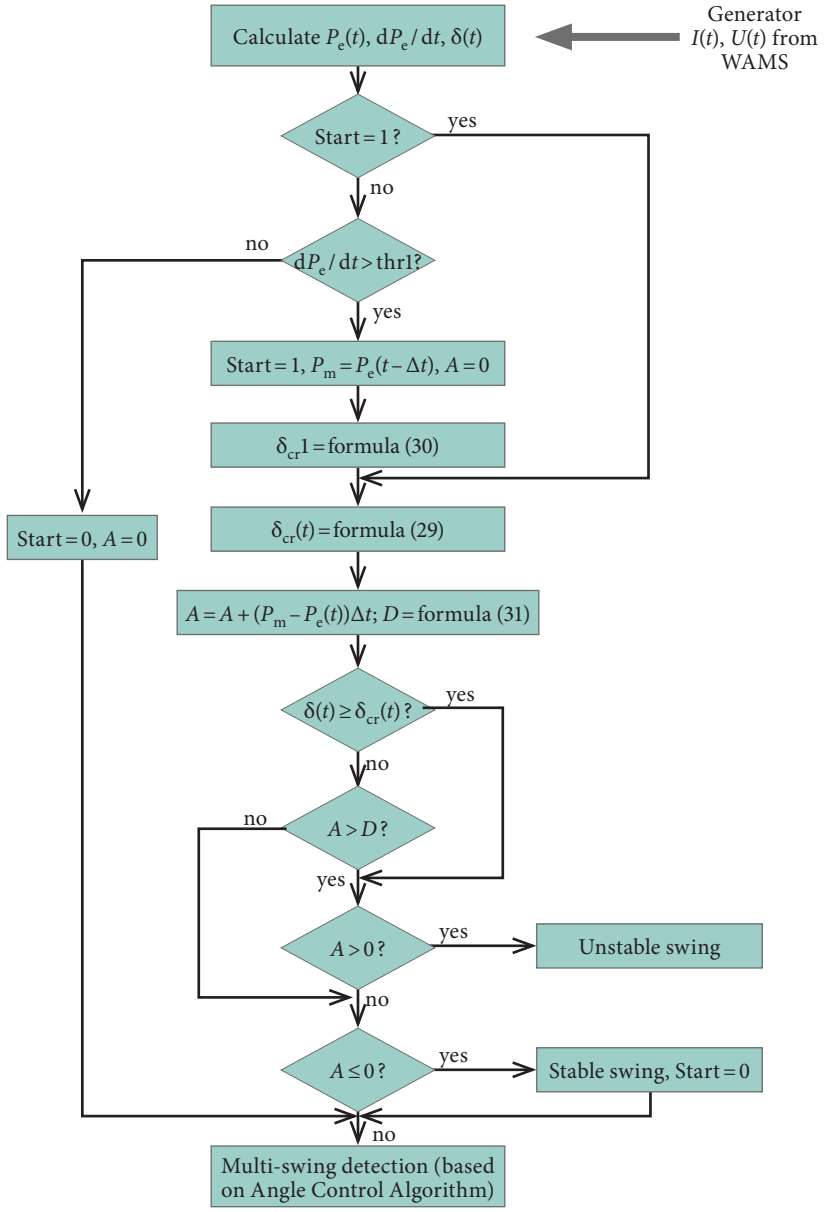

Fig. 5.16. EAC-in-time-domain method with angle control algorithm

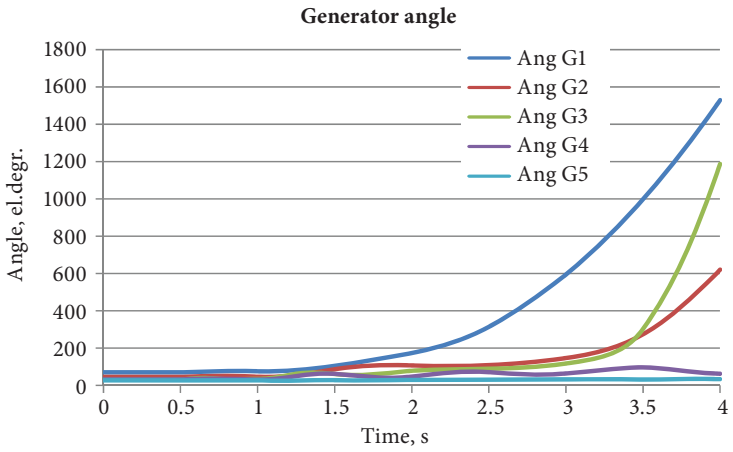

Fig. 5.17. Generators G1, G2, G3 going out of step as a result of transmission line short circuit followed by unsuccessful autoreclosing

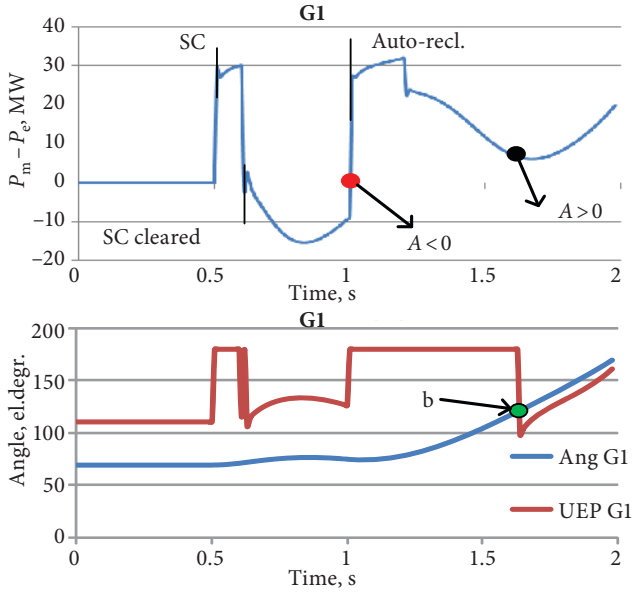

Fig. 5.18. Generator instability detected at point b (taken from [93])

Similarly, the unmodified algorithm has concluded that generators G2 and G3 do not lose stability (for G2: $A<0$ at $t=0.9$ s; for G3: $A<0$ at $t=0.75$ s), which is not a correct decision. The improved algorithm correctly identifies instability of generators G2 and G3 (for G2: $A>0$ at $t=1.95$ s; for G3: $A>0$ at $t=3.1$ s) (Fig. 5.19 a), b)).

Generators G4 and G5 do not lose stability (Fig. 5.20) as evidenced by the fact that the $\delta_{cr}(t)$ angle curves (*UEP G4, UEP G5*) do no cross the respective $\delta(t)$ curves (*Ang G4, Ang G5*).

It is assumed by the algorithm that generators' real power and generators' rotor angles could be calculated from the PMU's synchronised measurements. A detailed technique of rotor angle estimation from phasor measurements is described in [94] and [95]. It is also supposed that the generators' angles are computed with respect to a common reference. In the simulations presented in Figs. 5.17–5.20, the generators' angles are referenced with respect to an infinite bus, which in real life corresponds to the voltage phasor angle measured at the point of the interconnection of the Latvian power system with neighbouring power systems.

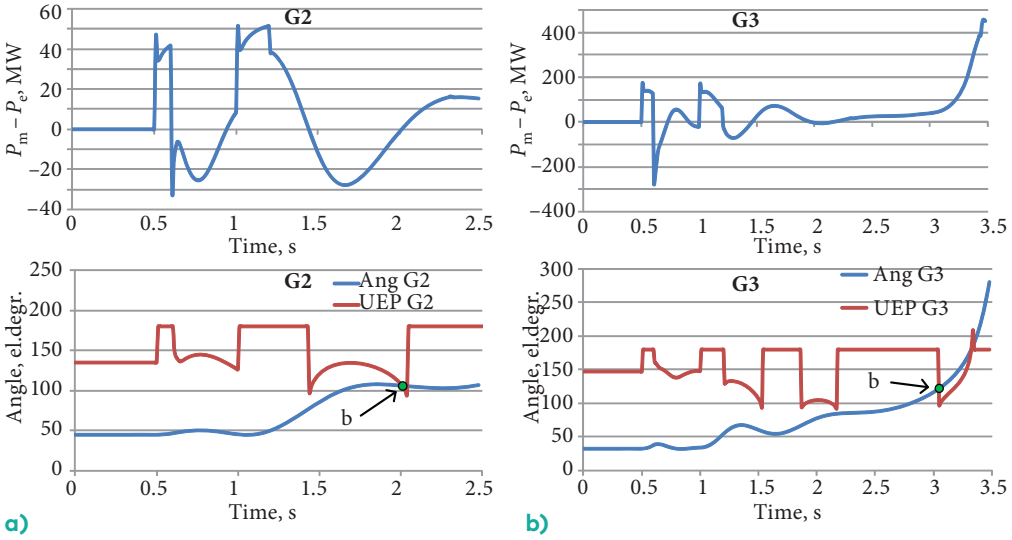

Fig. 5.19. Generator instability detected at point b (taken from [93])

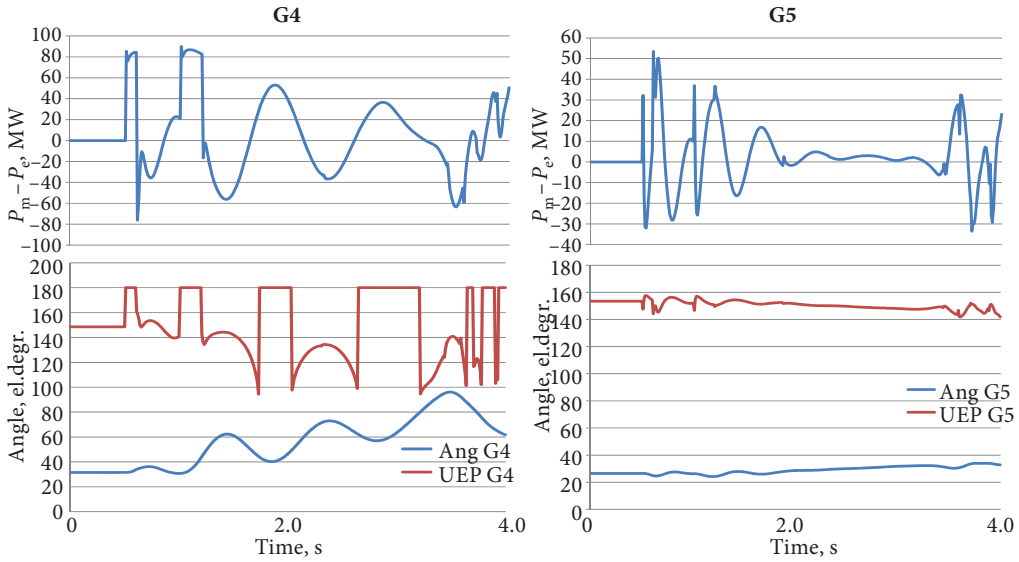

Fig. 5.20. Generators G4 and G5 remaining stable (taken from [93])

The last block of the algorithm flowchart (Fig. 5.16) implements the generator angle difference control principle (Fig. 5.21). Since the absolute values of the angles between the generators are available online, the angle difference for each pair of generators $\delta_{mn}(t)$ can be computed and traced in real time. Then a straightforward approach of comparing the angle difference with pre-defined setting $\delta_{cr(mn)}$ could be used (Fig. 5.21 a)). The loss of synchronism is declared as soon as the absolute angle difference exceeds the critical value defined by an appropriate setting. The value of the setting could be defined as a result of extensive transient stability studies applied to the network model. In some cases, the setting can be chosen as large as

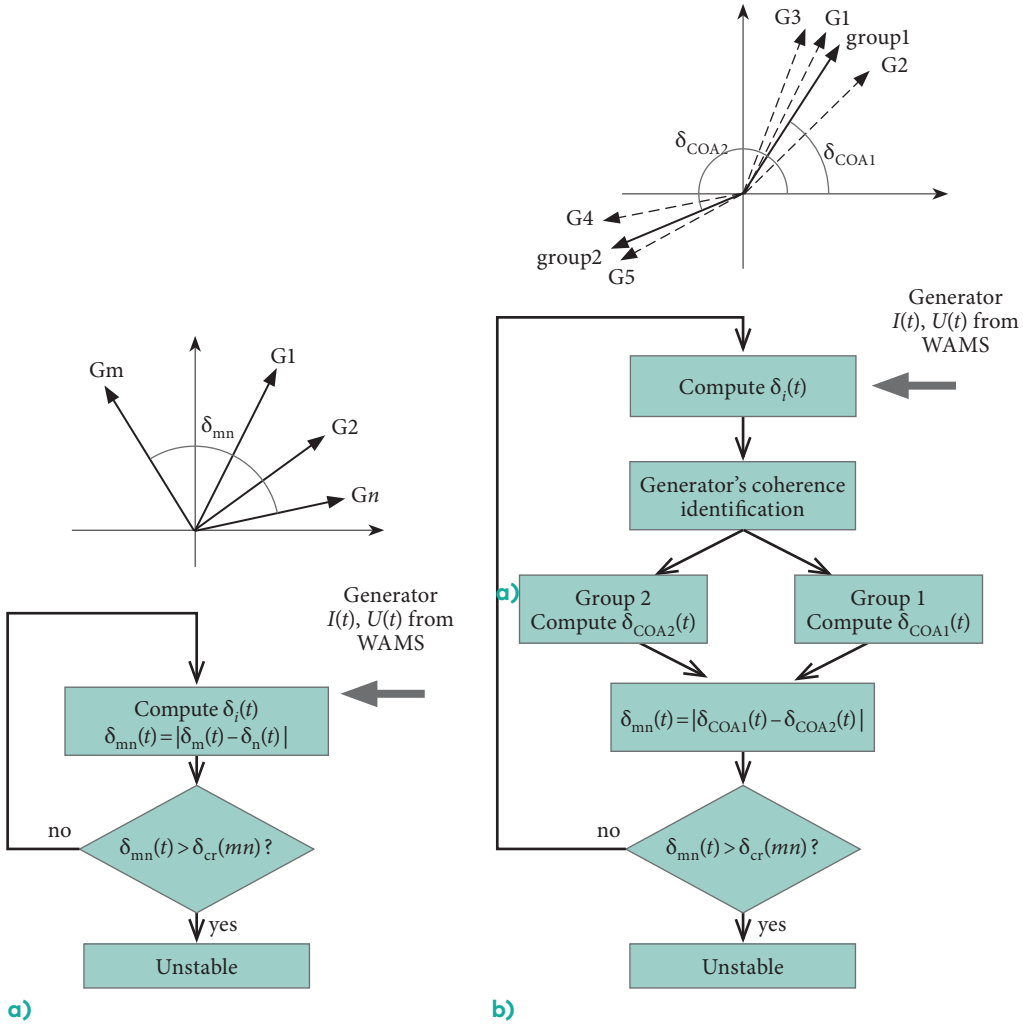

Fig. 5.21. Generator angle difference control algorithms

several complete rotation cycles. This can be useful for systems which are tolerant of asynchronous operation for a short period of time.

Alternatively, the algorithm may respond to the angle difference between groups of coherent generators (Fig. 5.21 b)). In this case, the COA should be calculated for each group of coherent machines according to (5.16) and (5.17) and the difference between the COAs is then compared with the critical angle value.

A generalised flowchart of the WAMS-based OOS protection system is shown in Fig. 5.22.

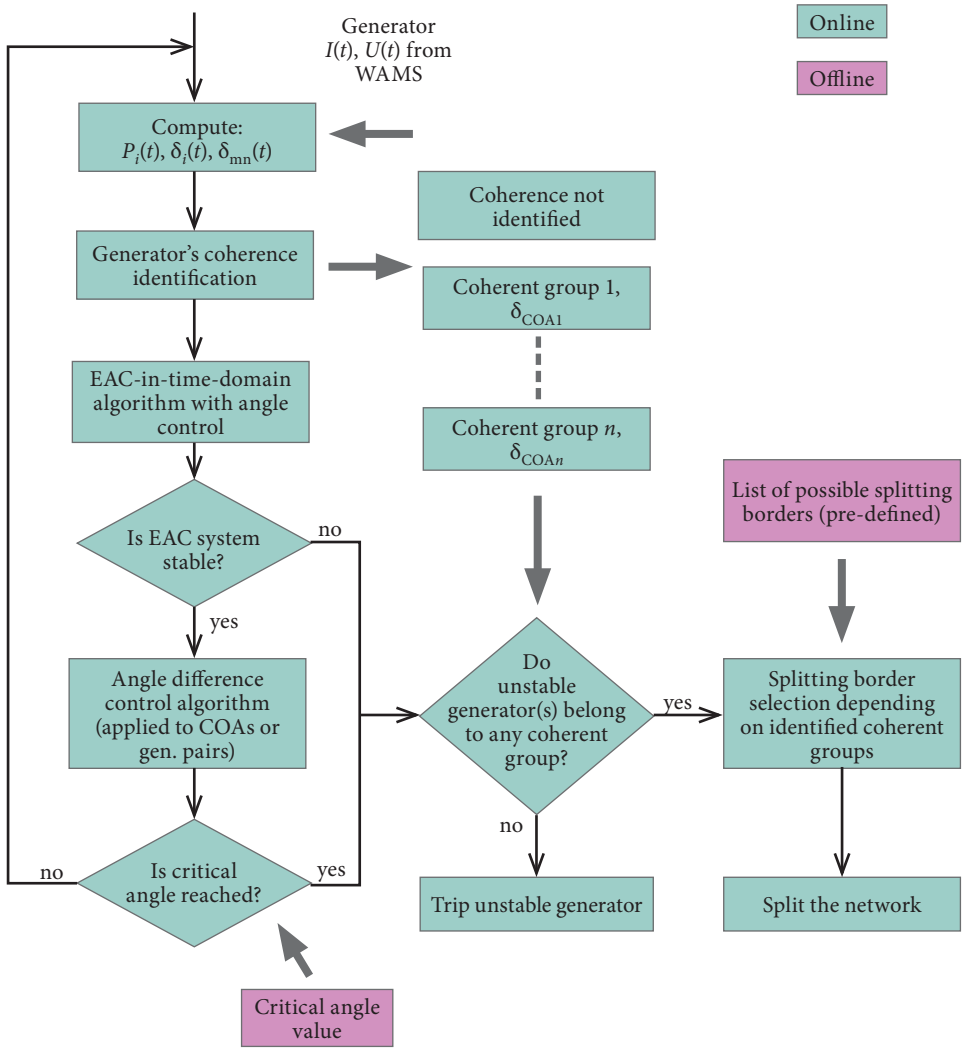

Fig. 5.22. Generalised flowchart of WAMS-based OOS protection system

At the off-line stage, the critical angle values should be known for two cases. The first case assumes that the generator's coherence has been identified online and thus, the critical angle setting will be applied to the COAs of the generator clusters. The most credible generator clustering patterns along with the associated critical angles could be derived during off-line simulations. Then that critical angle value is taken which suits the actual clustering pattern detected online. In the second case, it is assumed that the algorithm has been unable to reliably form groups of coherent generators. Then, the largest angular difference is chosen among all the pairs of machines and the advancing generator of the selected pair is tripped first.

If the coherent groups have been reliably detected by the time when instability occurs, then a suitable splitting decision can be chosen online. A list of transmission lines allowed to be tripped should be created at the offline stage and periodically updated with the actual state of the network. The choice of the particular splitting decision relies on the identification of coherent groups. Among all the possible splitting decisions, those that satisfy the condition regarding the separation of coherent groups have to be chosen. If there are several possible cutset patterns that allow separation, then each particular cutset should be analysed to fulfil the minimal power imbalance criterion. One of the methods described in Section 4.4. "Islanding Strategies" could be used to keep the imbalance to a minimum after splitting.

Network separation by itself may introduce a serious stress to the system. It is possible that at the post-splitting stage some of the generators within the islanded parts will diverge from the neighbours. Thus, an OOS condition may arise between generators within an island and should be treated accordingly. An EAC-based algorithm will not provide the correct decision in this case and should therefore be blocked. However, the angle difference control algorithm along with the detection of the coherence of generators can still be applied to each island separately. Care should be taken to avoid further splitting of the energy-deficient island because such splitting may worsen the situation and make questionable the self-healing ability of the island. On the other hand, for an energy-rich island, the angle difference control algorithm can be applied to trip individual generators that are accelerating in relation to the remaining machines.

6. CONSIDERATIONS ON PRACTICAL IMPLEMENTATION

6.1. PMU-based approach

The basis of WAMS consists in PMUs, which synchronously sample voltages and currents at the place of installation, calculate voltage and current phasors, the signal frequency and the frequency rate of change and streams these data in a standardised data frame through the communication channel to the higherlevel equipment (Fig. 6.1 a)). The WAMS-based OOS protection algorithm described in Chapter 5 expects that current and voltage measurements from all generators will be available at the control centre in real time and with minimal latency. At the control centre, the OOS protection algorithm is processed and a decision is taken. As soon as system instability has been detected and network cutset points have been chosen, feedback signals should be sent from the control centre to the protection relays or other IEDs, which trip the circuit breakers of the corresponding lines.

Several considerations need to be taken into account regarding a PMU-based OOS protection system:

1. The EAC-in-time-domain algorithm relies on transient energy calculation, and thus the moment of the transient needs to be captured with a high accuracy, and likewise all subsequent transients that may result from fault clearing and autoreclosing should be traceable with high resolution. Fault clearing time typically does not exceed 50 ms for a high-voltage transmission line; the switching time is even shorter during the autoreclosing cycle. Thus, generator electrical power should be sampled at a sufficiently high rate to have the ability to capture all those transients and thus provide an accurate estimation of generator energy. The IEEE C37.118 revision of the IEEE 1344 Synchrophasor standard stipulates several PMU synchrophasor reporting rates: 10, 25, 50 frames per second (fps) for 50 Hz systems and 10, 12 ,15, 20, 30, 60 fps for 60 Hz systems (see Section 3.3). Even in the best case with 50 fps, the minimum time step between two consecutive measurements is 20 ms, which may not provide the required accuracy. Modern PMUs are capable of much higher data reporting rates, and thus, high-resolution PMUs with a data reporting rate of 200 fps or higher should be used within the OOS protection scheme.
2. The angle control algorithm relies on the estimation of the generator angle difference, which in its turn is derived from the voltage and

current phasors. The phasor angle is defined within ±180°, and a phase-unwrapping procedure has to be implemented before the angle difference can be estimated. At low sampling rates, the phase-unwrapping algorithm may produce incorrect results, which is another reason why PMUs with a high sampling rate should be used.

3. The OOS protection algorithm suggests that PMU measurement for each generator of the network will be available in real time and with minimal latency. Measurements from several PMUs of a large power station will be aligned and processed by the phasor data concentrator

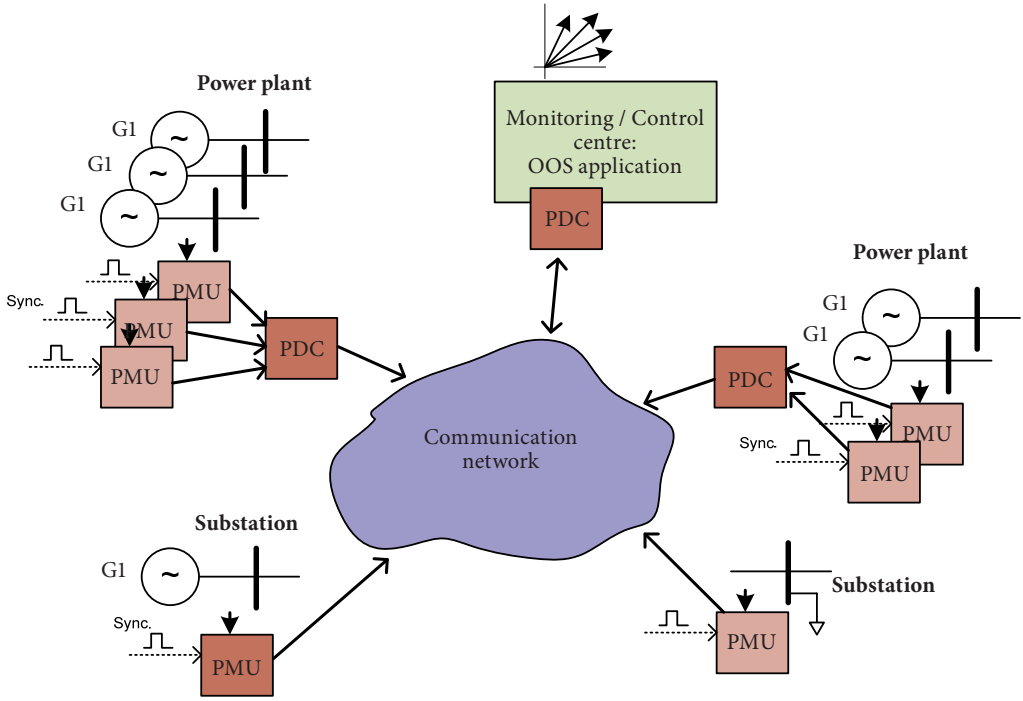

a) PMU-based OOS protection application

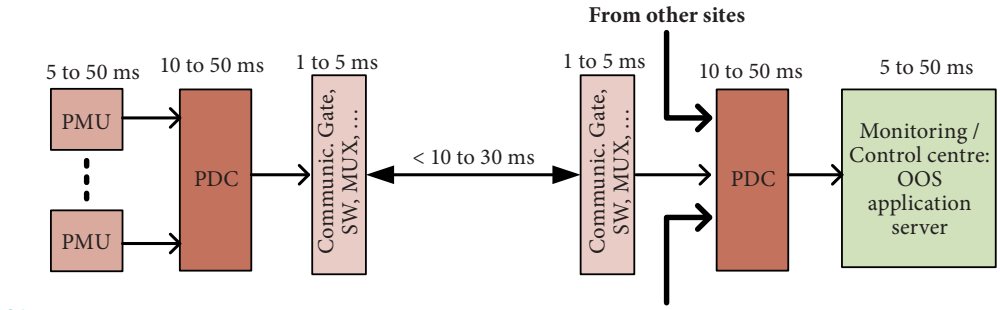

b) communication chain latencies

Fig. 6.1. a) PMU-based OOS protection application; b) communication chain latencies

(see Chapter 3.4) and then streamed to the next level in the communication chain. The large number of PMUs needed and higher-than-usual frame transmission rates will impose an additional demand on the capacity of the communication network. The communication channels' time delay and communication-equipment-introduced latency should be kept to a minimum to ensure real-time decision-making. The total time delay calculated from the moment when a row measurement is taken and up to the moment when a decision is taken by the control centre application should not exceed 200–300 ms. Typical communication chain latencies are shown in Fig. 6.1 b).

An obvious bottleneck of the PMU-based approach lies in the necessity to transmit the phasor data with a high time resolution towards the control centre. The latencies introduced by the communication equipment may seriously degrade the performance of OOS protection, especially during the detection of first-swing instability. The EAC-based part of the algorithm concurrently necessitates a high sampling rate and minimal time delays. The algorithm part based on generator angle control can in turn be used in a more relaxed environment with significantly lower sampling rates, and this is because the generator rotor angle trajectory changes smoothly and never changes abruptly, even in the presence of transients.

6.2. Dedicated-terminal-based approach

An alternative approach can be proposed which allows reducing the amount of information to be transmitted and, at the same time, ensures a high performance in first-swing instability detection. Such a protection system consists of several OOS-protection-dedicated terminals, which should be installed at large power stations. Each terminal measures the currents and voltages of the power station generators and computes the electrical power and angles for each generator (Fig. 6.2). The measurements of all remotely located terminals are synchronised by using a GPS-disciplined station clock. The terminal sampling frequency should be high enough (500 Hz or more) to be able to catch fast transients. EAC-based instability detection is processed locally, at power station level. The protection terminals exchange generator angle information in real time and EAC-based instability detection indications are transmitted. Because all the high-time-resolution tasks are accomplished locally, the data frame transmission rate can be significantly lowered (down to 20 fps).

The overall structure of such an OOS protection system can be implemented in two different ways. The first way is by using a centralised structure similar to the one in the PMU-based approach. Therefore, information

from all the remote station terminals is gathered in the control centre and the decision is taken by a dedicated OOS application server. The remote terminals inform the OOS application about the angular position of each machine and also stability/instability indication is provided for each particular machine. Then, the splitting decision is taken depending on the generators' coherence and in agreement with a pre-defined list of feasible splitting strategies (see Chapter 5, Fig. 5.22). When the decision has been taken, SCADA resources will be used to transmit commands to trip the corresponding CBs.

Another possible implementation is shown in Fig. 6.3. Unlike a centralised approach, this is a "flat" structure with data exchange between the power station's protection terminals. This kind of structure may be suitable for relatively small power networks with few generation sources, moreover, ones for which the list of possible splitting decisions is fixed and is known in advance. Reasoning for such a "flat" structure can be provided by several stipulations. Typically, large power stations are interconnected by at least one HV transmission line (or several lines in series) and there already exist communication links between major substations which are serving line current differential protection communication needs. Modern line current differential schemes support multi-terminal configurations with up to five terminals, which exchange data in real time [96]. Ordinarily, protection-grade communication is provided by means of a dedicated high-speed point-to-point communication link by using optical fibre technology. For less critical lines, the multiplexed channel can be used with the communication bandwidth defined as a multiple of 64 kbps. Using a similar technique

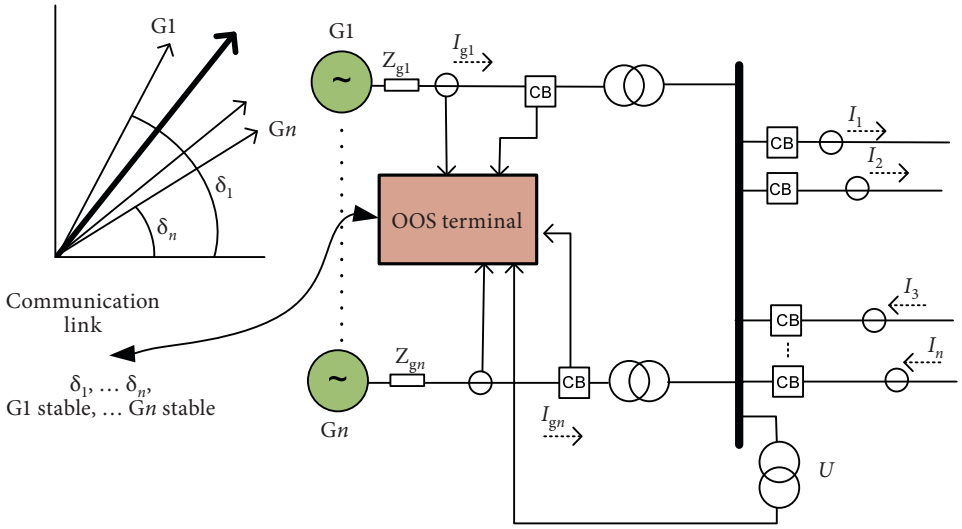

Fig. 6.2. OOS protection terminal measuring generators' terminal voltages and currents

and with minor modifications of the communication link at intermediate substations, it is possible to from a given station communicatively reach any other station. Assuming direct information exchange between the power station's OOS protection terminals (and presuming data passage at intermediate substations), the OOS protection algorithm can be implemented within each protection terminal. The data frame which circulates in the communication loop should contain dedicated fields for each generator of the system. Each terminal inserts into the data frame the information about the angles of "its own" generators and inserts stability/instability marks obtained as the output of the EAC algorithm. Then, the frame is retransmitted to the next terminal. Based on a 50-machine system, the frame length *FL* can be estimated as follows:

$$FL = 16bit \cdot 50\left(Generators\ angles\right) + 2bit \cdot 50\left(Generators\ status\ \frac{stable}{unstable}\right)$$
$$+2bit \cdot 50\left(control\ specific\ information\right) +$$
$$+150 \div 200bit\left(frame\ header, time-stamp\ and\ integrity\right) \approx$$
$$\approx 1200\ bits\ per\ frame.$$

Using a 64 kbit/s communication channel (which is considered to be the minimum communication bandwidth for line current differential protection duties), such a frame can be transmitted at a rate of 20 fps, which is adequate for the OOS protection system to perform flawlessly. The time delays introduced by the communication links will be minimal if a point-to-point link between the stations is used.

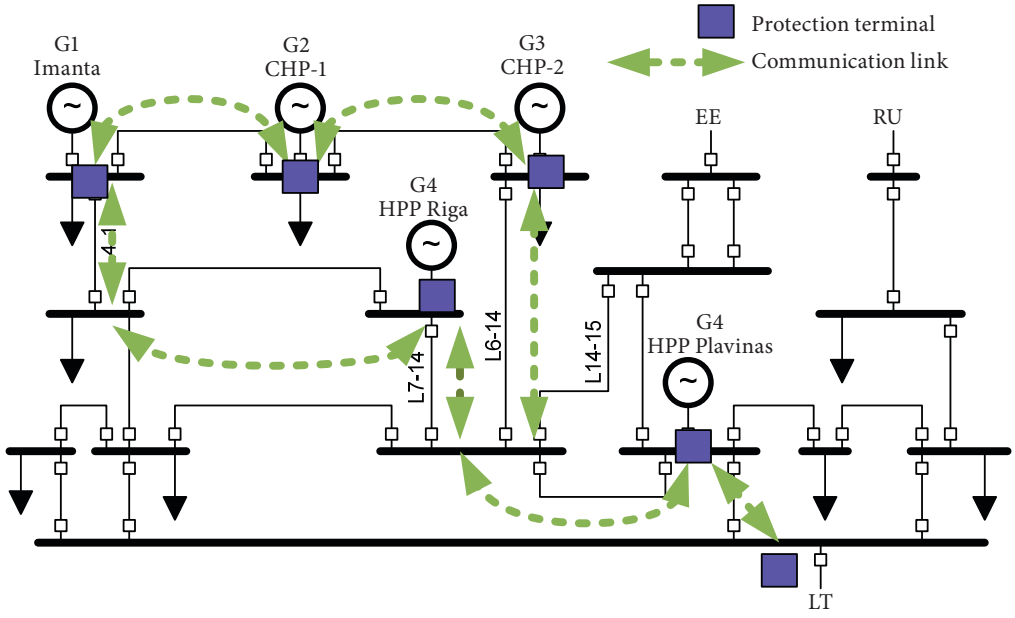

Fig. 6.3. Information exchange between protection terminals

Relying on local information and information from the terminals of the remote stations, each terminal implements the generator coherence identification algorithm. Typically, the generators of one power station will be coherent due to the straight coupling between the machines. Therefore, the task for the local terminal is to identify which of the remote stations swing in unison with the local station and which ones are diverging. The list of possible generator grouping scenarios should contain a reference to the particular lines to be tripped for each scenario. When an OOS condition has been detected (by EAC-based or angle-control-based algorithms) and a suitable splitting decision has been fetched from the list, the control fields of the corresponding CBs in the data frame are filled. Upon decoding the CBs' command fields, terminals at power stations or IEDs at intermediate substations will trip the corresponding CBs. The ample opportunities of the existing tele-protection equipment can also be used to transfer CB trip commands.

6.3. IEC 61850 implementation

The general principles and structural features of the communication based on the IEC 61850 standard are described in Chapter 8. Implementation based on the IEC 61850 communication standard can vastly improve the performance of the OOS protection system in terms of complexity reduction and hardware minimisation. At the power station level, current and voltage signals from all the generators should be wired up to the corresponding inputs of the OOS protection terminal. The problem of the hardwiring of analogue and status signals can be solved by implementing the Sampled Value (SV) communication technique within the power station process bus (Fig. 6.4) [97].

Here, the OOS protection terminal controls all the generators of the power station by means of subscribing to SV messages from the generators' merging units (MUs). Thus, the terminal is provided with all the necessary information (generator currents, bus voltages and generator status information). Additionally, information about the status of the circuit breakers (CBs) of the outgoing transmission lines (on/off) and the values of the currents of the transmission lines I_1, I_2,…I_n are also available for the OOS terminal as a subscriber and may be further used for the identification of the existing power network configuration. At station level, the OOS terminal may benefit by obtaining information from protection relays and various IEDs by means of subscribing to GOOSE messages from the relays of interest. The main point here is the availability of information about short-circuit events and other unbalanced conditions of the network. The OOS terminal does not need to trace the unbalanced conditions of the

network any more because this information is available from the neighbouring relays.

Reliable communication between different stations and substations is a critical part for the proposed OOS protection system. The present scope of the IEC 61850 standard is limited to data exchange within a substation [98]. Some attempts have been made to extend the already existing IEC 61850 communication services and models to wide-area communications structures [99]. The main problem here is that the inter-station communication bandwidth using a wide-area network is significantly lower compared with the intra-station 100 Mbit/s Ethernet. At the same time, the data frame transmission rate of the OOS protection terminals is much lower compared with other protection applications (line current differential protection). Considering the relatively low data transmission rate, various protocol-independent methods can be used for data transmission over WAN, including proxy and data tunnelling techniques. Inter-station communication and communication between stations and the control centre are covered by sections IEC61850-90-1 and IEC61850-90-2 of the standard (some parts are

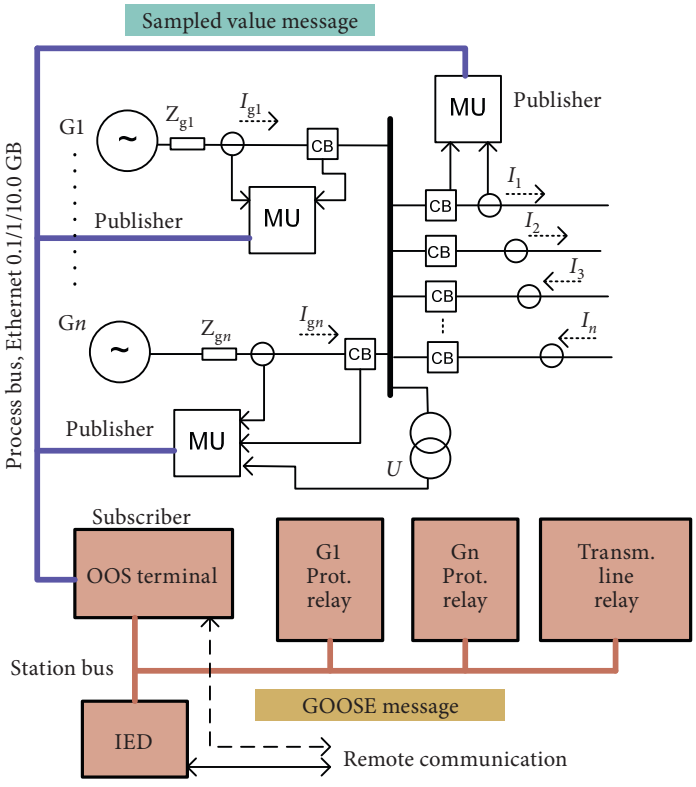

Fig. 6.4. OOS protection terminal measuring generators' signals using IEC 61850 communication (taken from [97])

under development). The IEC/TR 61850-90-1:2010(E) document [100] provides a comprehensive overview on the different aspects that need to be considered when using IEC 61850 for information exchange between stations.

7. COMMUNICATION IN A POWER SYSTEM

The modern electric power system is considered "the largest automatically operated machine made by mankind" [101]. The huge amount of synchronously operating equipment, the very large physical size of the system elements and the geographically distributed nature of the system makes proper functioning of the system virtually impossible in the case of lack of information. At each and every stage, starting from electricity production and towards electricity consumption, the operational conditions of the power system should be extensively monitored and controlled, thus ensuring the functioning of the system in a safe and optimal manner. Information exchange has always played a critical role in power systems and will become even more critical, considering that the amount of useful information is steadily growing.

The initial attempts to improve the reliability of power supply by using the "supervise and control" approach were made in the early 1930s. From those times into the present, the name "Supervisory Control and Data Acquisition" (SCADA) has become a synonym for power system monitoring and control applications. The functionality of the earlier SCADA systems was restricted mainly to power station operator actions, taken in response to changes in the system state. Nowadays, with all information digitalised, the list of power system applications which benefit from the system-wide information availability is constantly growing. The most important applications are as follows:

- detection of high-voltage equipment faults and abnormal conditions and equipment protection;
- substation automation and control;
- power station operation control;
- optimisation of transmission and distribution network management;
- distributed generation system management;
- optimisation of power flow and energy balancing;
- wide-area measurement system;
- system-wide emergency alarming applications and wide-area protection;
- processing, visualisation and archiving of power system data;
- updating and correction of power system mathematical models;
- demand-side management applications.

A suitable communication structure and a standardised way of information exchange are the essential prerequisites to support all of the listed functionalities. The data exchange structure of the typical power system utility is presented in Fig. 7.1. Power system entities (power stations, substations,

control centres) are located distantly from one another with the majority of measuring and control equipment concentrated at large substations and power stations. The data exchange should be provided at the power station/substation level where all the participating IEDs exchange information in real time by using a local area network (LAN) and thus a united substation automation system (SAS) can be formed. Inter-station communication should be provided to implement the tele-protection function [102] and transmission line current differential protection [103]. Station-to-control-centre data exchange by means of a wide-area communication network (WAN) is the core of the functioning of a SCADA system and is also the basis of wide-area measurements (WAMS) and system-wide protection systems.

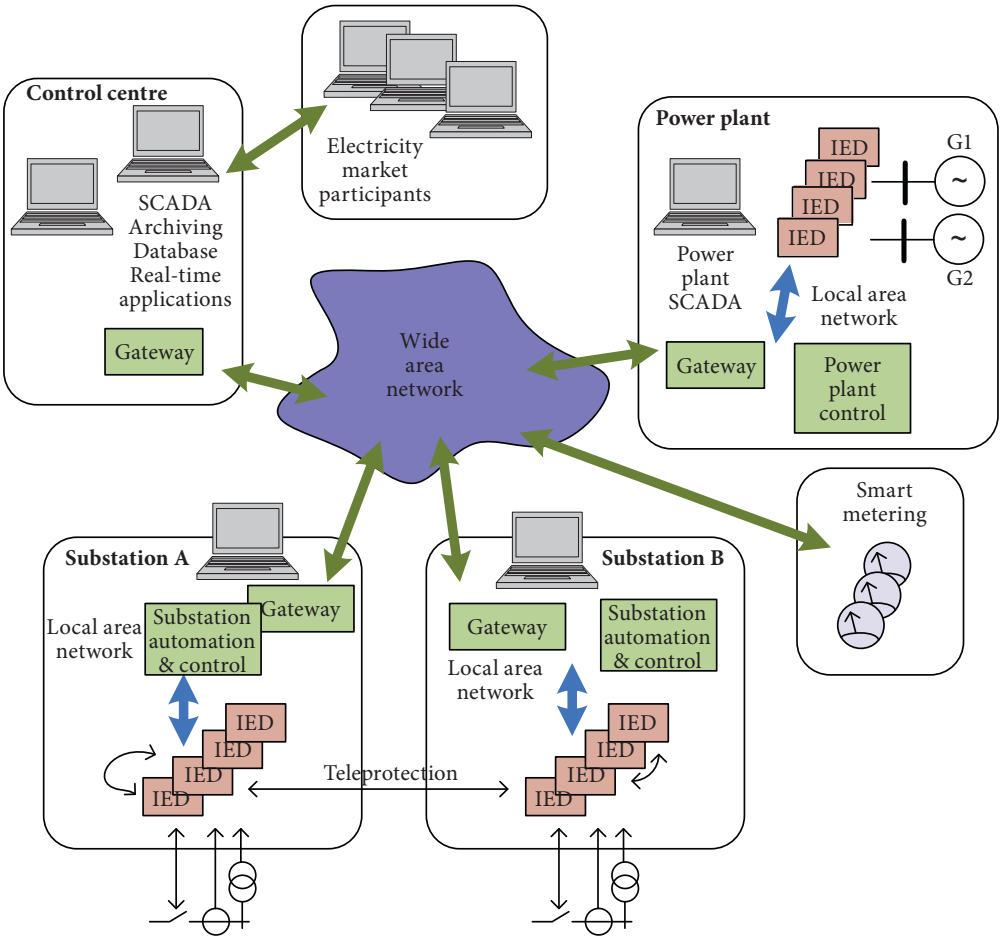

Fig. 7.1. The communication structure of the power system utility

Power system communication networks should conform to two main requirements:

1) the data exchange rate should meet the requirements of the particular application;
2) a very high level of network reliability and information security should be ensured (including cybersecurity).

The first obligation is dictated by the nature of power system operation, that is, the processes should be controlled in real time. Different types of power system applications have different understandings of the term "real-time". The real-time scales and the expected data traffic for typical power system applications are presented in Fig. 7.2.

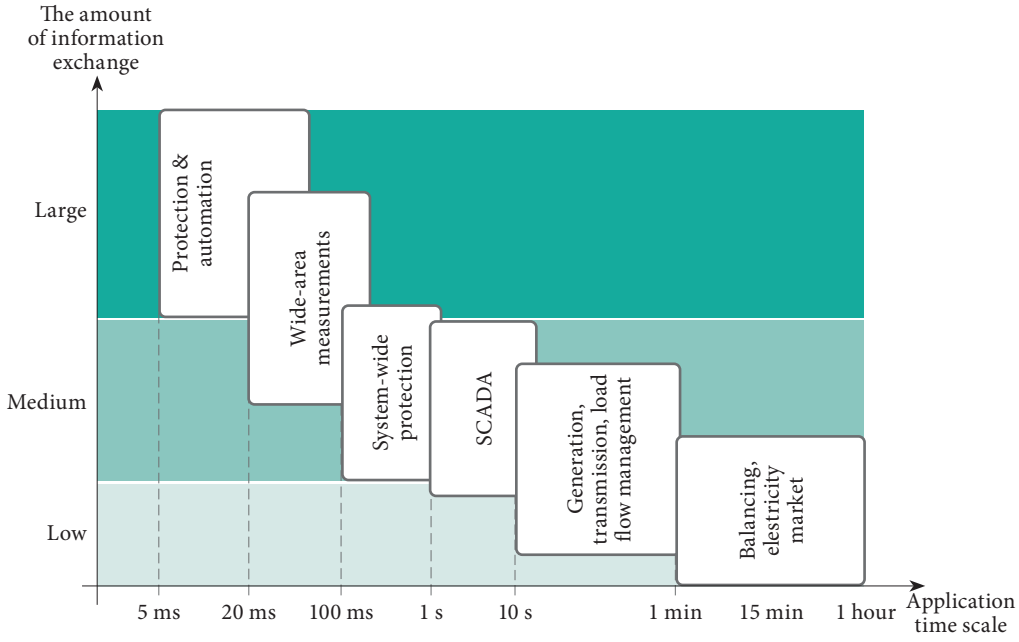

Fig. 7.2. Data exchange demand and real-time scales for different applications

Protection and automation applications have the highest demand on the data exchange rate with minimum tolerance for data latencies. Data availability is critical for protection applications because the decision should be taken within 20–100 ms after the disturbance and no data confusion or data retransmission is accepted. Other two demanding applications are wide-area measurements (WAM) and WAM-based system-wide protection systems. If the information is collected for post-fault analysis or is used by a database/archiving application, then real-time data availability is not so important; the main requirement is that the communicated data should not be lost. Measurements obtained from WAM could be used for time-critical applications (power-system-stability-related applications, wide-area protection). Then data availability in real time has the highest priority. The latency between data arrival from different locations in the network is acceptable by a small margin but data availability is paramount. The SCADA system is a less demanding application, but the availability of information is still very important because the system operator cannot take the decision relying on incomplete information. All the remaining applications can be considered non-real-time ones – the application response time may vary significantly because the control action is taken by a human or by non-real-time-operating software.

Network reliability and security is the second very important group of issues concerning the communication structures for a power system. General requirements can be formulated as follows [104]:

- Only ruggedised communication equipment accompanied by an appropriate physical medium should be used. All the communication-related equipment must be able to withstand harsh environmental conditions. Heavy EMI conditions should have minimum effect on the physical communication media.
- The communication network topology should provide a high level of redundancy. At least one alternative path should always be available.
- The communication network must be sustained in case any single point in the network fails. The network must be able to automatically recover from a failure.
- The network must be transparent to the user. All the information and devices must be easily managed, monitored and controlled by using network management software.
- Network management software must be applicable to multiple hardware, software, and network operating environments and support the object management structure as well as its expansion.
- Repairing of network components must be done in a very short time. Defective components must be hot-swappable with a new or repaired component.

- Network security mechanisms should provide the highest level of information security and should be capable of withstanding cyberattacks.
- The devices and the protocol profile chosen should presume network scalability, upgradability and future-proofing, and be robust enough for operation today and have a clear migration path to increased performance in the future [104], [105].

Nowadays, such tight requirements could be supported by at least several communication equipment manufacturers, and power system engineers should exercise care when choosing the particular vendor.

7.1. ISO reference model

The International Organisation for Standardisation (ISO) provides the overall structure of the complete communication system which is known as the ISO reference model for Open System Interconnection (OSI). The goal of the ISO-OSI model has been to provide interoperability between different communication systems by means of standardisation of the communication functions. The ISO-OSI model has a seven-layer architecture. It defines seven layers, or levels, within a complete communication system (Fig. 7.3) [106]:

- Layer 7 – Application layer – the end-user layer where the received information is processed by the user application and/or the user application creates the information to be sent.
- Layer 6 – Presentation layer – this layer ensures independence from differences in data representation by translating from application to network format and vice versa (e.g., data encryption, compression, character code translation) [106]. The presentation layer transforms data into the form that the application layer can accept.
- Layer 5 – Session layer – this layer establishes, manages and terminates connection sessions between applications. The session layer sets up, coordinates and terminates conversations, exchanges, and dialogues between the applications at each end [106].
- Layer 4 – Transport layer – ensures that the information delivered is error-free, in sequence, and without loss or duplication.
- Layer 3 – Network layer – ensures network routing, addressing, call set-up and call clearing. The physical/logical path of the data is established at this level.
- Layer 2 – Link layer – ensures error-free transfer of the data frames from one node to another over the physical layer.

- Layer 1 — Physical layer — defines the mechanical, electrical, optical, and logical properties of the interfaces between the user equipment and the network equipment.

A typical way of how information exchange between two devices is performed can be described as follows. The transmitting device passes the data to be transmitted to the applications layer, where it is processed and passed from layer to layer down the stack with each layer performing its designated functions. The data are then transmitted over the physical layer. Network switches and routers use the information assigned by Layers 3 and 2 to redirect the data frame to the destination device. Upon reaching the destination, the data are passed up through the layers again, each layer performing its assigned operations until the data is used by the receiving device. While the data pass through the seven-layer stack, each layer adds supplementary information (a header and a footer) to the data that directs and identifies the packet. The header and the data together form the data packet for the next layer, which in turn adds its header and so on. This process is called encapsulation. The combined encapsulated packet is then transmitted. The receiving device reverses the process, de-encapsulating the data at each layer with the header information directing the operations. Then, the application at the receiving end finally uses the data. The process is continued until all

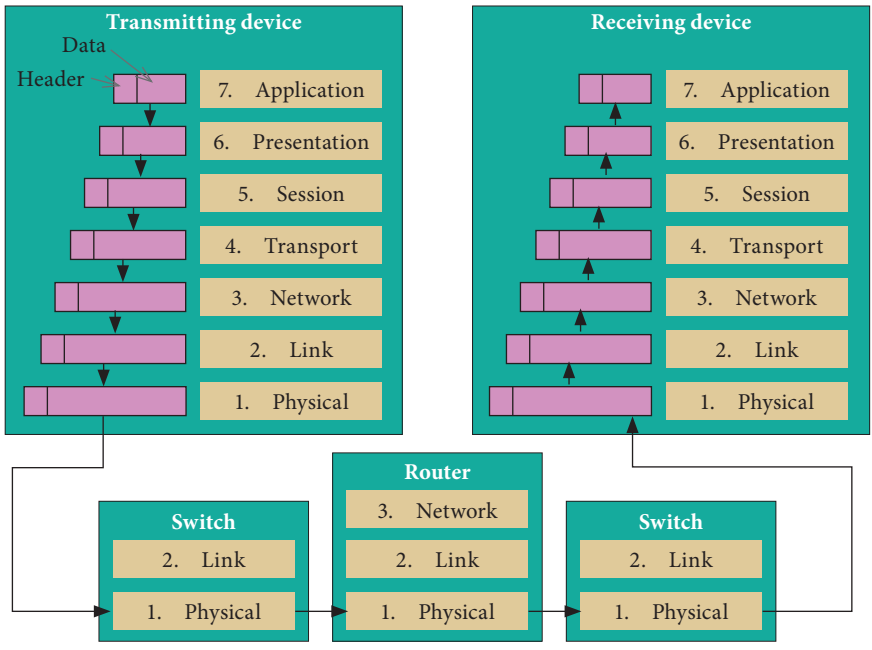

Fig. 7.3. Data flow in a seven-layer OSI model

the data have been transmitted and received. It should be noted that the OSI-ISO structure is a conceptual model which does not specify how each layer must be implemented. It is also assumed that the number of layers can be reduced for the particular application. Only Layers 1, 2 and 3 are mandatory for data transmission/receiving and thus, data-latency-critical application or applications with a less sophisticated data exchange procedure can use the simplistic approach to the OSI-ISO model with a reduced number of layers. An example of mapping of Internet TCP/IP protocols on an OSI-ISO model is presented in Fig. 7.4.

Referring back to Fig. 7.1, two major communication structures should be highlighted:

1) the LAN network, which provides information exchange within each individual substation/power station;
2) the WAN network, which provides inter-station and station-to-control-centre information exchange.

7.2. Substation local area network (LAN)

A substation automation system (SAS) is a mission-critical task where many protection relays, IEDs and automation systems coordinate their operation to provide secured and uninterrupted functioning of power system elements. The functions of SAS comprise control and monitoring of the switchyard, protection of the power equipment, recording of events and disturbances, energy metering and automation functions for energy asset management. Considering that all the processes should run smoothly even if the environmental conditions are at their worst, a well-proven and reliable

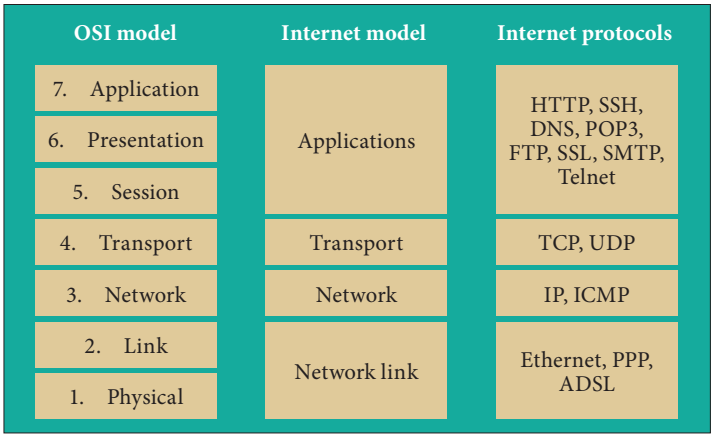

Fig. 7.4. Mapping of the TCP/IP protocol

technology should be used for providing the substation communication network. With the amount of digital-communication-enabled IEDs exponentially increasing, the Ethernet communication standard is a future-proof technology, which now is widely used to ensure communications between the devices on the substation network. The topology of a substation network comprises the following fundamental topologies: bus, tree, star, ring, or mesh (star-ring) ones [105]. Regardless of which network topology has been chosen, network reliability and redundancy should be a key requirement with the highest priority. An example of a substation network with a double-star (redundant-star) topology is presented in Fig. 7.5.

Redundant-star topology can be implemented by applying a physical double star with the most critical IEDs also doubled and with a connection with physically different LANs. For a logical double-star topology, each critical device should have a double-access interface (a double access node), which should be connected to two independent LANs. The communication protocol should provide the network fault detection methods and network reconfiguration mechanisms. The Parallel Redundant Protocol (PRP) and the Rapid Spanning Tree Protocol (RSTP) [105], [107] represent a typical and effective way to support network redundancy at the protocol level. The PRP protocol assumes that the two LANs (the main one and the redundant

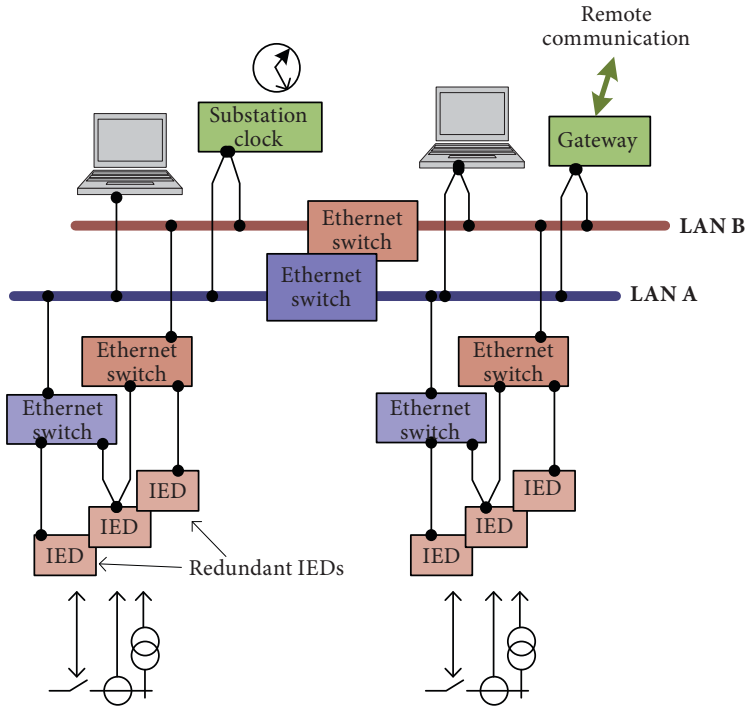

Fig. 7.5. Double-star topology

one) are completely separated and fail-independent. A source node simultaneously sends two copies of a frame, one over each port. The two frames travel through their respective LANs until they reach a destination node. The destination node accepts the first frame of a pair and discards the second one, making use of the sequence number in each frame, which is incremented for each frame sent.

The RSTP protocol is defined in the IEEE 802.1w standard [108]. The protocol sends out specific messages to the various nodes in the network to detect the broken paths and then performs communication path re-configuration, using the next available healthy communication path. RSTP is suitable for operation in star, ring and mesh configuration.

Another popular network topology is the ring, which uses point-to-point communication links (Fig. 7.6). All the Ethernet switches are connected in a loop and IEDs and other devices are connected with a switch. The data is transmitted between the source and the destination through nodes in one or two directions in the ring. Every node can simultaneously send a message to its neighbour. If the ring is broken, the data stream will be automatically redirected by the Media Redundancy Manager (MRM) switch, which operates according to the Media Redundancy Protocol (MRP) [105], [107]. For a ring-closed state (a healthy state), the data transmission path is as follows: MRM-to-Switch1-to-Switch2-to-Switch3 (shown with green arrows).

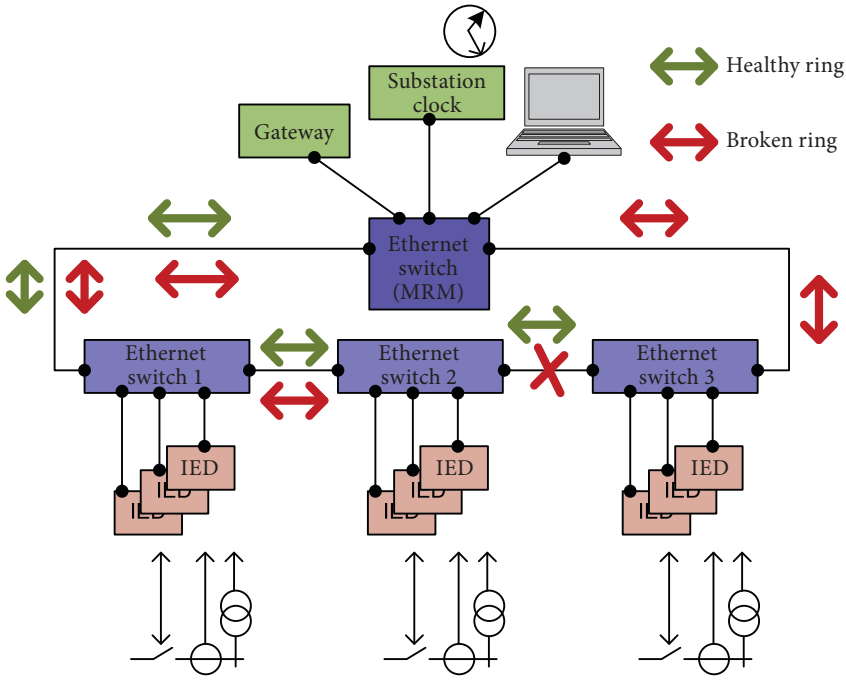

Fig. 7.6. Ring topology

The link between the MRM switch and Switch 3 is blocked (not used) for a healthy state of the network. When a network failure occurs, the MRM switch detects the ring-open state and uses the link between the MRM switch and Switch 3 to reach the IEDs connected to Switch 3 (the communication path for the ring-open state is shown with red arrows).

Depending on the size, complexity and design criteria of the substation network, topologies like the ring, the star, or a combination of the ring and star topologies can be implemented. The complete solutions for substation automation Ethernet LAN along with a comprehensive description are typically provided by several network equipment vendors [105], [107], [109].

The next important issue is the choice of the physical layer of the network. Today, the two most popular physical layer standards for Ethernet are twisted-pair copper cable (Category 5 or Cat 5) and fibre optic cable. Twisted-pair copper cables are easier to terminate and have lower installation costs but are susceptible to electrical noise and are limited to a distance of up to 150 metres (the shielded version) for a 100 MHz signal bandwidth [110].

Optical fibre, in turn, can easily carry a data bandwidth of up to 1 Gbps [110]. Multi-strand optical fibre cable makes it possible to share one cable among multiple users. Depending on type and the bandwidth required, the distance without amplification or signal repeaters can reach dozens of kilometres. Furthermore, optical fibre is among the most preferable communication media for substations because of its inherent immunity to EMI/RFI. The only disadvantage of using optical fibre is cost. The cost of optical fibre itself is still high, and installation of an optical Ethernet network is also very expensive, especially if it is used for remote controlling and monitoring applications in which data need to be transmitted over long distances.

Table 7.1

Typical copper and fibre optic interfaces of Ethernet switches (adopted from [110])

Port type	Port description	Typical distance	Power budget
10/100BaseT 10/100 Mbit	RJ45 Copper – unshielded	100 m	N/A
10/100BaseT	RJ45 Copper – shielded	150 m	N/A
100BaseFX 100 Mbit	Multimode ST Fibre Optic (full-duplex)	2 km	14 dB
100BaseFX 100 Mbit	Single mode SC Fibre Optic	40 km	12.5 dB
100BaseFX 100 Mbit	Multimode LC Fibre Optic	2 km	18 dB
1000BaseFX 1 Gbit	Multimode SC Fibre Optic	2 km	12.5 dB
1000BaseFX 1 Gbit	Single mode 1550nm SC Fibre	40 km	17.5 dB
1000BaseFX 1 Gbit	Single mode 1550nm LC Fibre Optic	70 km	20 dB

Ethernet interfaces are identified by the speed (in megabits per second), the modulation type ("Base" refers to baseband signalling, which means that only Ethernet signals are carried by the medium), and the physical interface (e.g., T or TX stands for Twisted Pair, FL or FX stands for Fibre). For optical fibre communications, signal attenuation is defined with the optical power budget parameter. The power budget can be thought of as the maximum permitted attenuation of the light signal as it travels from the transmitter to the receiver, while still permitting reliable recognition of received data [110]. Some common copper and fibre interfaces used in the protective relaying industry with the corresponding IEEE 802.3 definitions, distance and power budget are shown in Table 7.1 [110].

7.3. Wide area network (WAN)

The communication between substations and the substation-to-control-centre communication is implemented by using a wide area network (WAN). Substation LANs are connected to the WAN by means of gateways (Fig. 7.1). A typical WAN consists of meshed point-to-point interconnections of copper cables, fibre optic cables, radio links or satellite communication channels. The physical interconnections of the WAN are not exclusively available for the power system applications but are typically shared among several network users. This means that power-system-related communications should reserve dedicated channels to guarantee real-time data transfer and information security. These dedicated channels may form the private WAN, which is physically or logically separated from the public WAN. Considering all the types of information exchange within a power utility (voice, e-mail, video, telemetry, tele-protection, line current differential protection data, control and automation), the real-time operating systems have the highest demand on WAN performance. The highly deterministic character of the data and the minimal data latencies are paramount for real-time applications, and the wide area network should be capable of supporting these requirements.

The typical way of how the substation LAN is connected to the WAN is by using data multiplexor MUX (Fig. 7.7). The output of the multiplexor is connected to the public data network where several sources share the same communication channel [110].

There are two approaches of how data from several sources can be aggregated to use a single communication channel: the time-division-multiplexing-based technology with fixed time slots (TDM) and the packet-switched (PS) technology. TDM and the packet-switching technique differ in the way of how the shared transport channel is used. In TDM communication, the use of the transmission medium is divided into time

slots and each time slot is allocated to an individual source of data. Thus, the data packet at the multiplexor's output is represented by a series of time slots each containing the data from the particular input (Fig. 7.8 a)).

At the receiving end, the input data stream is sequentially de-multiplexed to the outputs. Therefore, there should not be a timing difference between the multiplexing and de-multiplexing procedures; the devices of the sending and receiving ends should be synchronised. Because each data source has dedicated time slots that can never be occupied by another source, the communication link established with the TDM can be considered as a dedicated channel. The data transmitted have minimum uncertainty, and the data latencies are nearly constant. On the other hand, the time slots are unnecessarily wasted if no data are transmitted from one of the sources, and this leads to inefficient use of the transmission link. The Synchronous Digital Hierarchy (SDH) and the Synchronous Optical Network (SONET) are typical examples of the implementation of the TDM technique [102].

When the packet-switching technique is used, the data from the input sources are acquired as they become available and fill the multiplexor's data buffer until the specified data packet length is reached. The data packet formed is then outputted at the maximum available speed (Fig. 7.8 b)). There are no dedicated allocations of transmission resources in PS-based communication, and if the particular application has no data to send, the shared resource is allocated to a different application [102]. Therefore, data allocation in the output frame is dependent on the data traffic at each

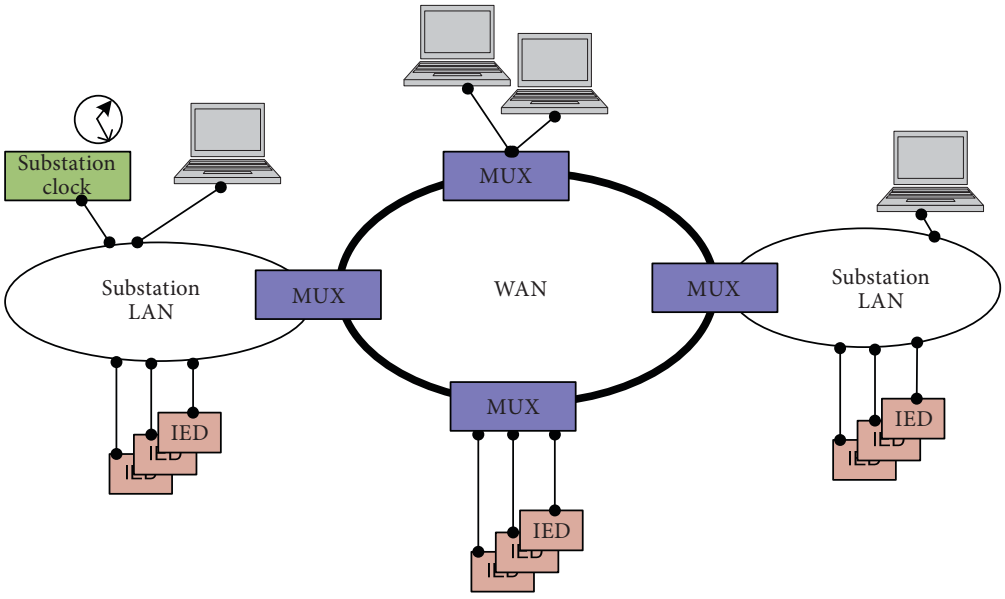

Fig. 7.7. Connection of substation LAN to WAN

particular input. Applications with high data traffic will dominate in the output data frame while infrequent data from a different application may be delayed or put in queue. Communication over Ethernet is a typical example of the packet-switching technology.

For real-time applications, an important issue is how quickly network faults can be detected and how quickly the network is able to recover after a fault. The mechanism of network troubleshooting and network recovery should be an integral part of the network protocols and should be transparent to the user. The network operation, administration and maintenance (OAM) functionality is a prerequisite for successful network implementation when mission-critical tasks are considered. A comprehensive set of OAM functions is a distinctive feature of the SONET and SDH networks. The network operation is monitored continuously and network failures are detected all the time. This is possible because a significant bandwidth of the network is allocated specifically for OAM-related data exchange [102]. The typical restoration time after a "path failure" event is within 50 ms for SONET/SDH networks.

In contrast, Ethernet has no integrated support of the OAM functionality. It has required the development of additional protocols to support OAM functions. These protocols access the shared transport channel in the same way as any other data service and are subject to the same variances in latency and lack of determinateness [102]. A significant improvement was made in Ethernet-/IP-based networking by introducing the multiprotocol label switching technique (MPLS). The MPLS provides the capability to

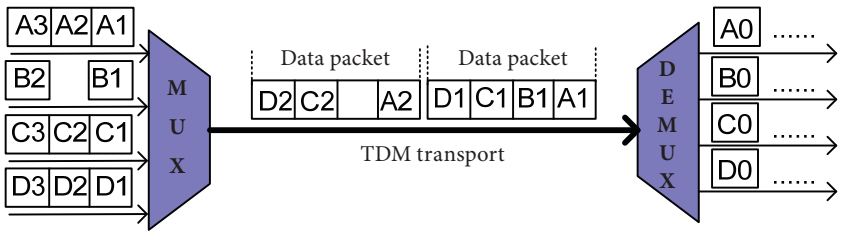

a) TDM communication

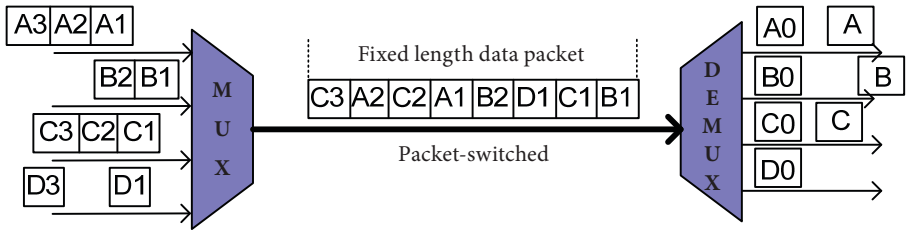

b) packet-switched communication

Fig. 7.8. a) TDM communication; b) packet-switched communication

establish connection-oriented paths or tunnels, called label-switched paths (LSPs). The MPLS technique is advantageous when it is desirable to force a packet to follow a particular route that is explicitly chosen at or before the time the packet enters the network, rather than letting it follow the route chosen by the normal dynamic routing algorithm as the packet travels through the network.

Upon comparing both technologies, the TDM and the Ethernet-based one, a conclusion can be made that the TDM-based communication technique might be preferable for time-critical, point-to-point applications when data consistency, minimal data latency and data certainty are paramount. In contrast, applications that are not time-critical or communication-delay-tolerant or ones that require point-to-multipoint data exchange will benefit from the packet-switching technology. This conclusion can be made on the basis of the operating principles of both technologies, but the ubiquity and universality of Ethernet as well as the latest advancements in technology push the protection relay manufacturers and power system engineers towards using the Ethernet/IP technology.

8. COMMUNICATION PROTOCOLS

The need for data exchange standardisation becomes obvious with digital communication-enabled equipment playing the major role in power system automation and protection. The desire for interoperability between devices from multiple vendors such as various relay manufacturers, SCADA system manufacturers, and communications equipment manufacturers has led to the development of several industrial communication protocols. Communication protocols are considered a "language" by which the equipment and software applications exchange information. Communication protocols are formal descriptions of digital message formats and rules that the participants should use to establish successful data exchange. Communicating devices have to agree on many physical and logical aspects of the data exchange process to ensure successful communication. There are many properties to the data exchange procedure that a protocol should define. The most important ones are as follows: data format, message type, data packet size, transmission speed, error correction types, handshaking and synchronisation techniques, address mapping, acknowledgement processes, flow control, packet sequence control, routing, etc. While protocol designs have classically been based on ISO-OSI reference model specifications, an optimised model also known as the Enhanced Performance Architecture (EPA) is often used to overcome the limited processing and communications capabilities of remote devices and wide area telemetry networks (Fig. 8.1). In practice, the EPA model allows achieving a much higher operational and communication performance compared with a seven-layer OSI

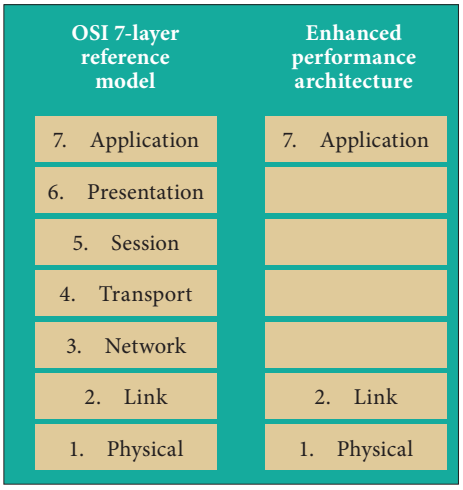

Fig. 8.1. EPA to OSI model mapping

reference model [111]. The 3-layer EPA architecture is a minimal architecture and can be expanded to support network communication capabilities (Layers 3 and 4 can be added accordingly).

Among the variety of communication protocols found in power system communication applications, the most common and widely accepted ones are as follows:

- DNP3
- IEC 60870-5
- MODBUS
- PROFIBUS
- IEC 61850

Because of the limited scope of the book, only general information about communication standards and protocols will be presented. For more technical details, the reader should refer to additional information sources [111]–[129].

8.1. Distributed Network Protocol (DNP3) and IEC 60870-5 Protocol

DNP3 and IEC60870-5 are two open communication protocols that share a similar approach to data communication and have similar structural and functional capabilities. Both protocols were intended for SCADA applications with DNP3 preferredly used in North and South America while IEC 60870-5 dominates in the European region [111]. The DNP3 standard protocol is supported by an active DNP3 User Group [112]. IEC 60870-5 refers to a collection of standards produced by the International Electrotechnical Commission (IEC), to provide an open standard for transmission of SCADA telemetry control and information [113]. Both protocols share the same basic concept but differ in some details and implementation peculiarities, which are summarised below:

- Enhanced Performance Architecture used to achieve the highest performance in data transmission (three-layered for IEC, four-layered for DNP3).
- Supported configurations include: peer-to-peer, multiple masters and slaves (DNP3); point-to-point, multipoint-to-point, point-to-multipoint (IEC).
- A range of physical interfaces can be employed: RS-232, RS-485, fibre optic, TCP/IP over Ethernet.
- Device addressing capability: 16-bit address (DNP3), variable address length (IEC).
- Polled and report-by-exception operation mode.

- Unsolicited messaging support.
- "Select-before-operate" control action.
- Time synchronisation and event time stamping.
- Broadcast messaging.
- Information grouping and classification (classes 0-3 for DNP3, Class 1 and Class 2 data for IEC).
- Unbalanced (master-only initiated) and balanced (master-/slave-initiated) mode of operation.
- High-security data transmission (16-bit checksum for DNP3, 8-bit checksum for IEC).
- File uploading/downloading capability.
- Standardised frame format (variable/fixed frame length for IEC, variable frame length for DNP3).

The choice between IEC 60870-5 or DNP3 depends on the industry and the particular application. Both protocols provide similar functionality and performance, enjoy a wide market acceptance and both are supported by the major equipment manufacturers. The decision can be based on the experience or preferences of the particular equipment vendor.

8.2. The MODBUS and PROFIBUS protocols

MODBUS and PROFIBUS are open protocols specifically designed for industrial communication. MODBUS was designed by the Modicon Corporation to provide communication between IEDs, programmable logic controllers (PLCs) and computers. MODBUS is an application-layer messaging protocol positioned at Layer 7 of the OSI model. The goal of creating the MODBUS protocol was to achieve an as simple and effective as possible way of data collection by the master station from multiple slave stations (sensors, actuators, IEDs, PLCs). Only one master station is allowed and only the master can initiate a data exchange. The protocol defines a series of write/read type commands to assign new binary/analogue values to slaves and to read information from slave equipment. The MODBUS protocol is comprised of three different implementations:

- MODBUS ASCII — the American Standard Code for Information Interchange (ASCII) is used for information coding (each character byte is coded as two ASCII characters) [114]. The message frame is limited to 252 bytes and the address space is limited to 247 bytes. Message broadcasting is possible. Data integrity is ensured by a checksum.
- MODBUS RTU differs from MODBUS ASCII in data encoding — the data are presented in binary form and transmitted as bytes. This

ensures a more compact form of data representation compared to MODBUS ASCII.

- MODBUS TCP/IP — a version with TCP/IP Ethernet functionality. A typical MODBUS message is encapsulated in a TCP/IP data packet.

The master-slave principle of the MODBUS protocols assumes that the master takes full control of communication whereas the slaves will only respond to the master's requests. The master writes/reads data to/from an addressed slave during every interrogation cycle and then passes on to the next slave. There are no time limits defined for slave response and no procedure has been specified for joining slaves to a communication bus. The physical layer of MODBUS is provided with an RS-232 interface (for a point-to-point link) and an RS-485 interface (for a multi-drop link). The MODBUS protocol does not provide an inherent time synchronisation function and, therefore, event time stamping should be done on the slave side. A detailed description of the MODBUS protocol is available in [115].

PROFIBUS (*Process Field Bus*) is also a master-slave protocol, which was designed in the 1990s to meet the industrial communication needs for process automation. Unlike MODBUS, PROFIBUS is multi-master-enabled protocol. If more than one master is present in a PROFIBUS network, they will pass the authorisation rights to communicate to one another with the help of a special "token" telegram. As soon as a particular master has a token, it can communicate with assigned slaves and other masters. Then the token is passed to the next master station. A specific procedure is provided to add a new station to the PROFIBUS network. A list of all added stations is created and dynamically updated, thus making it possible to add or remove stations without disturbing communication services. Special procedures are provided that allow bus scan cycle monitoring and passing of tokens. Broadcast messaging, time synchronisation and diagnostic functions are supported by the master station. There are two types of PROFIBUS in use today: PROFIBUS-DP (*Decentralised Peripherals*) and PROFIBUS-PA (*Process Automation*). PROFIBUS-PA was developed to extend the PROFIBUS-DP functionality, adding intrinsically safe data transmission in hazardous environmental conditions. DP uses the RS-485 physical layer (differential voltage signals are used for bit coding) while PA uses the physical layer defined by IEC 61158-2 [116] (differential current signals are used for bit coding), which ensures limiting of current flows so that explosive conditions are not created, even if a malfunction occurs. DP and PA buses can be interconnected by means of a special DP/PA coupler device to form a single PROFIBUS network. The data transmission rates are up to 12 Mbit/s for the DP bus (cable-length-dependent) and up to 31.25 Kbit/s for the PA bus. Detailed information on the operating principles of PROFIBUS can be obtained from [117]. PROFIBUS is not an Ethernet-enabled technology.

The solution known as PROFINET was developed by using the decentralised peripherals principles of PROFIBUS, but was inherently intended for Ethernet TCP/IP communications. PROFINET is not just PROFIBUS over Ethernet; it is a completely independent solution, which is maintained and supported by the "Profibus & Profinet International" organisation [118].

To conclude, both MODBUS and PROFIBUS are highly efficient and robust protocols that allow reliable solutions to be made for process automation tasks. MODBUS is a very effective and easy-to-implement tool when a single master-to-several-slaves configuration is sufficient. For applications that require more nodes, with several master stations, or if a hazardous environment is considered, PROFIBUS provides a reliable solution.

8.3. The IEC 61850 standard

While there are over 30 protocols that are used in substation automation, none of them can be expected to become a global standard that is able to meet all substation automation requirements and at the same time ensures full interoperability among different equipment manufacturers. IEC61850 "Communication networks and systems in substations" is the modern international standard that was released in 2003 and is managed by the working groups of Technical Committee 57 of the IEC (IEC TC57). Since then, the standard has been extended and improved to meet more of the needs of power system utilities, and the current version of IEC 61850 "Communication networks and systems for power utility automation" was successfully introduced in 2013 [119]. At present, IEC 16850 is accepted worldwide as the global standard that addresses all the needs in substation automation. The IEC 61850 standard was developed to achieve three main objectives:

1) allow interoperability and exchangeability among products from different vendors;
2) allow free allocation of system functions to electronic devices, thus providing a solution for almost any possible substation automation architecture;
3) the standard has to be future-proof to guarantee that the investments should not be lost in the years to come.

Instead of just defining how data will be transferred between communication participants, IEC 61850 uses an object-oriented approach to describe all the functionality, data and services which can be applied to existing and future substation automation tasks. The IEC 61850 standard provides a complex solution for substation automation by defining the following:

- object models to describe all types of information and functions available at the substation;
- communication services to be used between elements participating in substation automation;
- the configuration language to allow system/substation engineers to describe and configure regular and specific tasks of substation automation.

8.4. IEC 61850 modelling approach

Nowadays, the majority of substation-related functions (protection, measurements, control, metering, etc.) are implemented within dedicated intelligent electronic devices (IED), each containing a list of specific functions that the device is intended for. The IEC 61850 approach consists in describing a real device by its virtual model. The entire IED functionality is broken down into small pieces of automation-related information objects, which can be communicated over the network. The virtual model principle also applies to high-voltage equipment of the substation (circuit breakers, circuit switches, instrument transformers). These models have been termed logical nodes (LNs). Each LN provides some power-system-related services and is described by associated data objects. Data objects are grouped into several categories (general, status, command, measurements and settings), and data values can be monitored/modified. LNs can be addressed individually and thus, the entire substation automation system is comprised of a collection of LNs, each with designated functionality. Thereby, each particular substation automation task is performed as a result of information exchange between various LNs.

One of the popular examples for explaining the concept of LN is the LN of the circuit breaker (CB) (Fig. 8.2). The LNs' names (classes) and associated data are standardised, thus providing a unified approach to equipment design for different manufacturers [120]. A set of attributes is assigned to each data object with each attribute describing some of the data properties. Each attribute should belong to one of standard data classes with the attribute name, type and representation form also standardised (Boolean, integer, string; data quality; data time-stamping, etc.). Not all data objects and data attributes are mandatory for implementing; some of them may have an optional or conditional status.

As regards the example shown in Fig. 8.2, the circuit breaker is modelled with LN "Q0.1 XCBR". The LN name consists of the user-assigned part, "Q0.1", and the standard-defined name, "XCBR". The LN is described with several data objects: "Beh", "Mod", "Health", "Pos", etc. Data attributes (the type and format of data objects) are standardised in [121]. The CB position

("Pos") data are related to the Controllable Double Point (CDP) data class, which has several attributes (only two are shown for the sake of simplicity). The "StVal" attribute stands for status indication data; the data are in the Coded Enumeration format and the allowed values are Intermediate (00), OFF (01), ON (10), Bad State (11). The "CtlVal" attribute is a switch position control in Boolean format with ON/True, OFF/False values.

LN names are standardised and grouped according to their functional purpose. The first letter of the LN name ("X" for XCBR) defines the node class that the LN belongs to. Compatible node classes for substation automation are standardised [120] and are presented in Table 8.1.

Several LNs can be grouped together to form a new entity called a logical device (LD), to which a new name can be assigned by the user. Typically, this new name reflects the LD functionality as viewed from the perspective of substation automation functioning (Fig. 8.3). The model of a real physical device (IED) may in turn be comprised of several LDs. In the simplified example of the transmission line protection terminal shown in Fig. 8.3, the IED is equipped with several protection types (PDIF — current differential, PDIS — distance, PTOC — time overcurrent), performs CB monitoring/control and also has disturbance recording (RDRE) and fault location (RFLO) functionality. LNs named "LPDH" contain specific information about real IED and should be added to each LD. All the LNs' data are

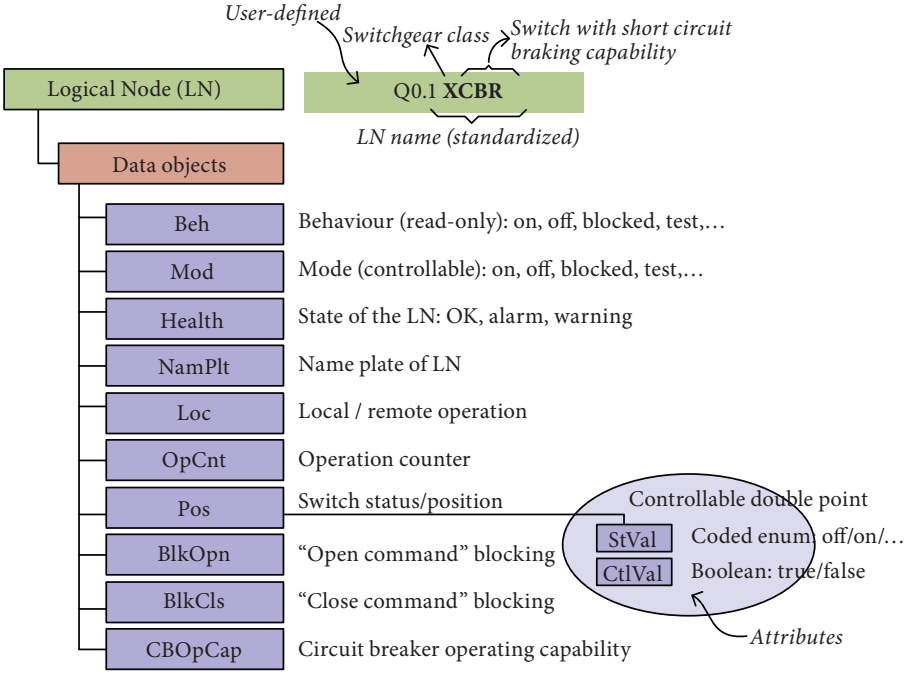

Fig. 8.2. The circuit breaker logical node (simplified)

accessible by means of the IED communication interface and the IED acts as a server from the communication network point of view.

LNs' data-communication-based approach allows logical interconnections to be performed between LNs that are residing in different physical

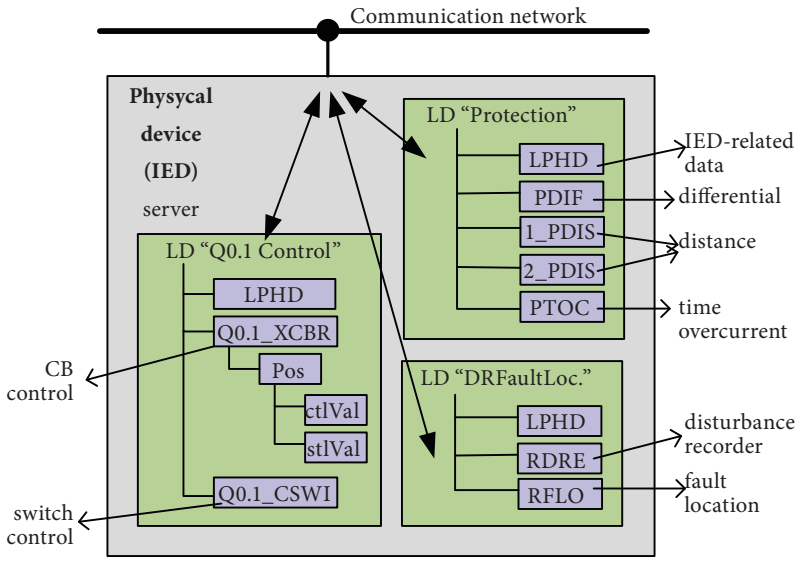

Fig. 8.3. Physical device model (simplified)

Table 8.1

Groups of logical nodes

LN class name	LN class description	Number of LNs	Examples
Axxx	Automatic control	4	ATTC (tap changer), AVCO (volt. contr.)
Cxxx	Supervisory control	5	CILO (interlocking), CSWI (switch control)
Gxxx	Generic functions	3	GGIO (generic input/output)
Ixxx	Interfacing and archiving	4	IHMI (human-machine interface)
Lxxx	System	2	LPDH (physical device), LLN0 (common)
Mxxx	Metering and measurement	8	MMXU (measurement), MMTR (meter)
Pxxx	Protection	28	PDIS (distance), PDIF (differential)
Rxxx	Protection-related	10	RREC (autorecl.), RFLO (fault locator)
Sxxx	Sensor and monitoring	4	SPDC (partial discharge), STMP (temperature)
Txxx	Instrument transformers	2	TVTR (voltage), TCTR (current)
Xxxx	Switchgear	2	XCBR (circuit-breaker), XCSW (circuit switch)
Yxxx	Power transformers	4	YPTR (transformer), YLTC (tap changer)
Zxxx	Other power system equipment	15	ZMOT (motor), ZREA (reactor)

devices. This concept is illustrated in Fig. 8.4. Each LN data object should be referenced with its full logical path containing unique LD and LN names (Fig. 8.4) [122], [123].

The abstract data models of IEC 61850 provide a systematic approach to information presentation and data exchange to accomplish the substation automation tasks. Data models can be mapped to a number of communication protocols, and several communication technologies can be used. To ensure the compatibility of the standard with communication technologies of the future, the Abstract Communication Service Interface (ACSI) was introduced [124]. The ACSI principle allows splitting the domain-related data models and communication services from the communication protocol/communication medium itself (Fig. 8.5).

Thus, substation-domain-specific functionalities, which do not change often, become independent of the communication technology in use. The specific communication service mapping procedure lays a bridge between abstract communication services and real communication technology. The communication method is based on the 7-layer ISO-OSI reference model with the Ethernet technology chosen for Layers 1 and 2. Two methods of information exchange are considered for real-time applications. For time-critical messages, the Generic Object Oriented Substation Event

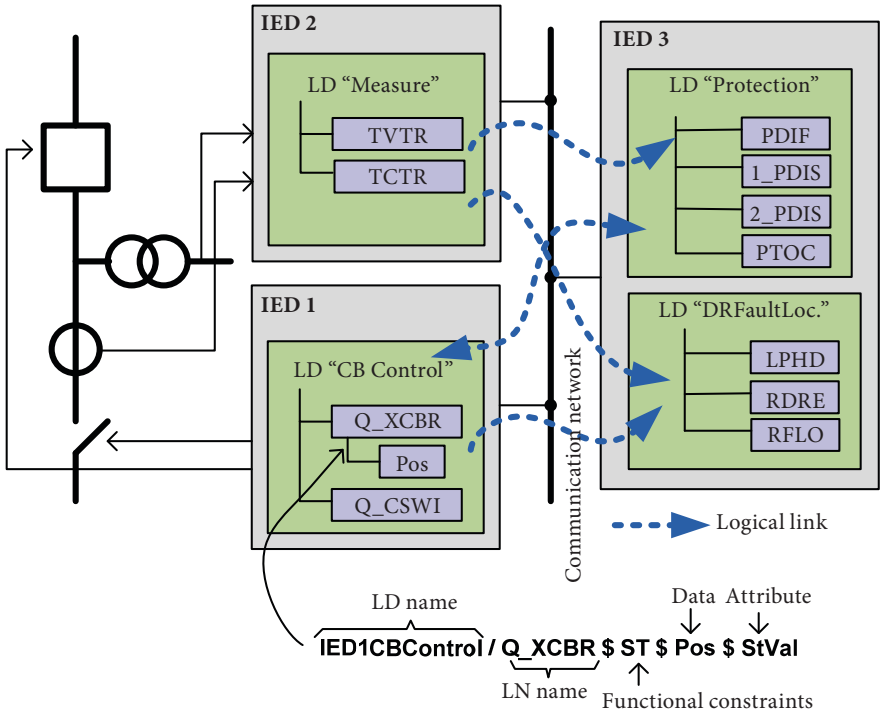

Fig. 8.4. The logical links between LNs residing in different IEDs

(GOOSE) and Sampled Value (SV) services are used. Both types of messages are mapped directly to the Ethernet link layer and thus, the fastest possible data transfer can be achieved (Fig. 8.5). Other communication services that also should run in real time but with less strict requirements (information polling from SCADA, data management and system operation maintaining applications) are implemented with Manufacturing Message Specification (MMS) and the TCP/IP service (Layers 3 to 7) (Fig. 8.5).

MMS is an application-layer protocol defined by the international standard ISO 9506, which specifies a set of services to be used in exchanging information between networked devices and/or computer applications. MMS is a connection-oriented method for communication between two entities: the client and the server. MMS specifies the messaging system to establish client/server communication and provides a definition, structure and meaning to the messages by means of standardising the following:

- objects that are contained in the server (variables, events, etc.);
- messages that can be used to manipulate server-contained objects;
- message encoding rules;
- message exchanging rules.

MMS allows any application or device to provide both client and server functions simultaneously. The communication between the client and the

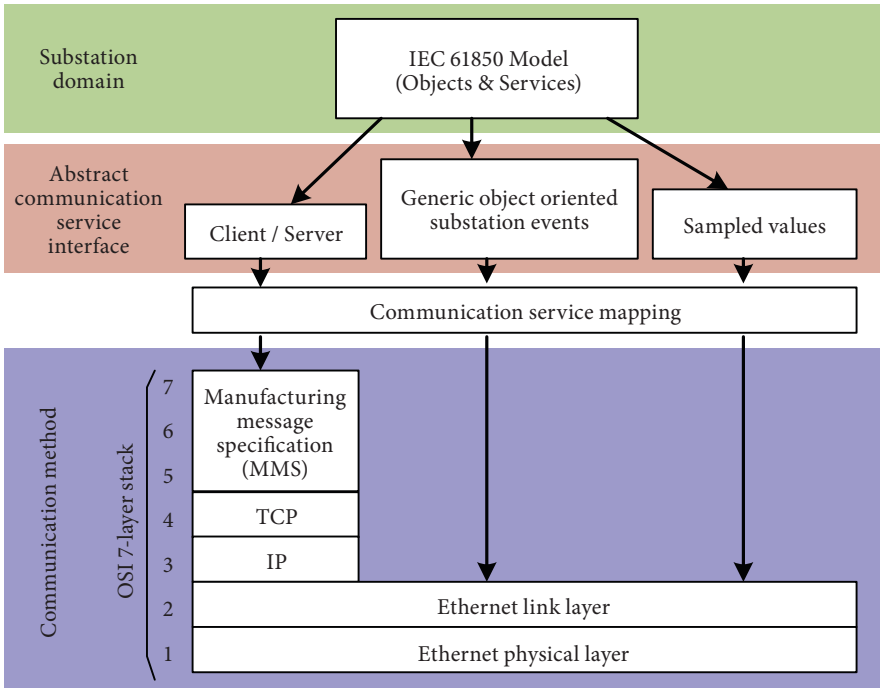

Fig. 8.5. IEC 16850 abstract communication service mapping

server is based on the request/response messaging principle (Fig. 8.6). The client sends a request message to the server and the server responds after the request has been processed. A spontaneous event messaging procedure from the server to the client is also provided.

The important feature of MMS lies in the Virtual Manufacturing Device (VMD) model, which specifies how the MMS server behaves in response to a specific service request as viewed from an MMS client application perspective. VMD is a way of virtualising the data/behaviour of real devices. The objects that exist in a real device are substituted with their virtual counterparts in the VMD. Then, the MMS client communicating with the MMS server sees the VMD that contains the objects (variables, events, files, etc.) of the real devices (Fig. 8.7). The VMD can be treated like a

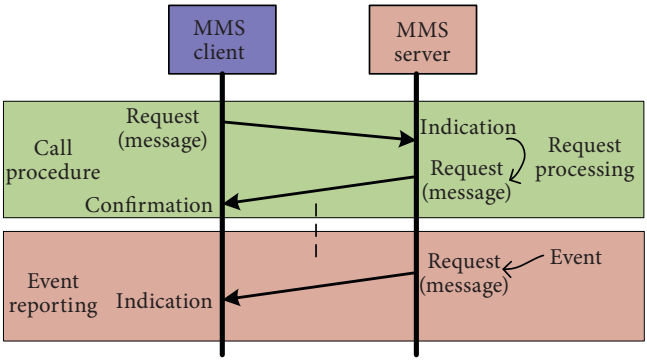

Fig. 8.6. MMS client-server communication principle

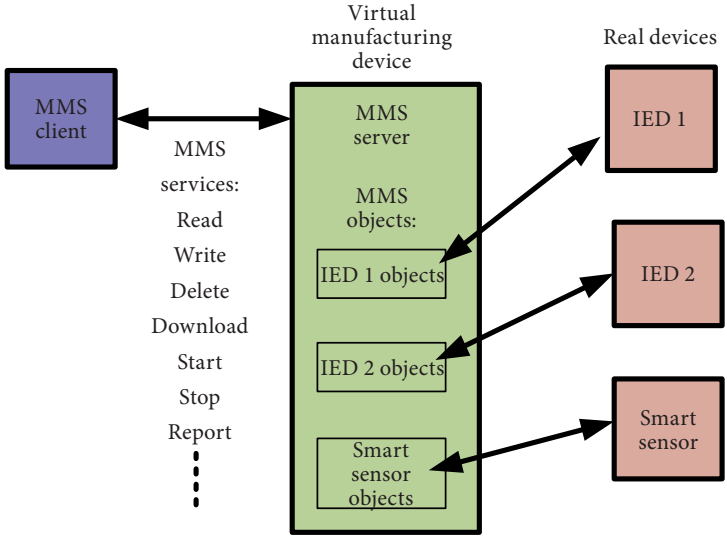

Fig. 8.7. VMD representation of IEDs

communication driver between the client and the real device, which images all the accessible information of the real device to the networked participants. This approach allows MMS services to be implemented in a unified manner for any vendor-specific equipment.

Object-oriented modelling is used to define the standard object classes: Named Variable, Named Variable List, Domain, Journal, Events, etc. Typical MMS services are: read, write, report information, download, read Journal, etc. The MMS client/server model is typically used for non-time-critical tasks and cannot be used for protection purposes.

To satisfy the information exchange needs for substation protection and automation applications, specific multi-cast messaging services are provided. Multi-cast messaging enables devices to broadcast status, control and input/output information to a number of devices simultaneously. Three types of multi-cast service are provided:

- Generic Substation Status Event (GSSE) message is intended for station-wide distribution of 2-bit status information;
- Generic Object Oriented Substation Event (GOOSE) message supports distribution of user-defined data sets;
- Sampled Values (SV) messaging service ensures distribution of discrete-time-sampled measurements and status data acquired from the high-voltage equipment.

8.5. IEC 61850 GOOSE message

The IEC 61850 standard provides a peer-to-peer communication model called Generic Substation Event (GSE), which is aimed at supporting time-critical activities between IEDs [125]. Time-sensitive information such as protection tripping commands, changes in equipment status, interlocking functions and multi-terminal-based protection information exchange has the highest priority with minimal communication latencies tolerated. One of the messages associated with the GSE services is the Generic Object Oriented Substation Event (GOOSE) message. The GOOSE service was intended to replace relay-to-relay wiring within a substation. The abbreviation GOOSE can be explained as follows: Generic — any type of data can be transmitted; Object-Oriented — information representation is defined according to the IEC 61850 data model; Substation — information is transmitted across the entire substation network; Event — the message is event-driven. A GOOSE message is transmitted as a broadcast/multicast message without being addressed to a specific receiver and without expectation of message reception acknowledgement. This mechanism is described in IEC 61850-8-1 and is known as the "publisher-subscriber" model. The "publisher" IED creates a new GOOSE message as soon as a new event appears.

Information transmitted by the GOOSE message is time-stamped and prioritised (a high-priority level guarantees the fastest message delivery). The message is distributed across the substation LAN and is accessible to any "subscribed" IED (Fig. 8.8). To make sure that the message was successfully delivered to the subscribers, the same message is retransmitted with a gradually increased time interval between retransmission moments (*T1, T2, T3, …*) until the maximum interval *To* is reached (Fig. 8.8). Then the message is continuously transmitted with a period of *To* until the new GOOSE message, driven by the new event, replaces the previous message. Such an approach provides a high reliability of message delivery in the absence of a message acknowledgement mechanism. Communication failures and disturbed/missed messages can be detected at the subscriber side by means of a number of mechanisms:

- Each GOOSE message has a "status number" (*stNum*), which is associated with the message driving event. The status number increases each time a new event appears and a new GOOSE message is generated. Lost messages can be detected by the subscriber by analysing the *stNum* field of the message.
- A "sequence number" (*sqNum*) is embedded in the GOOSE message frame and increases with every repeated GOOSE message. The sequence number is set back to zero every time the GOOSE "status number" increases; the *sqNum* field allows detection of out-of-sequence messages and lost messages.
- A GOOSE message is becoming "suspicious" if the time between the previous received message and the new one exceeds the Time Allowed to Live (TATL) (typically, *Ttal = 1.5 To*). The TATL value (fixed or varied) is embedded within the GOOSE message frame, and this is the way the publisher informs the subscribers when the next GOOSE message should be expected.

The IEC 61850 standard specifies the performance of the GOOSE message for control and protection applications (Table 8.2) [126].

Table 8.2

GOOSE message transmission time requirements

Performance class	Message type: fast messages	Message transmission time: not more than (ms)
P1: distribution bay/substations	Type 1A: "Trip"	10
	Type 1B: "Other"	100
P2: transmission bay/substations	Type 1A: "Trip"	3
	Type 1B: "Other"	20
P3: transmission bay /substation with top synchronising performance	Type 1A: "Trip"	3
	Type 1B: "Other"	20

Message transmission time includes all the necessary handlings at the sending and receiving ends. The time is counted from the moment the sender puts the data content on top of its transmission stack up to the moment the receiver extracts the data from its transmission stack [126]. The standard requires the "trip" (circuit breaker) type command transmission to be completed within 3 ms, which is even faster than typical relay-contact-wire-based command transmission. Thus, traditional applications like fast bus tripping schemes, breaker failure protection (Fig. 8.9), reclosing control, etc. can be replaced with GOOSE-message-based data exchange between participating IEDs.

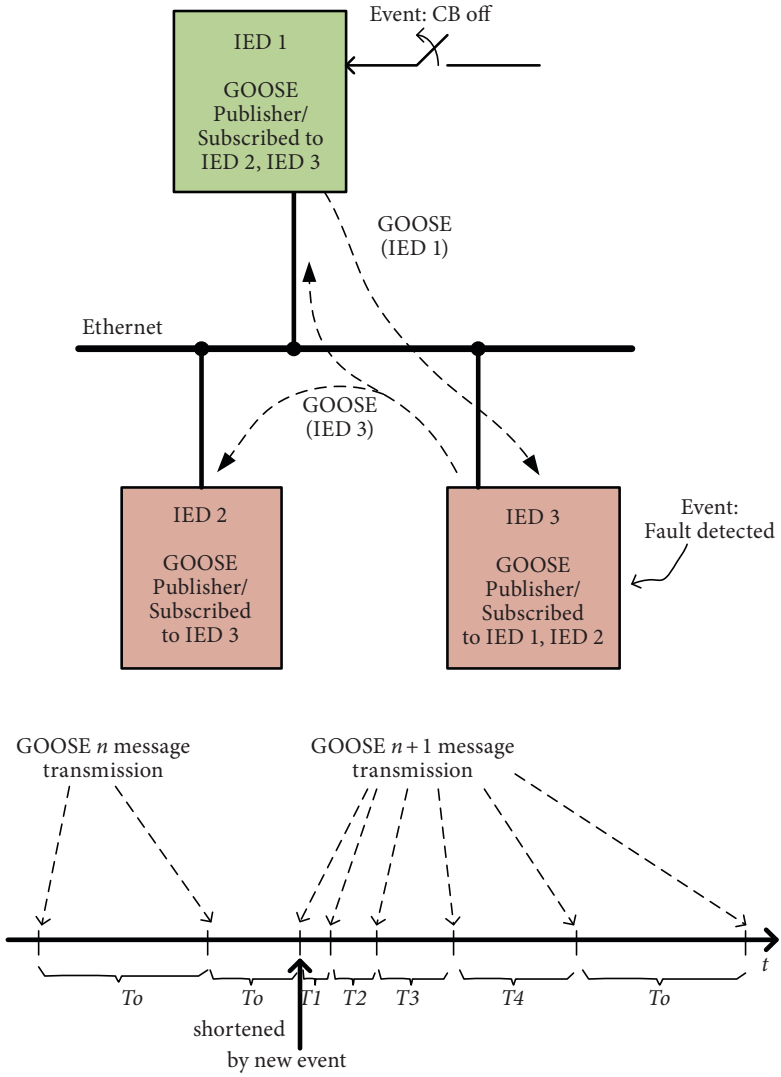

Fig. 8.8. GOOSE message transmission mechanism

While faults of the traditional hardwiring-based signalling schemes cannot be detected during steady-state conditions, the message retransmission mechanism ensures the knowledge of the communication channel health in nearly real time. As soon as the subscribed IED detects expiry of the TATL time limit, the communication channel/publisher fault can be declared and appropriate signalling can be activated. Another obvious advantage over the traditional approach is that the GOOSE message is not only a command-oriented/status-oriented message. Different data types like string, Boolean, integer values can be transmitted in the same GOOSE message. Therefore, all the data required by the specific protection scheme can be transmitted by means of a single GOOSE message.

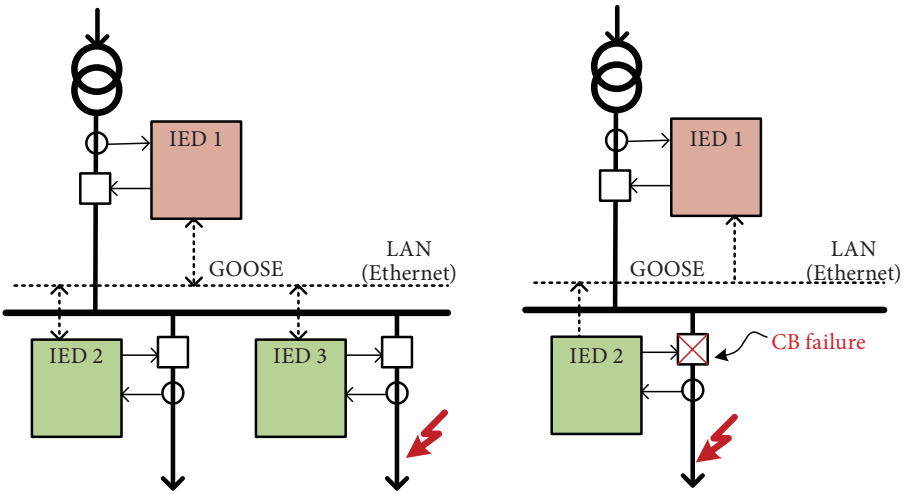

a) IED3 detects a feeder fault and transmits a message to block the fast-tripping element of IED1

b) the IED2-controlled CB fails to trip and the message is transmitted to IED1 to trip the incoming CB

Fig. 8.9. Traditional wiring schemes replaced by GOOSE message exchange over substation LAN

8.6. IEC 61850 Sampled Value message

IEC 61850, part 9-2 [127] has proposed an Ethernet-based communication network between process-level switchyard equipment and bay-level protection and control IEDs, which is referred to as the process bus. The process bus is intended for the transmission of the digitised instantaneous values of power system analogue quantities gathered from current (CT) and voltage (VT) transformers, sensors as well as status signals from high-voltage switching equipment (Fig. 8.10). Analogue signals from the instrument transformers are sampled and converted into a digital data stream by means of a dedicated IED called a merging unit (MU). The name "merging unit" originates from the fact that the MU merges (combines) sampled values acquired from several input signals in a single digital data packet. The MU can be treated as an external analogue-to-digital converter, which outputs digital data in a standardised way. A MU is typically a ruggedised device, which is specifically designed for use in a harsh environment and can withstand extreme temperatures. Placing the MUs right in the switchyard in close proximity to CTs and VTs allows radically reducing copper wirings

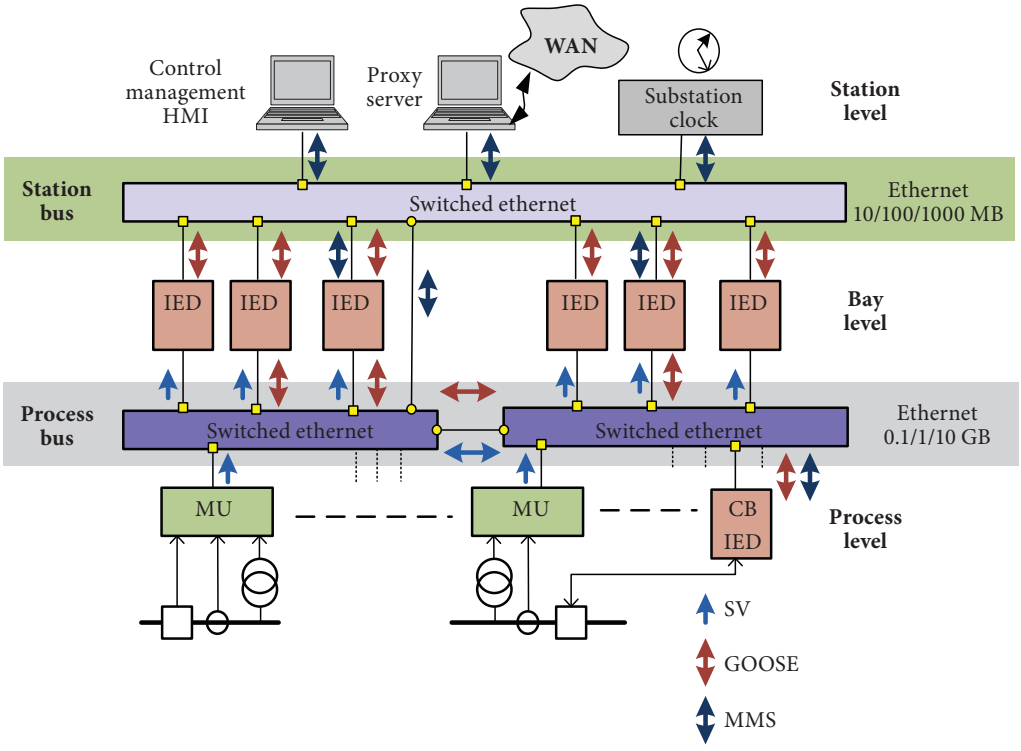

Fig. 8.10. Typical substation topology of IEC 61850

between primary equipment residing at the process level and control/protection IEDs at the bay level.

Two sampling rates are specified for a MU [128]: 80 samples per power system circle for protection and monitoring purposes and 256 samples per circle for power quality and other high-resolution applications. All station MUs are precisely synchronised in time (<1 μs) from the substation master clock. One pulse per second (1PPS) signal and IRIG-B are typical options. The sampled values are numbered in ascending order using a sample counter ("smpCnt"), which is forced to zero with the reception of each next synchronising pulse. Thus, sampled values obtained from different MUs can be aligned according to their "smpCnt" number and can be used by any IED within the substation (Fig. 8.11).

The output of the MU is connected to the substation process bus Ethernet network, using copper/optical connection. In the communication domain, a MU can be represented with several logical nodes (LN); typically, voltage measurements are referenced with TVTR LN and current measurements, with TCTR.

IEC 61850-9-2LE specifies how sampled value measurements shall be transmitted over an Ethernet network by an MU or by an IEC 61850-capable instrument transformer with an electronic interface. The sampled-value (SV) data set is packed in a multi-cast SV message and the SV messages are transmitted continuously at a specified rate without a data reception acknowledgement procedure. The SV protocol implements the same publisher/subscriber principle used by the GOOSE service. The MU is a publisher of SV messages and any subscribed IED can access the SV data. The

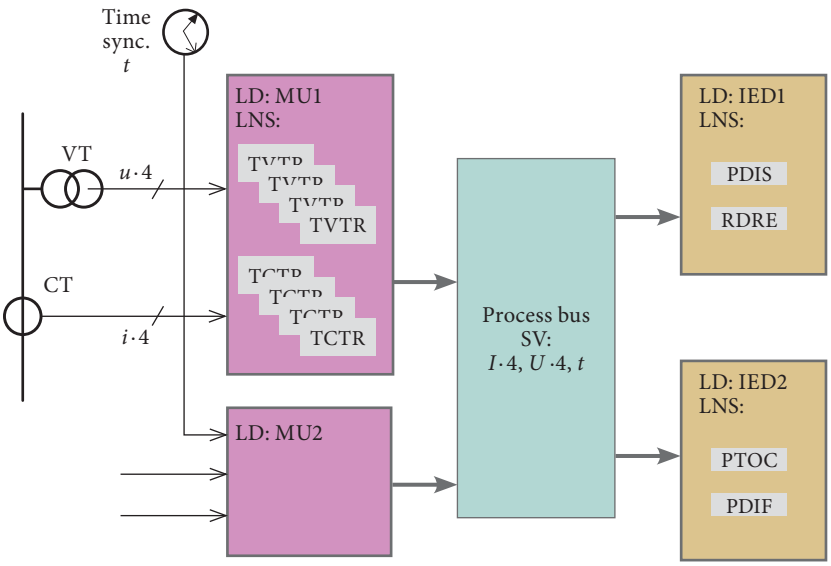

Fig. 8.11. Sampled Values service of IEC 61850-9-2LE

amount of traffic generated by SV message transmission depends on the number of MUs, the number of samples transmitted in one message and the signal sampling rate. Increasing the number of samples in one message will not lead to a proportional increase in data traffic because the same common part of the frame is used and thus, the optimum bandwidth of the Ethernet-based network is achieved with maximum frame length. A typical SV message contains instantaneous values of four currents (those of the three phases and the neutral) and four voltages (those of the three phases and the neutral).

The exact network topology to be used for the station bus and the process bus is not laid down in the IEC 61850 standard. Substation network architecture may differ for substations of the transmission, generation and distribution level. In a simplistic case, the station bus and the process bus may even be merged, thus forming a united station bus where all the services – GOOSE, MMS and SV – coexist, sharing the same physical medium. The most critical issue that should be accounted for is whether the expected SV and GOOSE message traffic will overload the network capacity in a worst-case scenario (typically when faults and abnormal regimes need to be addressed). Definitely, network redundancy, feasibility of access and isolation of the faulted network segment are of paramount importance when choosing a particular architecture.

8.7. Inter-station communication

Time-critical messages like GOOSE and SV were originally not intended for inter-station communication. Both are multicast messages mapped directly to the Ethernet link layer of the OSI model (Fig. 8.12) and thus, communication is limited to the station's LAN. To extend the GOOSE and SV messaging capabilities to inter-station and station-to-control-centre communications, encapsulation and tunnelling techniques can be used [129]. Tunnelling provides a mechanism to transport data packets of one protocol (the "passenger" protocol) within another ("transport") protocol. The tunnel behaves like a virtual point-to-point link with appropriate tunnel source and tunnel destination addresses. In typical implementation, GOOSE and SV services are delivered by using a high-speed SDH/SONET communication network as a tunnel. Another option is GOOSE and SV services communicating over Internet Protocol (IP) networks. An example of the mapping of GOOSE and SV services onto an IP-based protocol is shown in Fig. 8.12. Technical report IEC TR 61850-90-5:2012 [130] extends the application of GOOSE and SV from LAN to WAN by specifying the Routed

GOOSE (R-GOOSE) and Routed Sampled Value (R-SV) profiles. The message is encapsulated in an IEC TR 61850-90-5 session layer and published by using UDP/IP multicast services providing IP priority tagging, security and encryption services.

Traditional tele-protection and directional comparison schemes can be replaced with R-GOOSE messaging over WAN. To preserve the point-to-point communication mechanism, the Virtual LAN (VLAN) principle is used, which allows the expansion of substation LAN into an inter-station communication domain. A VLAN tag is added to every GOOSE and SV message that has to be sent outside the substation LAN. The VLAN tag then is used by the substation router to convert Ethernet frames into routable IP messages and transmits them to the destination address. While the majority of event-based activities between remote relays can be successfully covered with R-GOOSE, the protection applications like line current differential protection are still questionable. IEC TR 61850-90-5 [130] also provides a way of exchanging synchrophasor data between PMUs and WAMPAC (wide area monitoring, protection and control) systems using R-SV messaging. It is supposed that the R-SV service can be used for line differential protection needs, but special attention should be paid to WAN bandwidth capacity, packet drops and network collision scenarios. Several publications are devoted to R-GOOSE and R-SV implementation issues [129], [131].

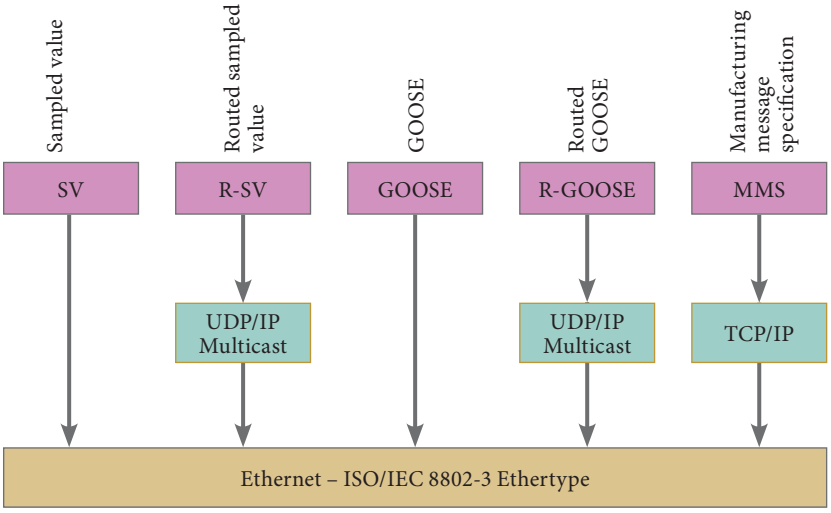

Fig. 8.12. Routed SV and Routed GOOSE mapping

8.8. Substation Configuration Language

The IEC 61850 standard uses abstract models to describe the primary and secondary substation equipment, substation automation functions and communication systems. Although the substation object models define each of the devices in the substation, these models do not specify how they interact. IEC61850 part 6 [132] provides the mechanism which allows describing and setting the relationship between real components, implemented functions and component interactions. This mechanism is known as the Substation Configuration Language (SCL) [132]. The SCL is based on the Extensible Markup Language (XML) and is a standardised tool to configure an IEC61850-based substation. The entire system is described at different hierarchical levels and each level is represented by an individual XML file (Fig. 8.13):

- The System Specification Description (.ssd) file describes the single-line diagram of the substation equipment, and substation automation functions are associated with logical nodes (LNs). No LN allocation to specific IEDs is made at this stage.
- The IED Capability Description (.icd) file describes IED functional capability as defined by the IED manufacturer (default functionality). This file could be considered as a default template of IED containing all the available IED LNs, LN types, LDs as they were instantiated. This self-describing file can be downloaded directly from an IED or from the database of IEDs and then passed to the system configuration tool.

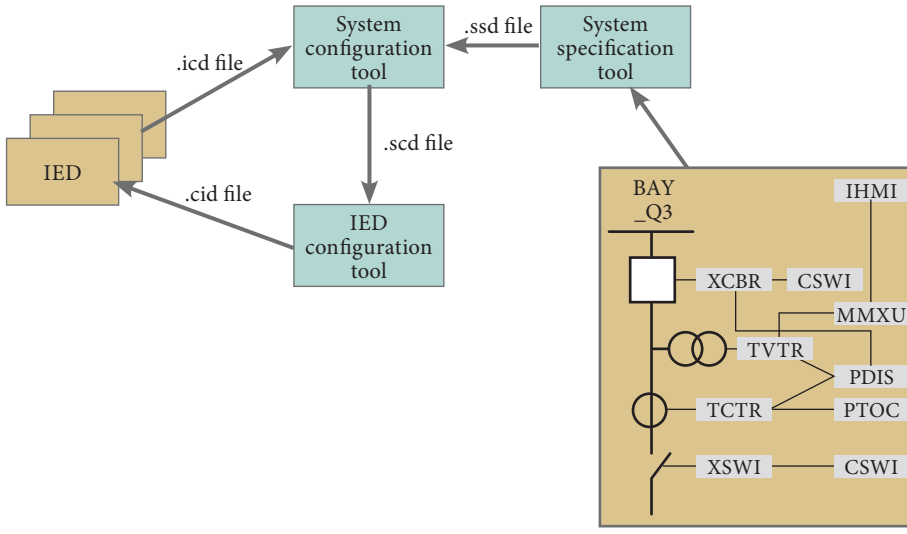

Fig. 8.13. The IEC 61850 substation engineering process

- The Configured IED Description (.cid) file describes the functional capabilities of an IED after the IED has been configured to meet the specific needs of substation automation. The file specifies how an IED's LNs are mapped to substation-specific LNs, LDs and IED communication is described as well. The file can be uploaded directly to the IED.
- The content of the Substation Configuration Description (.scd) file describes the complete system configuration including substation specification, all configured IEDs and the configuration of the communications.

References

[1] Final Report on the August 14, 2003 Blackout in the United States and Canada. U.S.-Canada Power System Outage Task Force, April 2004. Available: https://www.energy.gov/oe/downloads/blackout-2003-final-report-august-14-2003-blackout-united-states-and-canada-causes-and

[2] Final report of System disturbance on 4 November 2006. UCTE, 2006.

[3] Final Report of the Investigation Committee on the 28 September 2003 Blackout in Italy. UCTE, 2004.

[4] Final report on the course of events of Power failure in Eastern Denmark and Southern Sweden on 23 September 2003. UCTE, 2003.

[5] Y. V. Makarov, V. I. Reshetov, A. Stroev, and I. Voropai, "Blackout Prevention in the United States, Europe, and Russia," in *Proceedings of the IEEE*, Vol. 93, No. 11, pp. 1942–1955, Nov. 2005.

[6] P. Kundur et al., "Definition and classification of power system stability IEEE/CIGRE joint task force on stability terms and definitions," in *IEEE Transactions on Power Systems*, Vol. 19, No. 3, pp. 1387–1401, Aug. 2004.

[7] E. W. Kimbark, *Power System Stability*, Vol. I, New York: IEEE Press Classic Reissue, March 1995.

[8] Siemens, "SIPROTEC 4 Distance Protection 7SA522 Application Manual," Feb. 2011.

[9] ABB, "Line Distance Protection REL670 Application Manual," July 2016.

[10] GE Industrial Systems, "D60 Line Distance Relay Instruction Manual," Dec. 2018.

[11] Schneider Electric, "MiCOM P44x Numerical Distance Protection Technical Manual," June 2012.

[12] Toshiba, "GRZ100 Distance Relay Instruction Manual," July 2015.

[13] Toshiba, "GRL100B Line Differential Relay Instruction Manual," Sep. 2014.

[14] G. Benmouyal, D. Hou, D. Tziouvaras, "Zero-Setting Power-Swing Blocking Protection," Feb. 2005.

[15] RTU, "AGNA Technical Description and Operating Manual", June 2005.

[16] A. Sauhats, I. Svalova, A. Svalovs, D. Antonovs, A. Utans, and G. Bochkarjova, "Two-terminal out-of-step protection for multi-machine grids using synchronised measurements," *2015 IEEE Eindhoven PowerTech*, pp. 1–5, 2015.

[17] A. G. Phadke, J. S. Thorp and M. G. Adamiak, "A New Measurement Technique for Tracking Voltage Phasors, Local System Frequency, and Rate of Change of Frequency," in *IEEE Transactions on Power Apparatus and Systems*, Vol. PAS-102, No. 5, pp. 1025–1038, May 1983.

[18] V. V. Terzija, M. B. Djuric, and B. D. Kovacevic, "Voltage phasor and local system frequency estimation using Newton type algorithm," in *IEEE Transactions on Power Delivery*, Vol. 9, No. 3, pp. 1368–1374, July 1994.

[19] T. S. Sidhu and M. S. Sachdev, "An iterative DSP technique for tracking power system frequency and voltage phasors," *Proceedings of 1996 Canadian Conference on Electrical and Computer Engineering, 1996*, Vol. 1, pp. 115–118, 1996.

[20] Jun-Zhe Yang and Chih-Wen Liu, "A precise calculation of power system frequency and phasor," in *IEEE Transactions on Power Delivery*, Vol. 15, No. 2, pp. 494–499, April 2000.

[21] A. A. Girgis and R. G. Brown, "Application of Kalman Filtering in Computer Relaying," in *IEEE Transactions on Power Apparatus and Systems*, Vol. PAS-100, No. 7, pp. 3387–3397, July 1981.

[22] Chi-kong Wong, Ieng-tak Leong, Chu-san Lei, Jing-tao Wu, and Ying-duo Ham, "A novel algorithm for phasor calculation based on wavelet analysis," *2001 Power Engineering Society Summer Meeting. Conference Proceedings*, Vol. 3, pp. 1500–1503, 2001.

[23] J. A. de la O Serna, "Dynamic Phasor Estimates for Power System Oscillations," in *IEEE Transactions on Instrumentation and Measurement*, Vol. 56, No. 5, pp. 1648–1657, Oct. 2007.

[24] J. A. de la O Serna, "Synchrophasor Estimation Using Prony's Method," in *IEEE Transactions on Instrumentation and Measurement*, Vol. 62, No. 8, pp. 2119–2128, Aug. 2013.

[25] V. Madani, D. Novosel, "Guidelines for Synchronization Techniques Accuracy and Availability," North American SynchroPhasor Initiative (NASPI), Dec. 2008.

[26] B. Baumgartner, C. Riesch, M. Rudigier "The Future of Time Synchronization in the Electric Power Industry".

[27] *IEEE Standard for a Precision Clock Synchronization Protocol for Networked Measurement and Control Systems*, IEEE Standard 1588-2008, 2008.

[28] *IEEE Standard for Synchrophasor Measurements for Power Systems*, IEEE Standard C37.118.1-2011, 2011.

[29] *IEEE Guide for Phasor Data Concentrator Requirements for Power System Protection, Control, and Monitoring*, IEEE Standard C37.244-2013, 2013.

[30] F. Aminifar, M. Fotuhi-Firuzabad, A. Safdarian, A. Davoudi, and M. Shahidehpour, "Synchrophasor Measurement Technology in Power Systems: Panorama and State-of-the-Art," in *IEEE Access*, Vol. 2, pp. 1607–1628, 2014.

[31] M. Begovic, "Inter-Area Oscillations in Power Systems: A Nonlinear and Nonstationary Perspective (Messina, A.R.)," in *IEEE Power and Energy Magazine*, Vol. 9, No. 2, pp. 76–77, March–April 2011.

[32] J. H. Chow, *Time-Scale Modeling of Dynamic Network with Application to Power Systems*. Berlin: Springer Verlag, 1982.

[33] Haibo You, V. Vittal, and Zhong Yang, "Self-healing in power systems: an approach using islanding and rate of frequency decline-based load shedding," in *IEEE Transactions on Power Systems*, Vol. 18, No. 1, pp. 174–181, Feb. 2003.

[34] H. You, V. Vittal, and Xiaoming Wang, "Slow coherency-based islanding," in *IEEE Transactions on Power Systems*, Vol. 19, No. 1, pp. 483–491, Feb. 2004.

[35] R. Podmore, "Identification of Coherent Generators for Dynamic Equivalents," in *IEEE Transactions on Power Apparatus and Systems*, Vol. PAS-97, No. 4, pp. 1344–1354, July 1978.

[36] L. Wang, M. Klein, S. Yirga, and P. Kundur, "Dynamic reduction of large power systems for stability studies". in *IEEE Transactions on Power Systems*, Vol. 12, No. 2, pp. 889–895, May 1997.

[37] M. Jonsson, M. Begovic and J. Daalder, "A new method suitable for real-time generator coherency determination," in *IEEE Transactions on Power Systems*, Vol. 19, No. 3, pp. 1473–1482, Aug. 2004.

[38] K. Lo, Z. Qi, and D. Xiao, "Identification of coherent generators by spectrum analysis," in *IEEE Proceedings - Generation, Transmission and Distribution*, Vol. 142, No. 4, pp. 367–371, July 1995.

[39] N. Senroy, "Generator Coherency Using the Hilbert–Huang Transform," in *IEEE Transactions on Power Systems*, Vol. 23, No. 4, pp. 1701–1708, Nov. 2008.

[40] K. K. Anaparthi, B. Chaudhuri, N. F. Thornhill, and B. C. Pal, "Coherency identification in power systems through principal component analysis," in *IEEE Transactions on Power Systems*, Vol. 20, No. 3, pp. 1658–1660, Aug. 2005.

[41] M. A. A. Abd-EI-Rehim, I. D. Helal, and M. A. Hassan Omar, "Multi-machine power system dynamic equivalents using artificial intelligence (ANN)," *2006 Eleventh International Middle East Power Systems Conference*, *2006*, pp. 197–207, 2006.

[42] M. Davodi, H. Modares, E. Reihani, M. Davodi, and A. Sarikhani, "Coherency approach by hybrid PSO, K-Means clustering method in power system," *2008 IEEE 2nd International Power and Energy Conference*, pp. 1203–1207, 2008.

[43] G. C. Pyo, J. W. Park, and S. I. Moon, "A new method for dynamic reduction of power system using PAM algorithm," *IEEE PES General Meeting*, pp. 1–7, 2010.

[44] H. A. Alsafih and R. Dunn, "Determination of coherent clusters in a multi-machine power system based on wide-area signal measurements," *IEEE PES General Meeting*, pp. 1–8, 2010.

[45] T. N. Nababhushana, K. T. Veeramanju, and Shivanna, "Coherency identification using growing self-organizing feature maps," in *Proceedings of International Conference on Energy Management and Power Delivery*, Vol. 1, pp. 113–116, March 1998.

[46] Z. Lin, F. Wen, J. Zhao, Y. Xue, "Controlled islanding schemes for interconnected power systems based on coherent generator group identification and wide-area measurements," *Journal of Modern Power Systems and Clean Energy*, Vol. 4, Iss. 3, pp. 440–453, July 2016.

[47] M. Jonsson, M. Begovic, and J. Daalder, "A new method suitable for real-time generator coherency determination," in *IEEE Transactions on Power Systems*, Vol. 19, No. 3, pp. 1473–1482, Aug. 2004.

[48] A. Sauhats, A. Utans, D. Antonovs, and A. Svalovs, "Angle Control-Based Multi-Terminal Out-of-Step Protection System," *Energies*, Vol. 10, No. 3, p. 308, Mar. 2017.

[49] Kai Sun, Da-Zhong Zheng, and Qiang Lu, "Splitting strategies for islanding operation of large-scale power systems using OBDD-based methods," in *IEEE Transactions on Power Systems*, Vol. 18, No. 2, pp. 912–923, May 2003.

[50] Qianchuan Zhao, Kai Sun, Da-Zhong Zheng, Jin Ma, and Qiang Lu, "A study of system splitting strategies for island operation of power system: a

two-phase method based on OBDDs," in *IEEE Transactions on Power Systems*, Vol. 18, No. 4, pp. 1556–1565, Nov. 2003.

[51] Kai Sun, Da-Zhong Zheng, and Qiang Lu, "A simulation study of OBDD-based proper splitting strategies for power systems under consideration of transient stability," in *IEEE Transactions on Power Systems*, Vol. 20, No. 1, pp. 389–399, Feb. 2005.

[52] R. E. Bryant, "Graph-Based Algorithms for Boolean Function Manipulation," in *IEEE Transactions on Computers*, Vol. C-35, No. 8, pp. 677–691, Aug. 1986.

[53] R. E. Bryant. "Symbolic Boolean manipulation with ordered binary decision diagrams," *ACM Computing Surveys*, Vol. 24, No. 3, pp. 293–318, Sept. 1992.

[54] G. Xu and V. Vittal, "Slow Coherency Based Cutset Determination Algorithm for Large Power Systems," in *IEEE Transactions on Power Systems*, Vol. 25, No. 2, pp. 877–884, May 2010.

[55] X. Wang and V. Vittal, "System islanding using minimal cutsets with minimum net flow," *IEEE PES Power Systems Conference and Exposition*, Vol.1, pp. 379–384, 2004.

[56] A. Sen, P. Ghosh, V. Vittal, and B. Yang, "A new min-cut problem with application to electric power network partitioning," *European Transactions on Electrical Power 2009*, Vol. 19, pp. 778–797, March 2008.

[57] METIS. *A Software Package for Partitioning Unstructured Graphs, Partitioning Meshes, and Computing Fill-Reducing Orderings of Sparse Matrices*.

[58] G. Karypis and V. Kumar, "Multilevel Algorithms for Multi-Constraint Graph Partitioning," *SC '98: Proceedings of the 1998 ACM/IEEE Conference on Supercomputing*, pp. 28–28, 1998.

[59] G. Karypis and V. Kumar, "Parallel Multilevel k-way Partitioning Scheme for Irregular Graphs," *Supercomputing '96: Proceedings of the 1996 ACM/IEEE Conference on Supercomputing*, pp. 35–35, 1996.

[60] G. Karypis and V. Kumar, "A fast and high-quality multilevel scheme for partitioning irregular graphs," *SIAM Journal on Scientific Computing*, Vol. 20, pp. 359–392, Jan. 1999.

[61] R. Moreno and A. Torres, "Security of the power system based on the separation into islands," *2011 IEEE PES Conference on innovative smart grid technologies Latin America (ISGT LA)*, pp. 1–5, 2011.

[62] M. Fiedler, "Algebraic Connectivity of Graphs," *Czechoslovak Mathematical Journal*, Vol. 23, No. 98, pp. 298–305, 1973.

[63] M. Fiedler, "A Property of Eigenvectors of Nonnegative Symmetric Matrices and its Application to Graph Theory," *Czechoslovak Mathematical Journal,* Vol. 25, No. 4, pp. 619–633, 1973.

[64] S. Najafi, M. Abedi, S. H. Hosseinian. "A Strategy for Frequency Stability of Islanded Power Systems," *Power and Energy Conference, 2008. IEEE 2nd International*, Johor Bahru, Malaysia, Dec. 2008.

[65] H. You, V. Vittal, and Xiaoming Wang, "Slow coherency-based islanding," in *IEEE Transactions on Power Systems*, Vol. 19, No. 1, pp. 483–491, Feb. 2004.

[66] N. Senroy, G. T. Heydt, and V. Vittal, "Decision Tree Assisted Controlled Islanding," in *IEEE Transactions on Power Systems*, Vol. 21, No. 4, pp. 1790–1797, Nov. 2006.

[67] R. Schainker, P. Miller, W. Dubbelday, P. Hirsch, and Guorui Zhang, "Real-time dynamic security assessment: fast simulation and modeling applied to emergency outage security of the electric grid," in *IEEE Power and Energy Magazine*, Vol. 4, No. 2, pp. 51–58, March 2006.

[68] U. Kerin, G. Bizjak, S. R. Krebs, E. Lerch, and O. Ruhle, "Faster than real time: Dynamic security assessment for foresighted control actions," *2009 IEEE Bucharest PowerTech*, pp. 1–7, 2009.

[69] K. Kumar, T. Kyriakidis, M. Kayal and R. Cherkaoui, "Distributed real-time dynamic security assessment using ,intelligent techniques," *2013 IEEE Innovative Smart Grid Technologies-Asia (ISGT Asia)*, pp. 1–5, 2013.

[70] H. Jóhannsson and M. Wache, "System security assessment in real-time using synchrophasor measurements," *IEEE PES ISGT Europe 2013*, pp. 1–5, 2013.

[71] J. C. Cepeda, J. L. Rueda, D. G. Colome, D. E. Echeverria, "Real-time transient stability assessment based on centre-of-inertia estimation from phasor measurement unit records," *IET Generation, Transmission & Distribution*, Vol. 8, Iss. 8, pp. 1363–1376, 2014.

[72] C.-W. Liu, J. Thorp. "Application of synchronised phasor measurements to real-time transient stability prediction," *IEE Proceedings - Generation, Transmission and Distribution*, Vol. 142, Iss. 4, pp. 355–360, July 1995.

[73] Chih-Wen Liu and J. S. Thorp, "New methods for computing power system dynamic response for real-time transient stability prediction," *in IEEE Transactions on Circuits and Systems I: Fundamental Theory and Applications*, Vol. 47, No. 3, pp. 324–337, March 2000.

[74] T. Athay, R. Podmore, and S. Virmani, "A Practical Method for the Direct Analysis of Transient Stability," in *IEEE Transactions on Power Apparatus and Systems*, Vol. PAS-98, No. 2, pp. 573–584, March 1979.

[75] M. A. Pai and P. W. Sauer, "Stability analysis of power systems by Lyapunov's direct method," in *IEEE Control Systems Magazine*, Vol. 9, No. 1, pp. 23–27, Jan. 1989.

[76] A. Michel, A. Fouad, and V. Vittal, "Power system transient stability using individual machine energy functions," in *IEEE Transactions on Circuits and Systems*, Vol. 30, No. 5, pp. 266–276, May 1983.

[77] N. Kakimoto, Y. Ohsawa, and M. Hayashi, "Transient Stability Analysis of Multimachine Power System with Field Flux Decays via Lyapunov's Direct Method," in *IEEE Transactions on Power Apparatus and Systems*, Vol. PAS-99, No. 5, pp. 1819–1827, Sept. 1980.

[78] E. Carton, M. Ribbens-Pavella, "Lyapunov methods applied to multimachine transient stability with variable inertia coefficients," *Proceedings of the Institution of Electrical Engineers,* Vol. 118, Iss. 11, pp. 1601–1606, Nov. 1971.

[79] A. H. El-abiad and K. Nagappan, "Transient Stability Regions of Multimachine Power Systems," in *IEEE Transactions on Power Apparatus and Systems*, Vol. PAS-85, No. 2, pp. 169–179, Feb. 1966.

[80] E. Farantatos, R. Huang, G. J. Cokkinides, and A. P. Meliopoulos, "A Predictive Generator Out-of-Step Protection and Transient Stability Monitoring Scheme Enabled by a Distributed Dynamic State Estimator," in *IEEE Transactions on Power Delivery*, Vol. 31, No. 4, pp. 1826–1835, Aug. 2016.

[81] P. D. Aylett, "The energy-integral criterion of transient stability limits of power systems," *Proceedings of the IEE – Part C: Monographs*, Vol. 105, Iss. 8, pp. 527–536, Sept. 1958.

[82] P. C. Magnusson, "The Transient-Energy Method of Calculating Stability," *Transactions of the American Institute of Electrical Engineers*, Vol. 66, Iss. 1, pp. 747–755, Jan. 1947.

[83] M. Ribbens-Pavella, F. J. Evans, "Direct methods for studying dynamics of large-scale electric power systems – A survey," Elsevier Automatica, Vol. 21, Iss. 1, pp. 1–21, January 1985.

[84] L. F. C. Alberto, F. H. J. R. Silva, and N. G. Bretas, "Direct methods for transient stability analysis in power systems: state of art and future perspectives," *2001 IEEE Porto Power Tech Proceedings*, Vol., 2, p. 6, 2001.

[85] T. Athay, V. R. Sherket, R. Podmore, S. Virmani, and C. Puech, "Transient Energy Stability Analysis," in *Proc. Conf. on System Engineering for Power: Emergency operating State Control*, Davos, Switzerland, 1979.

[86] R. T. Treinen, V. Vittal, and W. Kliemann, "An improved technique to determine the controlling unstable equilibrium point in a power system," in *IEEE Transactions on Circuits and Systems I: Fundamental Theory and Applications*, Vol. 43, No. 4, pp. 313–323, April 1996.

[87] H. -D. Chiang, F. F. Wu, P. P. Varaiya, and C. -W. Tan, "Theory of the potential energy boundary surface," *1985 24th IEEE Conference on Decision and Control*, pp. 49–51, 1985.

[88] H. D. Chiang, F. F. Wu, and P. P. Varaiya, "Foundations of the potential energy boundary surface method for power system transient stability analysis," in *IEEE Transactions on Circuits and Systems*, Vol. 35, No. 6, pp. 712–728, June 1988.

[89] M. Pavella, D. Ernst, D. Ruiz-Vega, *Transient Stability of Power Systems. A Unified Approach to Assessment and Control.* Springer Science & Business Media, 2000.

[90] Y. Xue, T. Van Custem, and M. Ribbens-Pavella, "Extended equal area criterion justifications, generalizations, applications," in *IEEE Transactions on Power Systems*, Vol. 4, No. 1, pp. 44–52, Feb. 1989.

[91] S. Paudyal, G. Ramakrishna, and M. S. Sachdev, "Out-of-step protection using the equal area criterion in time domain – SMIB and 3-machine case studies," *TENCON 2008 – 2008 IEEE Region 10 Conference*, pp. 1–6, 2008.

[92] A. Sauhats, A. Utans, D. Antonovs, and E. Biela-Dalidovicha, "Out-of-step protection using equal area criterion in time domain," *2016 57th International Scientific Conference on Power and Electrical Engineering of Riga Technical University (RTUCON)*, pp. 1–6, 2016.

[93] A. Sauhats, A. Utans, and E. Biela-Dalidovicha, "Equal area criterion and angle control-based out-of-step protection," *2017 IEEE 58th International Scientific Conference on Power and Electrical Engineering of Riga Technical University (RTUCON)*, pp. 1–6, 2017.

[94] D. E. Echeverría, J. L. Rueda, D. G. Colomé, and I. Erlich, "Improved method for real-time transient stability assessment of power systems," *2012 IEEE Power and Energy Society General Meeting*, pp. 1–8, 2012.

[95] M. Jha, S. Chakrabarti, and E. Kyriakides, "Estimation of the rotor angle of a synchronous generator by using PMU measurements," *2015 IEEE Eindhoven PowerTech*, pp. 1–6, 2015.

[96] H. Miller, J. Burger, N. Fischer, and B. Kasztenny, "Modern line current differential protection solutions," *2010 63rd Annual Conference for Protective Relay Engineers*, pp. 1–25, 2010.

[97] A. Sauhats, A. Utans, and E. Biela-Dailidovicha, "Wide-area measurements-based out-of-step protection system," *2015 56th International Scientific Conference on Power and Electrical Engineering of Riga Technical University (RTUCON)*, pp. 1–5, 2015.

[98] *IEC 61850-3 Ed.2: Communication networks and systems for power utility automation – Part 3: General requirements IEC 61850 Standard*, IEC standard, 2010.
[99] Guo Yan Chen, Xianggen Yin, Kai Zhang "Communication Modeling for Wide-Area Relay Protection Based on IEC 61850," *Telkomnika*, Vol. 10, No. 7, pp. 1673–1684, Nov. 2012.
[100] *IEC/TR 61850-90-5:2012, Communication networks and systems for power utility automation – Part 90-1: Use of IEC 61850 for the communication between substations,* IEC Technical report, 2012.
[101] J. D. McDonald, *Electric Power Substations Engineering.* CRC Press, 2016.
[102] E. O. Schweitzer, D. Whitehead, K. Fodero, and P. Robertson, "Merging SONET and Ethernet Communications for Power System Applications," SEL *Journal of Reliable Power*, Vol. 3, No. 2, August 2012.
[103] S. Ward, W. Higinbotham, "Network Errors and Their Influence on Current Differential Relaying," *Protective Relay Engineers, 2011 64th Annual Conference*, April 2011.
[104] BELDEN, "White Paper – Data Communication in Substation Automation System (SAS)".
[105] BELDEN, "White Paper – Data Communication in Substation Automation System (SAS). Introduction of modern substation communication. WP1004HE-Part3".
[106] F. Halsall, *Data communications, computer networks and open systems,* 3rd Edition, Addison-Wesley, 1992.
[107] Siemens AG, "Redundant networks for industry," Nov. 2012.
[108] *IEEE 802.1w-2001 – IEEE Standard for Information Technology -Telecommunications and Information Exchange Between Systems – Local and Metropolitan Area Networks - Common Specifications – Part 3: Media Access Control (MAC) Bridges: Amendment 2 – Rapid Reconfiguration*, IEEE standard, 2001.
[109] ABB, "Substation Automation Solutions. SAS 600 Series".
[110] C. Wester and M. Adamiak, "Practical applications of Ethernet in substations and industrial facilities," *2011 64th Annual Conference for Protective Relay Engineers*, pp. 67–78, 2011.
[111] G. Clarke, D. Reynders, *Practical Modern SCADA Protocols: DNP3, 60870.5 and Related Systems*, Elsevier, Jan. 20, 2004.
[112] DNP User group: www.dnp.org
[113] IEC Protocols: www.iec.ch
[114] J. Makhija, "Comparison of protocols used in remote monitoring: DNP 3.0, IEC 870-5-101 & Modbus," *M.Tech. Credit Seminar Report, Electronics Systems Group, EE Dept, IIT Bombay,* 2003.
[115] MODBUS Protocols: www.MODBUS.org
[116] *IEC 61158-2, Digital data communications for measurement and control – Fieldbus for use in industrial control systems – Part 2: Physical layer specification and service definition*, IEC standard, 2003.
[117] M. Felser, *Profibus Manual*, 2017.
[118] www.profibus.com
[119] *Communication networks and systems for power utility automation-ALL PARTS*, IEC 61850:2022 SER standard series, 2020.
[120] *IEC 61850-7-4: Basic communication structure for substation and feeder equipment – Compatible logical node classes and data classes*, IEC standard, 2003.

[121] *IEC 61850-7-3: Basic communication structure – Common data classes*, IEC standard, 2010.
[122] B. G. Liptak, H. Eren, *Instrument Engineers' Handbook*, 4th Edition, CRC Press, 2011.
[123] B. M. Buchholz, Z. Styczynski, *Smart Grids – Fundamentals and Technologies in Electricity Networks*, Heidelberg: Springer, 2014.
[124] *IEC 61850-7-2: Basic communication structure for substation and feeder equipment – Abstract communication service interface (ACSI)*, IEC standard, 2003.
[125] *IEC 61850-8-1: Communication networks and systems in substation – Specific communication service mapping (SCSM) - Mappings to MMS (ISO 9506-1 and ISO 9506-2) and to ISO/IEC 8802-3*, IEC standard, 2011.
[126] *IEC 61850-5: Communication networks and systems in substations – Communication requirements for functions and device models*, IEC standard, 2003.
[127] *IEC 61850-9-2: Communication networks and systems in substations – Specific communication service mapping (SCSM)-Sampled Values over ISO/IEC 8802-3*, IEC standard, 2004.
[128] C. Brunner, G. Lang, F. Leconte, F. Steinhauser, "Implementation Guideline for Digital Interface to Instrument transformers Using IEC 61850-9-2," UCA International Users Group, 2004.
[129] C. H. R. D. Oliveira, A. P. Bowen, "IEC 61850 GOOSE Message over WAN," *International Conference on Wireless Network*, 2012.
[130] *IEC TR 61850-90-5:2012: Communication networks and systems for power utility automation – Part 90-5: Use of IEC 61850 to transmit synchrophasor information according to IEEE C37.118*, IEC standard, 2012.
[131] S. R. Firouzi, L. Vanfretti, A. Ruiz-Alvarez, H. Hooshyar, F. Mahmood, "Interpreting and implementing IEC 61850-90-5 Routed-Sampled Value and Routed-GOOSE protocols for IEEE C37.118.2 compliant wide-area synchrophasor data transfer," *Electric Power Systems Research,* Vol. 144, pp. 255–267, 2016.
[132] *IEC 61850-6: Communication networks and systems in substations – Configuration description language for communication in electrical substations related to IEDs*, IEC standard, 2004.